Tuning liquefier dynamics: A strategy for accuracy improvement in extrusion based additive manufacturing with PEEK

Reinout Holtrup

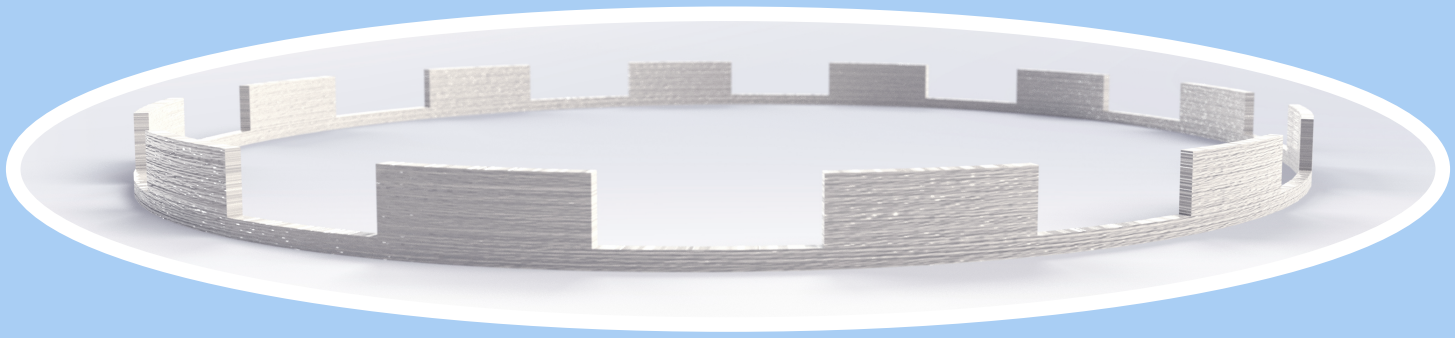

MASTER THESIS INDUSTRIAL DESIGN ENGINEERING

06/2019

University of Twente

Reinout Holtrup

Education
Master Industrial Design Engineering - *Management of Product Development track*
Faculty of Engineering Technology
Department of Design, Production and Management

Institution
University of Twente
Drienerlolaan 5
7500 AE ENSCHEDE

Company
Bond High Performance 3D Technology
Institutenweg 25a
7521 PH ENSCHEDE

Examination date
1 July 2019

Examination board

Chairman	Prof. dr. ir. I. Gibson
Supervisor	Dr. ir. T. H. J. Vaneker
External member	Dr. ir. R.G.K.M. Aarts
Company mentor	Dr. ir. K.H. Kuit

Report

pages	95
appendices	12
confidential inlays	1

This report is confidential until 1 September 2022

Tuning liquefier dynamics: A strategy for accuracy improvement in extrusion based additive manufacturing with PEEK

Reinout Holtrup

University of Twente

June 6, 2019

Abstract

Extrusion based 3D printing is an additive manufacturing technique in which a material is robotically dispensed through a nozzle or orifice on prescribed locations.

Bond 3D printing develops a new system that uses PEEK as the feeding material and has formulated three main challenges within their extrusion based printing process: enhancement of lead time, strength and accuracy (personal communication, 2017). The focus of this study was set on the enhancement of material dispensing accuracy for small single line width features with PEEK.

Bond3D states that due to the high performance applications inevitable small features show up in applications such as small tubes in manifolds, porosity in implants and thin walls in lightweight structures (personal communication, 2017). Additionally, the lack of accuracy and discontinuities can cause weaknesses in the final products (Gibson, Rosen, & Stucker, 2009, p. 155).

To enhance this accuracy, two approaches were employed: an empirical approach and an analytic model approach. The first approach studies the real-world effects and is well suited to find local optima, while the latter one provides better fundamental support and can often be used to extrapolate results to experimentally unverified testing conditions.

For both approaches, a custom-built 3d printer prototype was used to print single wall test geometries with abrupt velocity changes. Accuracy was assessed visually.

In the empirical study, individual or combination of process settings were varied, or accuracy enhancement "tricks" were applied (priming, coasting, retracts, wipes), after which the accuracy of the product was determined. However, it resulted that the effects of changing the process variables, such as line height, segment length and setting and coasting length were highly interdependent and setting up the experiments to obtain predictable results proofed to be challenging. Still, some qualitative results were found. Experiments that used retraction of the plunger, decreased travel time of the print head and thereby the time that oozing can take place and experiments which used coasting, led to the highest vertical stop-straightness. Wiping in some cases enhanced the vertical straightness of the printed structures during starts, but increased the risk of smearing, resulting in completely inaccurate prints.

Furthermore, in all experiment setups, the line width of deposited strand deviated strongly from the expected line width, which indicated that there were dynamic effects that affected the final accuracy.

As such, the system dynamics were analysed through a system identification consisting of two experiment types that characterised the dynamics: a step response and frequency response experiment. They characterise the response of the flow rate to the changes in plunger velocity. The responses were assessed by measurements of the oozed length and the resulting line width. It was found that the compressibility of the feeding material and its thermal expansion were the factors dominating dynamic effects. The dynamics were controlled using a controller making real-time system adjustments. The systems dynamics showed strong non-linear behaviour, while the implemented controller assumed linearity. This complicated extrapolating the accuracy as a function of plunger velocity and controller settings.

The strong non-linearity was explained by the fact that the stiffness of the feeding material is a function of the consumed volume. The decreasing fluidic restriction value of the nozzle for increasing the flow rates was explained by shear thinning behaviour of the molten polymer. Thermal oozing was explained by the difference in average melt room temperature that is dependent both on time and temperature.

The first two effects were described by analytic expressions and also an expression of the maximum thermally induced oozing volume was given. The Boles model of flow through a converging die using power law viscosity functions that were derived from the Cross viscosity model of PEEK was proven suitable to predict the steady-state pressure drop accurately for two different nozzles for PEEK within the studied flow regime. The model are powerful tools in the design and optimisation of 3D printing nozzles, materials and tuning and development of a numerical model, however the effect on accuracy in real-world printing conditions needs to be proven in a future study as well as the development of the melt room temperature over time and extrusion rate.

Keywords Additive Manufacturing, Accuracy, PEEK material extrusion

Contents

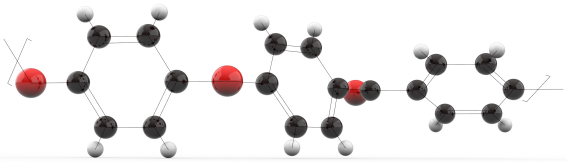

List of Figures

List of Tables

Acronyms

ABS acrylonitrile butadiene styrene. 10, 21

AM additive manufacturing. 9, 11

ASTM American Society for Testing and Materials. 9

CNT carbon nano tube. 23

DOE design of experiments. 25, 51, 54

FDM™ Fused deposition modeling. 10, 18

FEA finite element Analysis. 34, 80

FEM finite element Model. 88, 89

FeMo feasibility model. 12, 20, 49, 53, 55, 61

FFF fused filament fabrication. 18

FuMo functional model. 12, 13, 20, 71

G-code exchange file to describe target set points and velocities of machine motion and other actuators. 16, 18, 21, 37, 38, 43, 46–48, 50, 51, 58, 59, 64

ME material extrusion. 9

PLA polylactic acid. 10, 37

PLC programmable logical controller. 18, 21, 63, 64, 70

PoP proof of principle prototype. 4, 12, 16, 20, 48, 49, 53–55, 57, 61, 73, 90

SLA stereolithography. 10

SLS selective laser sintering. 10, 12

STL standard tesselation language. 18

Preface

The purpose of this report is to describe the master assignment that was carried out for the master Industrial Design Engineering at the University of Twente. This report describes the versatile, broad and thorough understanding of the topic and demonstrates the competence to conduct and report on scientific research.

This report is about the efforts that were taken to find a sophisticated strategy for accuracy enhancement in the extrusion-based 3D printing of the high-performance polymer PEEK. Although the emphasis was on applied science, a theoretical base had to be formed to gain understanding of the underlying complexity and solve the problem. Skills from other disciplines had to be developed, including mechatronics, chemistry and rheology.

Bond3D is the company that provided this graduation assignment. The company is founded by Aad and Thomas Bruggeman in 2013 with the purpose to make functional 3D printed products from high-performance polymers. It is a company with a high pressure to have a market release for their cutting-edge technology. The company attracted several rounds of venture capital with their prototypes, patents and business plans. Advanced hardware is being developed that can handle the difficulties of this material in collaboration with mechatronics company DEMCON.

I would like to thank dr. ir. Vaneker and dr. ir. Kuit for their support throughout this project. I would like to thank my colleagues for their great collaboration. They were always willing to help me. Finally, I would like to thank my girlfriend Miriam, my brother Arno, and parents Roland and Miep for their love and motivation and encouragement.

The chapter order of this publication differs from the order in which the research was carried out due to changes of insights along the way and the demand for readability of this report.

The target audience of this report consists of academic professors and students that would like to enrich knowledge about the design and application of extrusion based manufacturing or want to make enhancements to extrusion based manufacturing systems.

Chapter 1

Introduction

Material extrusion (ME) is one of the seven additive manufacturing techniques according American Society for Testing and Materials (ASTM) F2792 (ASTM, 2012). ME is an additive manufacturing (AM) process in which material is selectively dispensed through a nozzle or orifice (Silbernagel, 2018). In this thesis, the physics of the extrusion-based printing process are studied with the goal to enhance printing accuracy. Accuracy is often used as a concept to deal with the quality of small part sections. In this master thesis, accuracy refers to the placement of the right material volume at the right location.

The 7 categories of AM are:

- vat polymerisation,
- material jetting,
- binder jetting,
- **material extrusion,**
- powder bed fusion,
- sheet lamination,
- direct energy deposition

3D printing, in general, became popular during the last decade. The basic principles for 3D printing processes are no novelties. Most of the principles were invented in the eighties. At that time they were described as rapid prototyping techniques, while nowadays they are called 3D printing or additive manufacturing techniques. The first extrusion based printing was performed by Scott Crump by combining a hot glue gun and a Cartesian gantry and candle wax. The technology was patented in 1989 (Silbernagel, 2018). The first 3D modellers were sold in the second quarter of 1991 (Crump, Wales, & Walters, 1991).

In extrusion based printing, parts are built from layers and these layers are built from deposited lines of material. These lines are made by extrusion of material through a nozzle while moving with respect to the platform.

The material is deposited at a predetermined place. Extrusion-based printing can be applied to a wide range of material types, including concrete, chocolate, photo polymers and thermoplastics. Figure 1.1 shows a typical extrusion based 3d printing system for thermoplastic polymers. In this printing technology, a feeding material is supplied in solid form. Heater elements in the hot end section liquefy the material and a cold end functions as a barrier and sealing for the molten material. Thermoplastics are used as the base material when extrusion based printing is mentioned in this report.

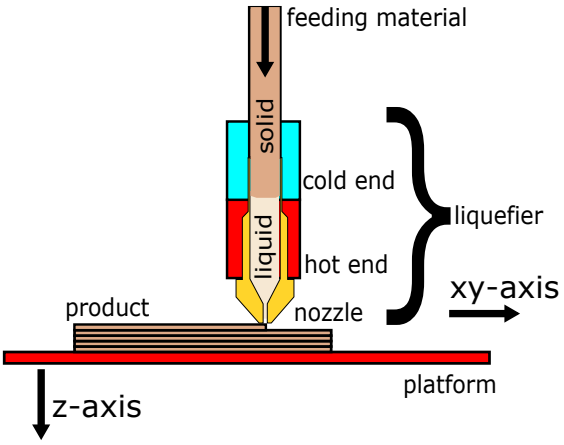

Figure 1.1: Material extrusion 3D printing with thermoplastic polymers

Extrusion-based printing is suitable for a wide range of polymers. The most common materials are polylactic acid (PLA) and acrylonitrile butadiene styrene (ABS). Depending on the material processed, a heated build environment is needed to provide suitable welding conditions. (Bellehumeur & Li, 2004)

The advantages of extrusion based 3D printing are the independence of batch sizes, the high grade of freedom of form, the ability to build with multiple materials including soluble and breakaway support materials and the high strengths that could be achieved, when comparing with other 3D printing techniques. For an overview see Appendix K.

The throughput is a subject that should be compared together with the post processing efforts: The actual printing may take longer when compared to selective laser sintering (SLS) or stereolithography (SLA), but post-processing takes much less time. It does not require powder removal and post-curing, but dissolving support material may take some time.

The main disadvantages of the technology is that the strength depends on the layer adhesion, which is very difficult to control. Part quality is highly sensitive to thermal conditions. Bed adhesion issues are common and the achievable detail level is not the highest due to the high layer thickness.

Wohlers (2016) writes that from 2007 the expiration of the key Fused deposition modeling (FDM™) patents held by Stratasys contributed to the rise of FDM™ clones including the RepRap project. While sales were limited to 66 low-cost (under $5000) units in 2007, the number increased to an estimate of 140000 by 2014. Compared to the number of industrial systems sold in the same year (12850 units), this is a very large number. The number of FDM™ clone manufacturers and start-up companies seems ever- increasing. (Wohlers, 2016)

3D printing experienced an attention boost in 2011. This can be observed by examination of stock values of listed companies from 2011 until the end of 2013 shown in Figure 1.2. The share values dropped dramatically from early 2014 to 2016 since 3D printing was actually not as valuable as people were made to believe. Although the hype cycle has ended, the industry kept on growing with 31.5% during 2013 and 2015.(Wohlers, 2016)

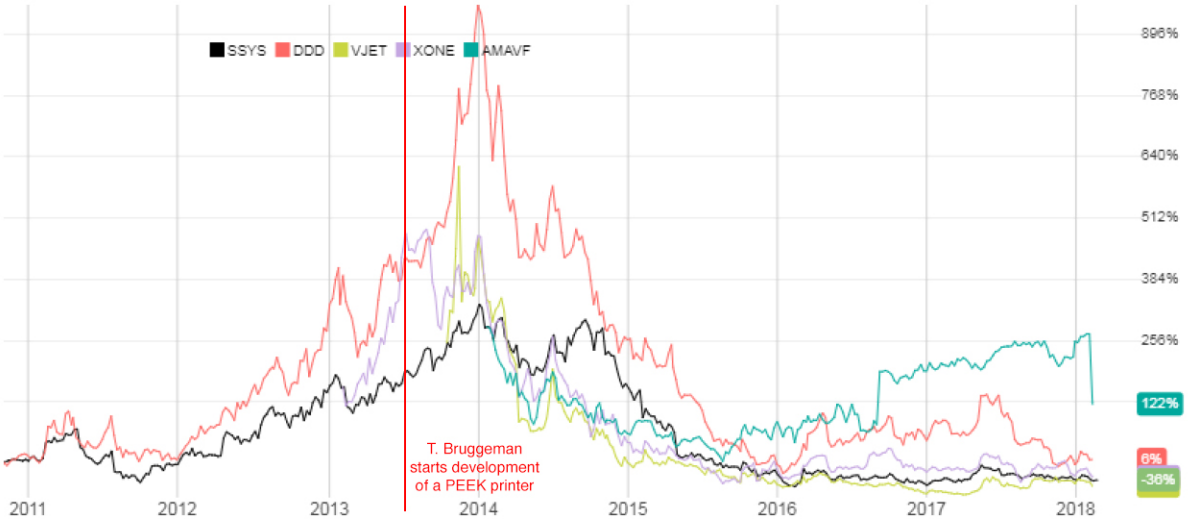

Figure 1.2: Stock price trends of public 3D printing companies. [Stratasys, 3D Systems, Voxeljet, ExOne and Arcam] (adopted from www.nasdaq.com)

1.1 State of the art at Bond3D

High performance polymers The market gap that Bond3D wants to fill is that of AM systems for high performance polymers. While in the last decade industrial AM systems have made their way to the market for metals, the number of industrial printers for high performance polymers is still limited, while the demand is high.

No official definition of a high performance polymer exist, but Hergenrother (2003) defines it as following: "A polymer with unusual stability to harsh environments and properties that surpass those of conventional polymers." High performance mainly refers to the high thermal stability, facilitated by the strong primary bonds and secondary bonds, high purity and high molecular weight.

Polymers can be arranged in a pyramid to visualise the taxonomy. The top section of this triangle contains the high-performance polymers, see Figure 1.3.

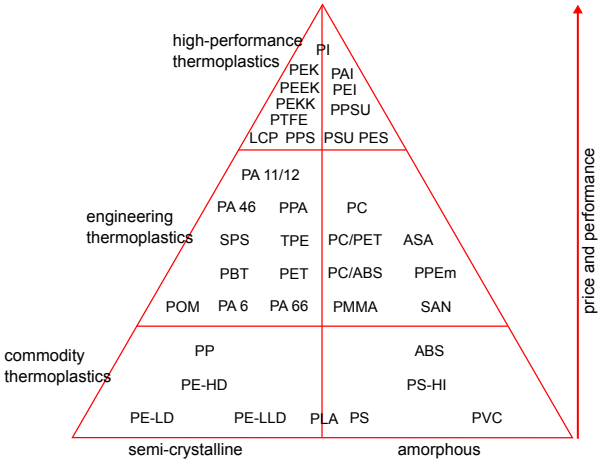

Figure 1.3: Thermoplastic performance pyramid, adapted from: Wikipedia (2018a)

The high thermal stability of these high performance polymers makes melt processing hard. Melt processing works by decreasing the viscosity by exposure to heat.

The pyramid is horizontally divided in semi-crystalline and amorphous polymers. Semi-crystalline polymers have a good fatigue resistance and are suitable for bearing, wear and structural applications. In contrast to

amorphous polymers, semi-crystalline polymers have a melt point. Semi-crystalline polymers are difficult to bond using adhesives, solvents and welding when compared to amorphous polymers.

In an extrusion based 3D printing system materials are layer-wise welded together. This is more challenging with semi-crystalline materials while obtaining strong inter-layer bonding. According to Martineau, Chabert, Boniface, and Bernhart (2019), the crystalline growth has an ambivalent effect on strength. Crystalline growth across the interface reinforces the interfacial strength. However it reduces molecular chain mobility and therefore the interdiffusion.

PEEK PEEK is the material that was chosen by Bond3D as the primary high performance material to develop the system for. PEEK is a semi-crystalline material, which has a crystallinity that is generally above 25% (Grasmeder, 2017b) and is dependent on the processing history according to Meyer and Keurentjes (2008, p.686). Injection moulded parts have a crystallinity of 30% to 35% what is optimal for strength. (Kurtz, 2012, p.3).

The applications that Bond3D has in mind require a robust and flexible system, capable of printing accurate and strong products with low throughput. The material costs are magnitudes higher than alternatives. The parts fabricated with PEEK often have critical functions. It can be concluded that for this reason, the design requirements for the 3D printer that would produce these parts are high.

Applications Although PEEK appears in niche applications, the following three application groups could be considered as the most important ones:

- High temperature applications
- High strength to weight ratio demanding applications
- Medical applications

PEEK has almost the highest service temperature (250°C) of all melt processable additive-free polymers. The heat deflection temperature is also high. This makes PEEK an suitable material for high-temperature applications.

The high strength-to-weight ratio of PEEK and the form freedom contribute to the fact that extrusion based printing of PEEK could be used for lightweight applications.

High strength, good steriliseability, and the high chemical resistance support the idea that the material is suitable for medical applications. PEEK has the advantage of radio-translucency and slight flexibility (that prevents stress-shielding) when compared to titanium. Kurtz (2012), Godara, Raabe, and Green (2007) and Valentan, Kadivnik, Brajlih, Anderson, and Drstvenšek (2013) suggested that 3D printed PEEK is promising for medical applications, due to its high mechanical properties. 3D printing technology can enable porosity in products with a fully interconnected channel network, controllable porosity and channel size (Zein, Hutmacher, Tan, & Teoh, 2002). Enabling porosity allows better integration, fixation or interaction with the surrounding tissue (Kurtz, 2012, p. 181).

The price and processability are the main reasons to consider other materials: the price of medical grade PEEK can raise up to over £2,000 per kilogram (Ganz, 2016). This was comparable to about €2600 in 2016. The costs of the industrial 450G variant range from €100 to €300 per kilogram granular material (Ashby, 2018).

Extrusion based printing is a high-cost, low-volume production technique. Other processing techniques for PEEK are: compression and injection moulding, cold press, machining and micro machining, extrusion and pultrusion, SLS and winding (Kurtz, 2012, p. 38-46). The low setup costs and high required freedom of form are the reasons for considering material extrusion with PEEK. For low complexity parts, the high costs probably cannot be justified.

Prototypes Bond3D had the following prototypes available at the start of this master assignment:

- 5 proof-of-principle test setupsPoPs
- 1 feasibility model (FeMo)
- 3 functional models (FuMos)

Most tests in this report were performed using a PoP prototype. This stands for proof-of-principle and is used to test all kind of new features and settings. They do not have a hot environment and have a polar motion system. The FeMos are the full feature prototypes that are constructed to ensure high repeatability and robustness. The FeMo prototype is a prototype with a combined polar and Cartesian motion system and uses a printhead without an automatic rod replenishing system. The FuMos are the most advanced test-setup that are designed to provide robust test conditions. These systems have a robust Cartesian gantry and a

heated build chamber that can reach a temperature of 250°C. The FuMos will be the most similar to the final 3D printing system.

Accuracy To realise high complexity parts, Bond3D needs to be capable of printing parts that have small features with high accuracy: The right volume of material has to be located at the right location.

Bond3D had produced a set of challenging 3D printable products and had them printed by a service provider using ULTEM 9085 (a brand of PEI) and ASA with a Stratasys Fortus 450mc machine. It should be mentioned that these are amorphous materials, see Figure 1.3. They are likely to have a larger processing, which eases obtaining accuracy.

The Fortus 450mc machine is the main competitor. The printed samples had the following challenging features:

- single wall segments and pins,
- single wall products with sharp corners,
- small objects with infill.

Relevant properties of small features within this study are:

- low thickness,
- high steadiness of line width,
- high straightness,
- high height-to-width ratio.
- low shortness,
- high placement accuracy of the start and stop.

Beyond the scope of this master thesis, more features may be present in products that are involved with accuracy:

- bridges,
- smooth fillets,
- vertical arcs.
- round holes,
- sharp outer corners,
- internal corners,
- surface roughness,
- general appearance.

Accuracy defects Extrusion AM based products may show many possible defects, the most important ones are:

- wrong placement of material due to stringing and oozing during pauses and travels,
- blobs and zits at the start and end of segments,
- unsteadiness of line width,
- displacement of material caused by dragging of the nozzle,
- warped geometry caused by thermal gradients after placement (Out of scope).

Stringing and oozing, blobs and zits and unsteadiness of line width and dragged material are direct effects of discontinuities in the extrusion process and are within the scope of this thesis. In this report they are grouped under the name: 'accuracy defects'. Warped geometry also causes inaccuracy, but is not within the scope of this master assignment and is treated in another work package of Bond3d.

Bond3D was unaware of any root causes of the accuracy problems at the start of this master thesis. Also, new print heads had become available and were installed on the prototypes. The behaviour of the print heads was unknown by that time. The control software was still in development.

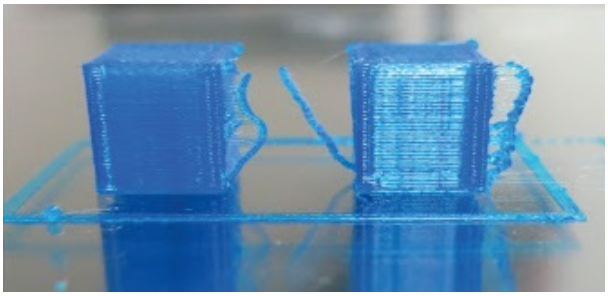

Figure 1.4: The oozing problem, adopted from Landry (2015)

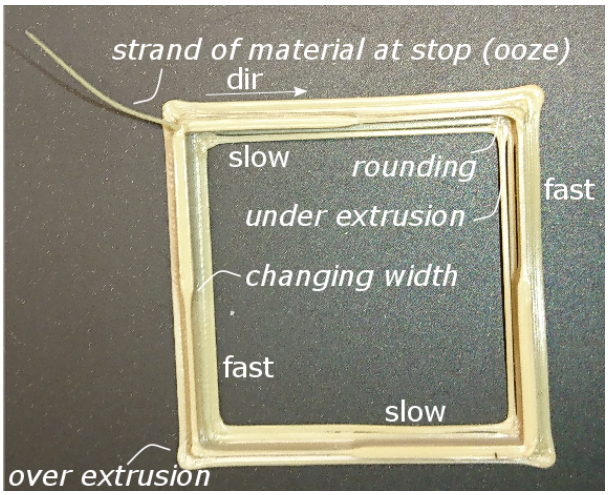

Figure 1.5: Unsteadiness of line width, oozing and rounding for a square of 30 by 30 mm with changing print speed (4 and 20 mm/s)

Motivation for solving the causes for accuracy defects

- The accuracy problems caused by discontinuities are not merely aesthetic but also result in structural problems.
- The aesthetic performance may be of great importance, since the perception of the product quality (such as strength) is also judged by its aesthetics. A surgeon would reject to use an implant if the quality looks poor.
- Accuracy problems may lead to unreliability of the process or even to total failure: Under extrusion in the first layer may lead to poor bed adhesion and the errors from consecutive layers can add up.
- Limited accuracy of small features limits the design space and/or increase the efforts that need to be taken to circumvent these features. Due to the high performance applications, the design space is already narrow and inevitable small features show up in applications such as small tubes in manifolds.

Gibson et al. (2009, p. 155) write: "Every additional weave pattern within a specific layer is going to cause a discontinuity that may result in a weakness within the corresponding part", hence the importance of the reduction of discontinuities by sophisticated path planning and control strategies to both improve the aesthetic and structural performance.

The ultimate goal is to find strategies for 3D printing product features that have little or no dependence on other features. When printing strategies for small features are found, a product composed by these features should be printable.

Competitors Bond3D is not an exclusive company that develops a 3D printing system for PEEK: Several 3D printing systems for PEEK are already available or announced in 2018. An overview was made from aggregated information from trade fairs, inquiries and several web pages and is shown in Figure 1.6. Pricing information should be considered as indicative. The quality of the products that they print varies, but will certainly improve. Some patented technologies from these companies are publicly available. The competitors themselves are not the topic of this thesis, but their information could reveal useful insights and background knowledge. From the

figure, it can be concluded that high-end printers do have a high-temperature building environment. Bond3D claims that for making high-quality PEEK parts with an extrusion printer, accurate and fast responding high-temperature liquefiers are required. Adequate control of the temperature during the solidification phase is needed: the semi-crystalline nature of the polymer contributes to the fact that the strength of the result is heavenly dependent on the thermal conditions during solidification (Grasmeder, 2017b). The costs of the high-end systems are high, since all conditions have to be realised with innovative solutions to make improvements and to work around patents including Swanson et al. (2000). In first instance Bond3D wants to become a service provider rather than a machinery seller since Bond3D expects higher price margin of products compared to machines. (Personal communication, 2018)

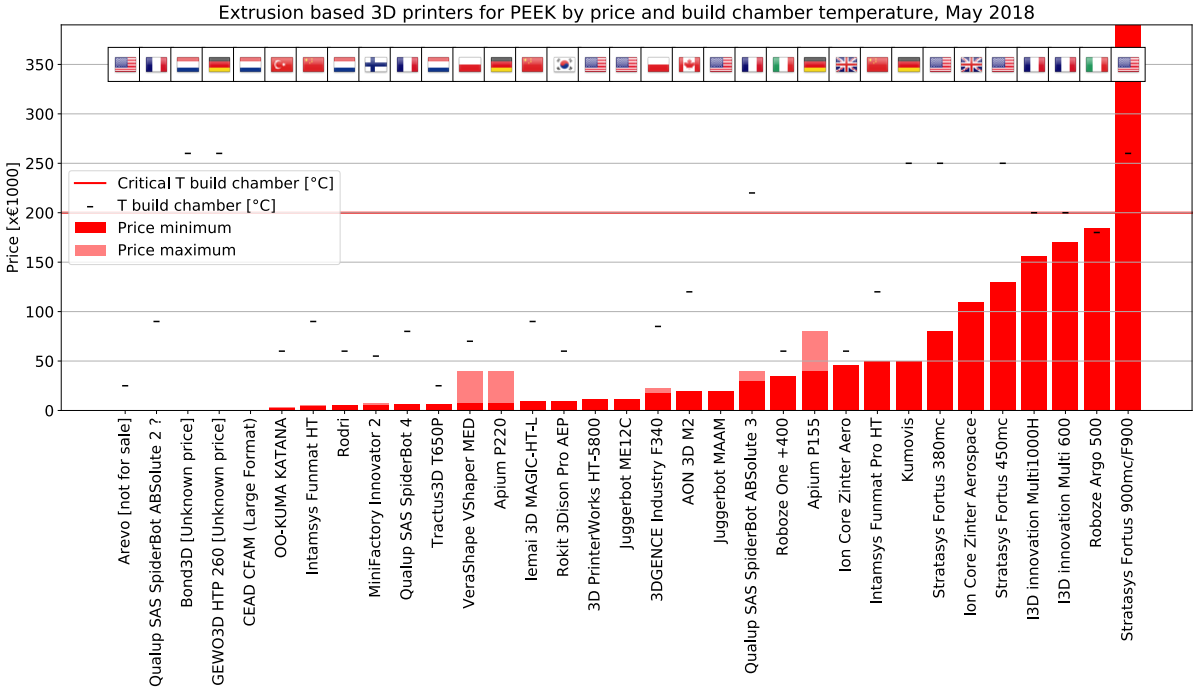

Figure 1.6: Overview extrusion printers for PEEK. The Stratasys printers (not for PEEK) are added for reference.

1.2 Problem statement and goal definition

PEEK is difficult to print due to the high processing temperature, the high viscosity and the small processing window in which everything has to be performed to deliver strong and accurate products.

Advanced hardware features that measure and manipulates noise- and inherent factors are required to provide stable, predictable and repeatable printing conditions. Thorough knowledge of the process is needed to make control logic dealing with the conditions.

- The process enhancement to a specific application relies on empirical studies rather than a fundamental understanding of the process.
- The problem with these empirical studies is that the results are hard to transfer to other machines, materials and geometries.
- Variations in extrusion rate impact dimensional accuracy (Turner & Gold, 2015).
- Some models that address problems related to accuracy and defects are available, but the publications in which they are described often lack demonstration cases and validation.
- The critical behaviour is hard to observe since it takes place in a closed liquefier or on micro-scale.

These problems lead to the following central problem:

Given a high-performance extrusion-based 3D printing system and PEEK 450G as the building material, develop a method to enhance small feature performance.

Four sub-goals were formulated:

1. *Find the relation between process settings and accuracy or available models in literature and explore what is done on this subject. What could be learnt from the available attempts on improvement of printing accuracy?* See: chapter 2.
2. *Find a set of combinations of process settings and empirical determined error compensations that show achievable small feature performance within a limited set of geometries and benchmark the performance.* See: chapter 3.
3. *Extrapolate the results to new sets of geometries and printer settings by exploration of the underlying problem. How could the extrusion process be modelled to find a more sophisticated, generally applicable accuracy enhancement approach?* See: chapter 4.
4. *Solve the underlying problem and find which system properties limit the achievable accuracy.* See: chapter 5.

1.3 Research topics

These are the topics that need investigation to find the state of the art knowledge that could provide answers to these questions:

- architecture of extrusion based 3D printing systems: Components and work flow,
- complications: failures and conditions,
- simple compensation strategies,
- material modelling of PEEK: melt behaviour, crystallinity, rheology, solidification, dynamics,
- behaviour of polymers in liquefiers (rheological modelling and thermal modelling),
- compensation using mechatronics and control engineering.

1.4 Scope and approach

The investigation is a quantitative research study. The goal is to find mathematical models to describe the behaviour of the system and to enhance accuracy by improvement of the control of the systems (numerical) control variables.

Since there is prior (validated) information about the design of the control of liquefiers is limited, the models themselves have to be designed and verified in this study. Since this is an attempt with a new system and a new material, the obtained models in this study should not be regarded as fully optimised models to enhance accuracy.

The emphasis of this study is the development of the method itself for improvement of accuracy, which should be adaptable to new systems with different configurations (other materials, nozzles).

Due to simultaneous (indescribable) development and changes to the systems inmature hardware, control software and g-code preparation software and due to confidentiality agreements, the repeatability of the experiments and their numerical outcomes is compromised: the discovered principles and the method to find numerical values are more important than the actual (system specific) values themselves.

In this research, a wide extent of scientific methods is used to find solutions to this problem. These include literature research, exploration experiments, bench marking, analytic modelling and empirical optimisation experiments.

Initially, the behaviour of the machine and its response to easy compensation tricks that are suggested by 3D printing web communities needed to be analysed. These are settings in slicer distributions such as Cura and Simplify3D. The settings include tricks, such as retracts, wipes, priming, coasting, z-lifts and snapping motions. They can be applied with measures such as distances and velocities and in different orders. They are typically tricks that are included in G-code. The G-code is generated with an in-house developed python script. It can be used to make the G-code and it allows to have accurate control of the actual motion planning of the machine and provides G-code generation for the polar motion system of the PoPs: proof-of-principle prototypes provided with the advanced print head, a simplified polar motion system and a heated build plate. A thermally controlled environment is not included.

Concurrently, a literature study is performed with the goal to find root causes of printing errors, material characteristics, modelling approaches, tuning strategies and working points that can support the understanding of the complex behaviour of the liquefier behaviour in this study.

The first step is to elaborate an overview of the prior art.

The second step is to explore the behaviour of the machine and to find optimal settings using the tricks suggested in literature chapter

The third step is to stress these settings to new situations and to find out how these settings have to be adjusted to provide satisfying results in the general case. An experimental (black box) model construction is needed. The system is modelled by observation of its behaviour.

To better understand the origin of the behaviour, an analytic model will be constituted. This model has to approach the behaviour of the system and will provide guidance for system modifications to improve accuracy.

1.5 Chapter overview

In line with the proposed problem and question breakdown described in this first chapter, the main contents of this thesis are divided into the following chapter structure:

- Chapter 2 describes prior art research publications on the topic of PEEK 3D printing and about the technical challenges. It also reports on earlier modelling approaches of the material extrusion process and compensation approaches in general.
- Chapter 3 explores the variables and conditions. It describes an accuracy enhancement attempt using simple compensation methods such as feeder retracts, wipes and coasting. It demonstrates the capability of the system in an early stage of process improvement, but also discusses the limitations of these approaches.
- In chapter 4 it is described that deviation of the line width was observed that was dependent on extrusion rate and time. The dynamics responsible for this problem are characterised by a step response and a frequency response experiment. A feed forward controller was implemented that compensates for the liquefier dynamics. The controller worked within a small domain of flow rates. The frequency response model shows that further study was necessary to improve the model and adequacy of the controller for a broader domain.
- In chapter 5 analytic expressions are obtained that can further enhance the adequacy of the controller. This included expressions for the pressure drop in the liquefier, the stiffness of the material rod and the thermal expansion. The Boles equation was was proven suitable to predict the steady-state pressure drop accurately for two different nozzles for PEEK.
- Chapter 6 contains the final conclusion, the answer to the central question and recommendations.

Chapter 2

Literature

This chapter describes the prior art research publications on the topic of extrusion based printing with PEEK. The literature study was organised into the following topics:

- An introduction to the general principle, workflow and components that have an influence on accuracy in an extrusion based 3D printer. See: section 2.1
- An introduction to behaviour of polymers in liquefiers and material properties of PEEK. See: section 2.2
- An introduction to compensation approaches and algorithms that are present in slicer software and open source controller software projects. See: section 2.3

This chapter ends with a set of concluding remarks, see section 2.4.

2.1 Introduction to extrusion based 3D printing

"Material Extrusion" is a group of 3D printing processes in which a material is robotically dispensed on prescribed locations. In this master thesis, the scope is set on the deposition of thermoplastics and PEEK in special. 'Extrusion based printing' is used as an alias to this particular process in this master thesis.

The used process is comparable the process protected by Stratasys: FDM™ and to fused filament fabrication (FFF), however the material is not fed in the form of a filament but as rods.

To make a new product, a designer translates an idea into a physical 3D printed product via sequential steps that require making the right design choices. The support for making these depends on the physical capabilities of the 3D printer, the performance requirements of the end product and the process requirements, for example: *Is it possible to print a product that includes a feature with a line width of* 0.6 mm *and a height of* 5 mm *and a length of* 4 mm *with a* 0.6 mm *diameter nozzle with a tensile strength of* 100 MPa *in* 10 minutes*?*

The next paragraph describes the work flow and transitions in a extrusion based 3d printing process, hereafter the components that have a significant influence to accuracy are presented. Section 2.1.3 describes performances and parameters that are used by prior studies in printing with PEEK. The consequences of wrong decisions are summarised in section 2.1.3.

2.1.1 Workflow

Figure 2.1 shows an overview of the workflow. From the first transition it should be noticed that the CAD design is triangulated during the conversion to an standard tesselation language (STL) file. When the polygon count is set too low, the polygons can become visible in the end product. In the second step, the STL file is sliced. The slicer has a large influence on accuracy, since it determines the print paths and the number of discontinuities in the print path. G-code is a representation of the way how the paths should be printed. It does merely prescribe the sequence and synchronicity of motions and their magnitude: For example: *move axis1 to* 200 units *and axis2 to* 10 units *synchronously with a combined feed rate of* 200 units/min. The units for axis1 can be in degrees while those of axis2 are in mm. The actual motion planning is done by the interpreter.

Feedback loops and time dependent information do not exist in G-code. The G-code needs to be interpreted by the real time control system (firmware) running on a programmable logical controller (PLC) or micro-controller. An interpolation algorithm creates linear motions between the coordinate points and a planner smooths out the motion paths. The result is written to buffers that are used by the execution loops that do the actual printing.

After the product has been printed, some post-processing steps may be required, such as the removal of support material and other unnecessary material. For some purposes an annealing process may be needed to increase the degree of crystallisation afterwards.

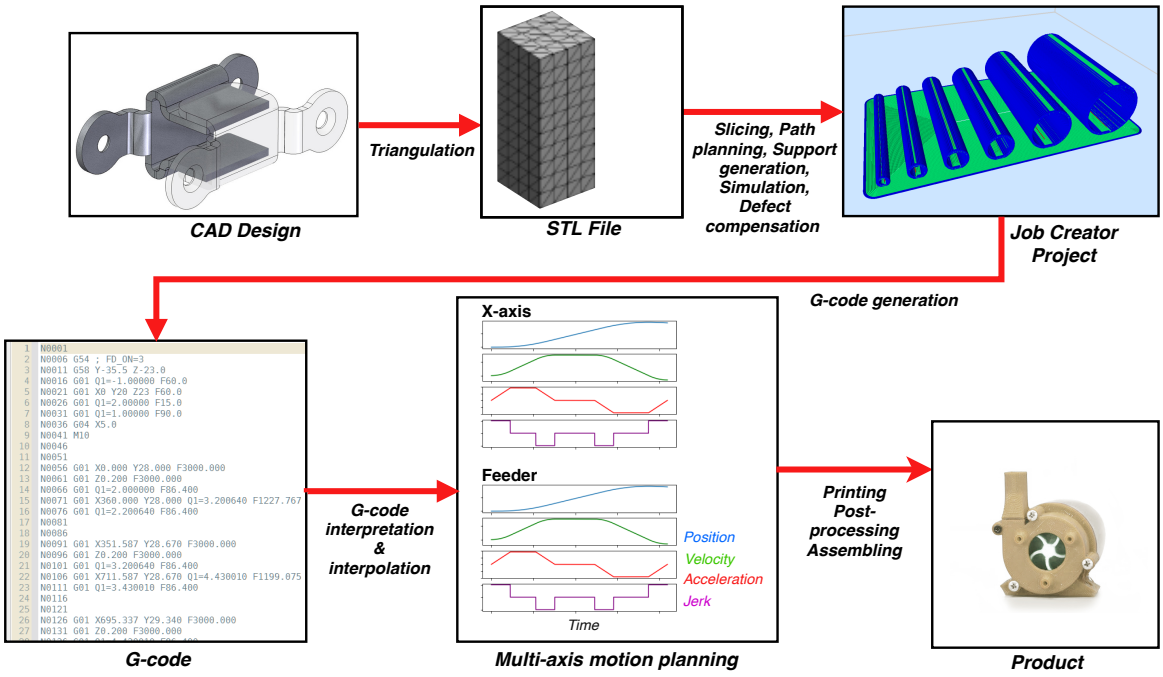

Figure 2.1: Overview of the workflow to transform a CAD design into a physical product

2.1.2 Components that influence accuracy during deposition

Advanced hardware and software have to provide working printing conditions. The next paragraphs describe some of the important hardware components that influence accuracy. Accuracy = aiming for state X and reach state X+dx, in this case applied to the position of the extruded material and the volume of this material. The following components are related to accuracy by some degree, see Figure 2.2:

- Liquefier
- Motion system
- Feeder
- Printer control

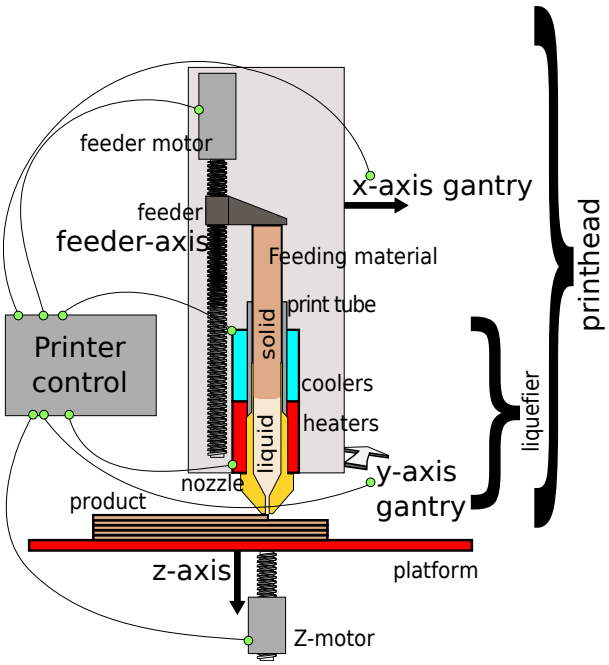

Figure 2.2: Schematic overview of the 3D printer components.

Liquefier The liquefier (part of the print head) consists of a hot end and a cold end that are separated by a thermal insulator, the heat break. The nozzle is part of the hot-end. The liquefier has to reduce the viscosity of the material by increasing the temperature above the melt temperature. This is needed in order to force the molten material to the narrow channel of the nozzle. The rate of degradation increases for temperatures above 370°C. Bond3D found that the bulk temperature of the material should be about 390°C. The geometry of the liquefier plays an important role in pressure management and thermal control, see section 2.2. Gibson et al. (2009, p. 145) write that the larger the chamber, the more difficult it can become to maintain the material at a constant and uniform temperature. The heat conductivity of the various parts is important: the nozzle needs to be of a highly conductive material in order to supply the material with heat from the heaters and copper should not be used according the processing guide for PEEK, since it can cause degradation (cross-linking and burning) of the material at the high processing temperatures (Victrex®, 2018, p. 5). The presence of copper was reported to increase the degradation rate a factor of 4-5 times (Prime, General, Division, California, & Seferis, 1986).

The print tube should be of a low conductive material to prevent back flow (Gilmer et al., 2017). The nozzle should be kept clean during printing since sticking material has a significant impact on accuracy.

Motion system Belt drives or lead screws are used to drive the print head in the horizontal plane. The latter are often used in higher cost systems. (Gibson et al., 2009, p.150).

Large, high precision, high force, pre-assembled industrial spindle axes for accurate positioning were integrated in the Bond3D machine. They were selected to ensure that they can deal with the velocity, accelerations and declarations of the print head module, making accuracy errors caused by them very unlikely. The heavy duty motion systems enables the use of multiple heavy print heads.

In general, various configurations are possible regarding the motion system such as: Delta configurations, SCARA or Cartesian gantries (Pierrot, Reynaud, & Fournier, 1990). Polar systems are another option.

Bond3D uses three different configurations:

- The FuMo has a Cartesian gantry, The build platform moves in the vertical dimension.
- The PoP has a polar motion system. It has a rotating bed, mounted to a linear axis. The print head moves along a vertical axis.
- The FeMo is a hybrid between the two: It has a Cartesian gantry with a build plate that can be rotated.

The PoP system was dominantly used in this study. The big advantage of using a rotating print bed is that it allows high speed continuous motion and high accelerations and decelerations without requiring much hardware. The downside is that it limits part design and that it requires specific G-code. The geometries that can be created with the PoP are limited.

Feeder The material in the liquefier is fed from a material stock by a feeder. This material stock could contain pellets, powder, liquids, granules or a roll of continuous filaments. Liquid material could be pumped, screw extruded, pressed by a plunger or pressed by compressed gas. (Gibson et al., 2009, p.145)

Regarding feeder mechanisms for filaments there are various options: most popular in consumer 3D printers are Bowden extruders. In a Bowden extruder the feeder mechanism is placed as a static element mounted to the body of the printer. The feeding material is pushed through a long flexible tube towards the moving liquefier. This makes the moving assembly lightweight and therefore significantly reduces the costs and complexity of the motion system. The main disadvantage is the lag and unwanted flexible behaviour in the feeding process.

An alternative is a direct drive mechanism, where the feeder mechanism is placed close to the liquefier of the printer. This mechanism is also applicable for feeding rods. The moving assembly is havier compared to Bowden type feeders, but direct drive feeders don't suffer from the inaccuracy caused by the compressibility of the filament and the flexibility of the guiding tube. Therefore they generally need less retraction or other compensation methods such as those described in section 2.3. They have the opportunity to provide higher accuracy than Bowden extruders.

In this project the material is fed in solid form by a feeder that advances the material using a kind of plunger that applies pressure. In regular filament based 3D printers this feeder has knurled or hubbed wheels that grip into the material. The feeder mechanism in the Bond3D system could be considered as a special form of a direct drive mechanism, See: Figure 2.2

Go and Hart (2017) reported that the advancing mechanism can be the critical component when high throughput rates have to be achieved. Slipping of the wheels, grinding and buckling of the filament should be prevented. A solution is to not use this kind of feeder mechanism at all and apply alternatives such as feed rods (Crockett et al., 1995), threaded filaments (Go & Hart, 2017) or a screw extruder with granular material (Tseng et al., 2018).

In commercial 3D printing systems, a force of 40 N to 60 N is applied on the filament surface. For ABS P430 filament with a diameter of 1.25 mm in a Stratasys™ Mojo™ system, the maximum sustainable extrusion pressure is in the order of 23.9 MPa (Go, Schiffres, Stevens, & Hart, 2017).

Printer control The printer controller is the hardware and software combination that plans and executes the motions and other behaviour of the machine and reads sensor information. Figure 2.1 shows an overview of the work flow to transform a CAD design into a physical product. The printer used in this project uses a software PLC, that allows easy customisation and modular design on a regular workstation computer using the structured text programming language. The system reads the inputs, then calculates new controls and then writes the controls to the buffers of the actuators. All the code is executed within a fixed sample time independent of length of the program. The controller reads the inputs from a G-code file using a function block called the G-code interpreter and calculates continuous motion profiles. G-code is also used in regular CNC-milling applications and is a programming language that describes the location of motion segments and corresponding set points and feed rates. When these segments are programmed within the same line, the controller knows that there is a desire for synchronous execution. The motion profile would then be adapted to the slowest axis. It is also possible to use special commands in G-code such as setting acceleration limits and commands to let the controller know that it has finished the job.

The path planner routine uses an algorithm that 'glues' motion blocks into continuous motions. This algorithm may cause slight rounding in corners that impact accuracy. Further discussion is left out of scope for this master thesis, however it is demonstrated in Figure 1.5.

2.1.3 State of the art of extrusion based printing with PEEK

Figure 1.6 showed an overview of companies that have presented 3D printing systems that are capable of printing with PEEK. A composition of components does not make an accurate 3D system, process control and tuning are essential.

Process tuning is required to achieve high performance print results. The behaviour of polymers in the liquefier is presented from a modelling point of view in section 2.2, while the reality is more complex. This section presents an overview of publications about the experimental findings in extrusion based printing with PEEK. The first publication that mentions extrusion based printing with PEEK was performed by Crockett et al. (1995). Valentan et al. (2013) was the first to spend a research dedicated to extrusion based printing with PEEK.

Black box approaches (empirical studies) on PEEK extrusion printing are reported by: W. Z. Wu et al. (2014), Yang et al. (2017), Zhao, Li, and Jin (2018), Deng, Zeng, Peng, Yan, and Ke (2018), W. Wu et al. (2015), Rahman,

Letcher, and Reese (2015), Davies, Shyng, Wang, and Ghita (2015), Vaezi and Yang (2015), Berretta, Davies, Shyng, Wang, and Ghita (2017), Yang et al. (2017), Kang et al. (2018), Zhao et al. (2018) and Deng et al. (2018).

It was chosen to not report on the details of these studies in the this master thesis. Different setups and parameter sets were used that make it hard to compare results. The actual values reported in the studies are not exactly relevant for this study for the same reason.

The topics are summarised for exploratory purposes:

- Setups
- Goals
- Performances
- Methods
- Parameters
- Failures
- Causality of failure
- Recommendations
- Conclusions

Setups The systems that are used by the researchers are often modified desktop printers or custom built machines. Crockett et al. (1995) used a rod based system. Valentan et al. (2013) and Berretta et al. (2017) used Cartesian printers with filament. Rahman et al. (2015) used a printhead mounted to a robot arm. W. Z. Wu et al. (2014) Kang et al. (2018), Zhao et al. (2018) used unspecified custom printers.

Motivations Valentan et al. (2013) wrote that they want to produce medical prostheses, facial prostheses more specifically. Kang et al. (2018) were motivated by the opportunity to solve respiratory failures caused by the rigidity of metal implants by making more flexible 3D printed ribs from PEEK. Vaezi and Yang (2015) want to print porous orthopaedics.

Performances The majority of studies focus on the tensile strength, but some others were described.

- Strength (parallel)
- Strength (perpendicular), filament-to-filament bonding
- Strength (Z-direction), layer adhesion
- Strength (flexural)
- Strength (compressive)
- Isotropy (% ordered state after printing)
- Youngs modulus
- Strain %, brittleness
- Surface quality
- Repeatability and consistency
- Crystallinity %

Most studies measured the strength by pulling printed tensile dumbbells, but the final geometry was not described to meet a certain standard (number of contour layers, if they were milled afterwards, etc. This makes it hard to make a fair comparison of the performances.

The Z-strength was not reported by any of the studies, possibly because no good results had been achieved yet. The strongest reported pull rod was published by the Solvay AM cup in 2018, this sample had a Z-strength of 80 MPa. (Solvay, 2018). Bond3D has achieved better results with another PEEK variant and probably with other test conditions.

Some researches Davies et al. (2015) and Berretta et al. (2017) reported slightly more about the crystal morphology but could not make a fair comparison with measured strength. Testing methods described in the studies are:

- Testing tensile dumbbells
- Testing of flexural strength of end products
- Testing of single wall samples
- DSC tracing
- SEM and Micro-CT imagery

Generally, the studies conclude that with 3D printing of PEEK, high crystallinity can be achieved, resulting in a high tensile strength (in longitudinal direction) but with low strain and brittleness. Z-strength and layer adhesion performances are remarked but the performances are not reported.

Parameters The number of parameters is large and so is the degree of coupling between them. The variation of the build plate temperature in a cold build room has a very different effect on tensile strength of relative low products than the variation of the build plate temperature in a hot oven, when looking at the results of Deng et al. (2018) and Kang et al. (2018) for example. This is an overview of the parameters:

- Material variant
- Heat treatment
- Rod diameter
- Part orientation
- Raster angle
- Filling ratio
- Build plate temperature
- Building chamber temperature
- Nozzle temperature
- Layer thickness
- Volume flow rate (print speed)
- Cooling rate (after deposition)
- Surface tension during printing
- Exposure to extra thermal radiation
- Additives (carbon nano tubes (CNTs))
- Surface tension

Failures Obtaining the high performances required for the proposed goals, is being limited by failures that limit the processing window. All these failures could be linked to the accuracy problem:

- Degradation, burning (Vaezi & Yang, 2015), (Yang et al., 2017) crosslinking (W. Z. Wu et al., 2014) and chain scission (Yang et al., 2017)
- Entrapment of moisture and bubbles and voids, (W. Wu et al., 2015), (Yang et al., 2017), (Zhao et al., 2018), (Berretta et al., 2017), (Vaezi & Yang, 2015)
- Thermal distortion, deformation and poor shape retainment (W. Wu et al., 2015), (Yang et al., 2017), (Zhao et al., 2018), (Vaezi & Yang, 2015),
- Weak inter-layer bonding and delamination and poor polymer diffusion (reptation) among layers. (Rahman et al., 2015), (W. Wu et al., 2015), (Yang et al., 2017)
- Uncontrolled or uneven crystallisation (W. Wu et al., 2015), (Berretta et al., 2017), (Vaezi & Yang, 2015)
- Poor adhesion to print bed (Vaezi & Yang, 2015)
- Nozzle clogging (Vaezi & Yang, 2015)

The design or process condition choices that optimise for one of these aspects, compromises with accuracy: High temperatures reduce the viscosity, hence less force is required to press the material. Less force means less compression and less compression means less oozing, but increases the chance of nozzle clogging due to the adhesion of burnt polymer. Bubbles cause distortions in the extrusion process. This can be prevented by using dried feeding material and purging in advance of the process. However, the printer extrudes material in predetermined places, shrinkage reduces the accuracy after cooling. Weak inter-layer bonding and crystallisation issues can be improved by subjecting the printed object to higher environment temperatures, but sagging of the building or support material may be the consequence.

To reduce the chance of clogging, the Bond3D printer system has print tube with a large diameter that prevents bending and buckling of the material. This reduces the chance on clogging, but increases the thermal resistance. The heat simply has to pass a longer distance. The effects are further discussed in section 2.2.

Causality of failure The system relations are hard to comprehend by describing them as stand-alone factors. Figure 2.3 presents an attempt to capture the causality of failure in an overview. In this master assignment, accuracy problems are the central topic.

It should be noticed that there are some contradictions in determining ideal process conditions. The causes for defects are better explained in section 2.2.

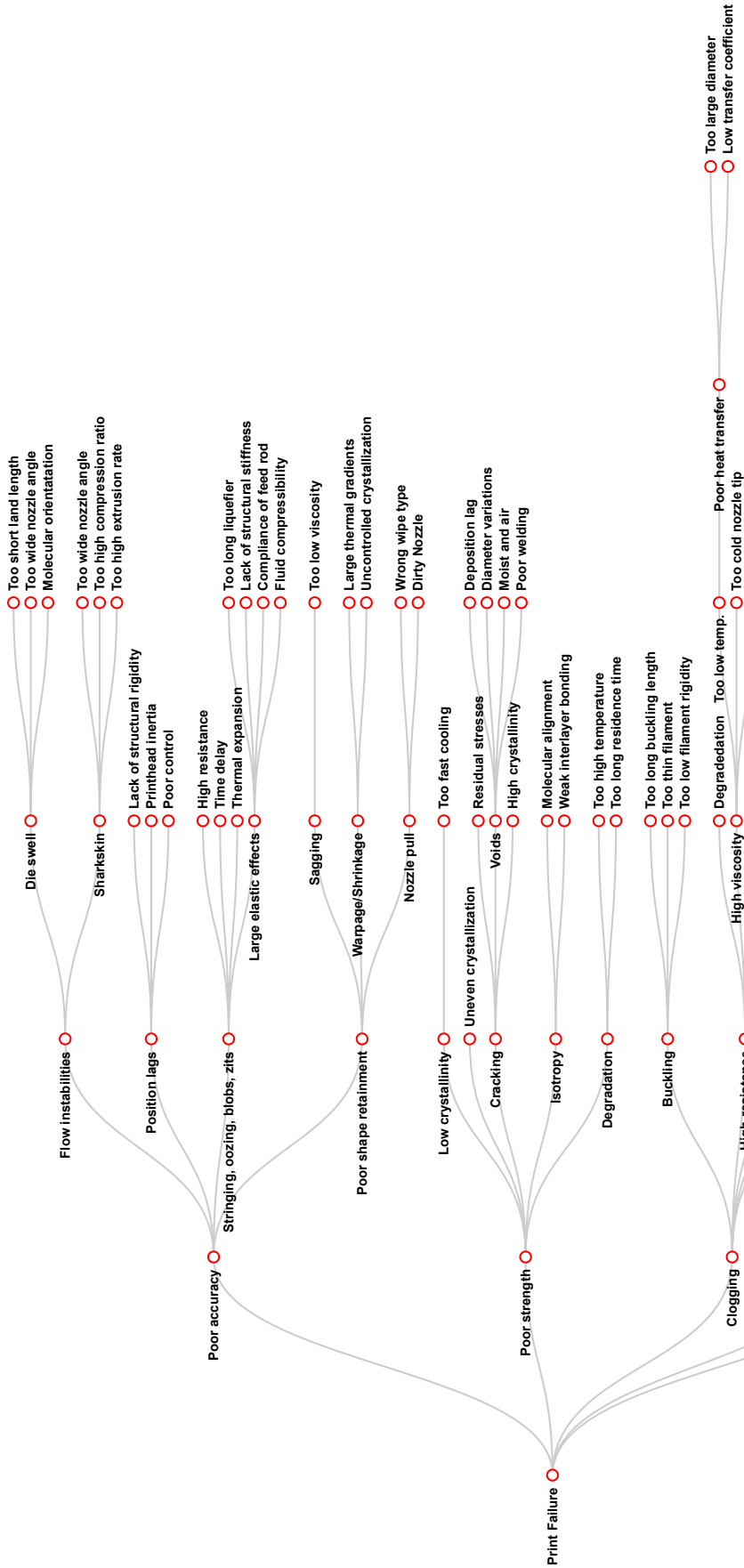

Figure 2.3: Fish bone diagram of printing failures in extrusion based printing

Recommendations The following topics are a selection of recommendations from the papers:

- Application of machine tricks
- Control of G-code generation
- Usage of parameter monitoring equipment
- Consideration of modelling anisotropy in FEM models
- Robust process control
- Active control of humidity and temperature in an enclosed environment

Conclusions The discussion of the literature helped to get insight about the problem, however specific to the central topic of this study, not much work has been written. Unambiguous conclusions are hard to draw from these research publications. The studies are presented as exploratory studies but optimisation methods where applied to study the subject, such as design of experimentss (DOEs).

The number of parameters is too large and optimisation is limited to local optima in the conducted experiments. They apply to the specific test configurations and are hard to transfer to other setups. Using DOE, a small number of factors can be varied on few levels. Performance measurements are performed after printing (strength, strain). Few scientists report on the (monitored) conditions during printing. Few other characteristics are studied that could influence performance, including crystal morphology and crystallinity (SEM imagery and DSC tracing). The setups that are used highly differ from the setup used in this project.

Accuracy is an uncovered topic in the studies, however they are useful for exploration of the problem and side effects.

2.2 Behaviour of polymers in liquefiers

In subsection 2.1.2, the liquefier and feeder were described as the components that are of particular interest when trying to solve accuracy related issues. The following topics were selected to make a basic model of the behaviour of the material inside the nozzle:

- Pressure drop in the nozzle, see: subsection 2.2.1 and viscosity models, see: subsection 2.2.2,
- Liquefier dynamics, see: subsection 2.2.3,
- Thermal behaviour, see: subsection 2.2.4
- Die swell, see: subsection 2.2.5

More factors influence the accuracy, such as material variants, variance of the properties and influence from the environment. They are left out in this list, since the control of these factors is not part of the design and the processing of the liquefier.

2.2.1 Pressure drop

The pressure drop dependency is the relationship between how much pressure has to be applied to generate a certain flow rate. This relation is needed for chapter 5. Various researchers tried to model the behaviour of material within liquefiers for filaments. The behaviour is expected to be similar for feeding rods since the thin channel in the nozzle tip is similar, which is a dominant factor in the pressure drop calculation.

The first topic is that of the calculation of the pressure drop in the liquefier. The pressure drop causes the compression (and storage of potential energy) of the feeding material, which is one of the reasons for oozing, explained in section 2.3. An adequate model for this pressure drop is key for compensation.

The model that will be obtained in this project will consist of the following components:

- Pressure drop relation, (this section)
- Viscosity model, see subsection 2.2.2
- Parameters for the viscosity model of PEEK, see: section 2.2.2
- Parameters of the liquefier geometry, see: Table 5.3

The material variables (power law coefficients) are described in the m and ϕ form, see subsection 2.2.2. This section provides an overview the models. In subsection 5.2.3 the Boles model and Bellini's model are compared with the measured pressure drop for two different liqufiers.

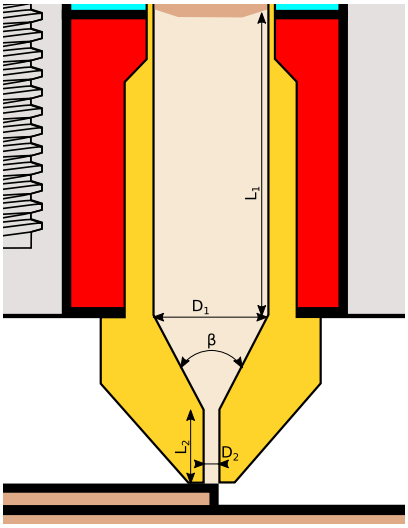

Figure 2.4: Close-up of the nozzle and dimension labels used in equations 2.2-2.5

The Hagen-Poiseulle model for Newtonian fluids

The biggest pressure drop occurs in the narrow channel of the nozzle. The pressure drop of a basic fluid in a narrow channel (see: Figure 2.4) can be modelled using the Hagen-Poiseuille equation (Richardson, 2018). Comb, Priedeman, and Turley (1994) mentions the usability of this model in the context of extrusion based printing.

$$\Delta P = \frac{8\mu \cdot L \cdot Q}{\pi R^4} = \frac{8\mu \cdot L_2 \cdot Q}{\pi(\frac{1}{2}D_2)^4} \tag{2.1}$$

This equation is derived from the Navier-Stokes equation, by making the following assumptions about the flow conditions: The flow is axial symmetric, steady, fully developed, laminar and incompressible. Inertial and gravity effects are negligible.

In the case that the material is isothermal, and behaves as a Newtonian fluid, the viscosity μ in Equation 2.1 is a constant, and the pressure drop could be considered as being linear dependent on the volumetric flow rate Q, when this model is applied.

Bellini's pressure drop model for a power law fluid in a liquefier

Polymers are long chained-molecules, hence their behaviour is more complicated. The pressure drop is by no means linear proportional with the feed rate:

Due to the molecular long-chained structure, a polymer in shearing conditions works like a lubricant that eases the flow. This reduces the viscosity of the fluid for higher shear rates.

This effect is called shear thinning and is most present in the narrow section of the nozzle due to the high shear rate in this section.

The viscosity of a a shear thinning polymer is dependent on at least two conditions: the shear rate and the temperature. The shear thinning behaviour can be modelled using a power law model See: Equation 2.12 on page 29

Yardimci, Hattori, Guceri, and Danforth (1997) and Bellini (2002, p. 150) used formulas for shear thinning fluids derived from die conductance formulas for cone and pipe sections for shear thinning materials from Michaeli (1992). They are described in the newer edition on p.69 in Hopmann, Christian and Michaeli (2016). The formulas that where obtained consider three situations that are summed together in a total pressure drop Equation 2.2:

- the thick channel of the nozzle Equation 2.3,
- the converging section of the cone: Equation 2.4,
- the thin channel: Equation 2.5.

The formulas take v as the input velocity of the filament (instead of a volumetric flow rate) at the entrance of the liquefier. In these equations, the inlet and outlet pressures are disregarded (Hopmann, Christian and Michaeli, 2016, p.65).

$$\Delta P_{total} = \Delta P_{1\_v} + \Delta P_{2\_v} + \Delta P_{3\_v} \tag{2.2}$$

$$\Delta P_{1\_v} = 2L_1 \left(\frac{v}{\phi}\right)^{1/m} \left(\frac{m+3}{(D_1/2)^{m+1}}\right)^{1/m} \tag{2.3}$$

$$\Delta P_{2\_v} = \left(\frac{2 \cdot m}{3 \cdot \tan(\beta/2)}\right) \left(\frac{1}{D_2^{3/m}} - \frac{1}{D_1^{3/m}}\right) \left(\left(\frac{D_1}{2}\right)^2 (m+3) \cdot 2^{m+3}\right)^{1/m} \tag{2.4}$$

$$\Delta P_{3\_v} = 2L_2 \left(\frac{v}{\phi}\right)^{1/m} \left(\frac{(m+3)(D_1/2)}{(D_2/2)^{m+3}}\right)^{1/m} \tag{2.5}$$

Where:

Table 2.1: Geometry constants. See: Figure 2.4. For Bond3D values, see Table 5.3

Bellini	Boles	Unit	Description
D_1	D	m	Inner diameter of liquefier melt room
D_2	d	m	Diameter of nozzle channel
L_1	$-$	m	Length of the melt room
L_2	l	m	Length of the nozzle channel
β	2α	rad	Angle of the nozzle

Table 2.2: Material constants. For PEEK values, see: section 2.2.4 and Figure 5.8

Bellini	Boles	Unit	Description
m	$\frac{1}{n}$	$[-]$	Power law flow exponent
ϕ	$\frac{1}{K}^{1/n}$	$\frac{1}{Pa \cdot s}$	Power law fluidity
$1/m$	n	$[-]$	Power law flow behavior index
$1/\phi^n$	K	$Pa \cdot s^n$	Power law flow consistency index
F	F	$[-]$	Thermal expansion factor

Table 2.3: Variables, see: Figure 5.10

Bellini	Boles	Unit	Description
P_{total}	P_{total}	Pa	The total pressure drop over the liquefier
v	$\frac{4Q}{F \cdot \pi D_1^2}$	m/s	Feed rate
$\frac{v \cdot F \cdot \pi D_1^2}{4}$	Q	m^3/s	Volumetric flow rate at the exit

The factor F is needed since the feeder pulls low temperature material and the flow rate in the tip of the nozzle has a high temperature, see:

Bellini's model includes an unexpected extra parameter L_1: The material is not molten in the full length of the print tube. The flow in this section is slow. Some tests of the influence of this parameter led to the conclusion that the difference in pressure drop is less than 5% for reasonable lengths between one and 30 mm. A dummy value in this range can be substituted for that reason.

section 2.2.4.

The pressure dependencies used by Bellini (2002), and Venkataraman et al. (2000) are criticised by Turner and Gold (2015) and Osswald, Puentes, and Kattinger (2018). Turner and Gold (2015) write that the pressure drop model does not consider a yield stress and requires validation and Osswald et al. (2018) states that the model is only suitable for low extrusion rates.

The Boles pressure drop model for a power law fluid in a liquefier

Mackay, Swain, Banbury, Phan, and Edwards (2017) applied rheology to find power law parameters for ABS and calculated the pressure drop using the Boles equation, that was described by Kwon, Shen, and Wang (1986). In a simplified form and for the condition that the nozzle diameter d is much smaller than the entrance diameter D, the Boles equation is:

$$\Delta P_{total} = \left(K \left[\frac{3n+1}{4n} \frac{32Q}{\pi d^3} \right]^n \right) \times \left[\frac{1.18}{n^{0.7}} + \frac{4l}{d} + f(\alpha) \right] \tag{2.6}$$

where:

$$f(\alpha) = \frac{2}{3n\sin(\alpha)} \left[\frac{3\sin(\alpha)}{4n[1-\cos(\alpha)]^2[1+2\cos(\alpha)]} \right]^n | d \ll D \tag{2.7}$$

For an explanation of the terms, see: table 2.1-2.3. Optionally the Arrhenius, or Cross model could be included to describe the temperature dependency.

Mackay et al. (2017) did not compare the calculated pressure drops with experimentally found pressure drop but observed buckling failure. Therefore they could not assess the accuracy of their implementation of the Boles equation. It also does not incorporate changes in the thermal situations at a range of flow rates. This may be the reason for unsatisfactory agreement between experimental and calculated data for high flow rates.

Bellini's model and Boles model differ for the main reason that Bellini's model is solely based on shear stress, while the Boles model incorporates an empirically determined factor to incorporate elongation stress.

Osswald's melting with pressure removal pressure drop model

Osswald et al. (2018) considers the problem at higher flow rates as a 'Melting with pressure removal' problem. This states that at high flow rates, the rate of melting controls the printing speed and that the heat transfer should be modelled as a melting film. Go and Hart (2017) and Go et al. (2017) also state that the rate of heat transport to the core of the material limits the extrusion rate.

Numerical pressure drop models

Additional to analytic models, some numerical approaches for pressure drop calculations are published: examples are: Bellini (2002, p.59), Ramanath, Chua, Leong, and Shah (2008), Nikzad, Masood, Sbarski, and Groth (2009), Jerez-Mesa, Travieso-Rodriguez, Corbella, Busqué, and Gomez-Gras (2016) and Go and Hart (2017). The quality of these approaches, due to the scarce validation and documentation is hard to assess, although they provide a good demonstration of the occurrence of thermal gradients in the liquefier. The temperature at the walls may be much higher than the temperature in the core.

2.2.2 Viscosity models for polymers

To calculate the pressure drop over the liquefier in subsection 5.2.3, a viscosity model is required.

Viscosity can be described with rheological models. The most basic model is that for a Newtonian fluid, that characterises viscosity with a single value, μ, in literature also described with η, see Equation 2.9. This viscosity can be applied in Equation 2.1. Water is an example of a fluid that can be modelled with a Newtonian fluid model.

Letting a material flow through a channel let the material shear. The material closer to the wall has a lower velocity compared to the material in the centre of the channel. The shear rate is highest in the thin channel of the nozzle.

Shear is best explainable by considering a fluid between two parallel plates, see: Figure 2.5. Under the assumption of the absence of stick-slipping, the velocity of the material at the stationary wall is 0 mm/s and the material at the moving wall has the velocity of that moving wall. The shear rate of this situation can be described by Equation 2.8.

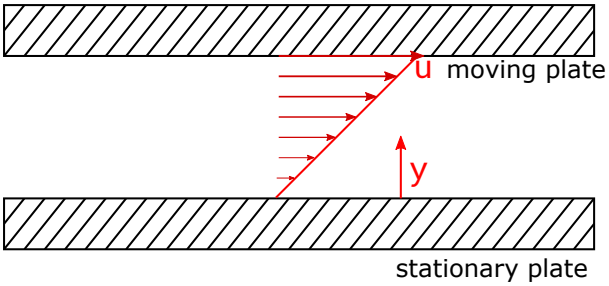

Figure 2.5: Shear between parallel plates

$$\dot{\gamma} = \frac{\mathrm{d}u}{\mathrm{d}y} \tag{2.8}$$

Deforming the fluid will incur a shear stress. The two are related by the viscosity term μ:

$$\tau = \mu \cdot \dot{\gamma} \tag{2.9}$$

The shear stress can be used to calculate the shear force, by multiplication with the contact area:

$$F_{shear} = \tau \cdot A_{contact} \tag{2.10}$$

This shear force has an equal magnitude as the force needed to move the plate, but the opposite direction.

Shear incurs also in a cylindrical tube. When assuming non-stick slipping behavior, the material at the wall has a velocity of zero, while the material in the center has a high velocity.

Introduction of generalised Newtonian fluid models

Polymer molecules are long chains. These chains make the behaviour more complex. A single viscosity term cannot describe the behaviour accurately. The molecules close to the wall experience friction from the wall and move slower than the molecules in the centre of the channel. The effect is that they line-up along the wall and work as a lubricant for the other molecules. As a result, the viscosity is lower than expected for higher flow rates. This effect is known as shear thinning.

For a polymer, the viscosity is dependent on the shear rate itself:

$$\tau = \mu(\dot{\gamma}) \cdot \dot{\gamma} \tag{2.11}$$

The models that are able to deal with shear thinning (and thickening) are called Generalised Newtonian Fluid models. Two examples of these models are: the power-law model of Ostwald and de Waele, see Equation 2.12 or Equation 2.13, and the Cross viscosity model, see: Equation 2.15.

The parameters in these models need to be experimentally determined or extracted from a database. The characterization of the models can be done using rheometers, such as dynamic testing, melt flow indexers etc. The more parameters a model has, the more tests need to be executed and the more difficult the model is to apply.

The viscous behaviour is temperature dependent. The time-temperature superposition principle enables translation of the model parameters at a reference temperature to parameters at other temperatures. This temperature dependency $a_T(T)$ can be described by the Williams-Landel-Ferry (WLF): Equation 2.17 or Arrhenius model: Equation 2.20. The viscosity decreases for higher temperatures due to the increased mobility of the polymer chains.

Power law model Shear rate is defined as the velocity gradient, the ratio between the difference in velocity between two layers, divided by the difference in distance between the two layers:

This equation occurs in two forms in literature. In k an n form (Bellini, 2002, p. 54) this equation becomes:

$$\mu(\dot{\gamma}) = k \cdot \dot{\gamma}^{n-1} \cdot a_T(T) \tag{2.12}$$

The power law also appears in m an ϕ form. (Bellini, 2002, p. 150):

$$\tau = (\frac{\dot{\gamma}}{\phi})^{\frac{1}{m}} \tag{2.13}$$

The power law is simple, but does not account for low shear rates, since the viscosity would become infinity, hence the Newtonian region cannot be estimated with the power law. They are valid for a narrow band of shear rates.

Steffe (1996, p. 102) writes that the wall shear rate for a polymer in a cylindrical channel can be de calculated from the volumetric flow rate using Equation 2.14:

$$\dot{\gamma}_w = \frac{3n+1}{4n} \cdot \frac{4Q}{\pi \cdot R^3} \tag{2.14}$$

Cross model The Cross model, for PEEK shown in Figure 2.6 is a common model in engineering that covers a broader range of shear rates, but needs more parameters and is more difficult to apply.

The Cross viscosity model is given in Equation 2.15:

$$\mu(\dot{\gamma}) = \frac{\mu_0}{1 + (\frac{\mu_0 \cdot \dot{\gamma}}{\tau^*})^{1-n}} \tag{2.15}$$

$$\mu_0 = D_1 \cdot a_T(T) \tag{2.16}$$

WLF temperature dependency:

$$a_T(T) = e^{\frac{-C_1(T-T_s)}{C_2+(T-T_s)}} \tag{2.17}$$

In the database that is used in this project, the coefficients are described with the following experimentally determined parameters:

$$C_2 = A_3 + D_3 p \tag{2.18}$$

$$T_s = D_2 + D_3 p \tag{2.19}$$

Arrhenius temperature dependency: Another way to describe the temperature dependency involves the Arrhenius equation:

$$a_T(T) = e^{\frac{\log k_0}{\log k_1} = (\frac{E_a}{R}) \cdot (\frac{1}{T} - \frac{1}{T_0})} \tag{2.20}$$

Power law viscosity model for PEEK Parameters of a power law viscosity model for PEEK were not found in literature. In Figure 5.8 on page 83 they are obtained through fitting to the Cross model.

Cross-WLF viscosity for PEEK The cross viscosity for PEEK is given in Figure 5.6. The values are given in Table 2.4. Note that the data does not include a pressure dependency, hence $D_3 p = 0$.

variable	C_1	A_3	D_1	D_2	D_3	n	τ^*	$lowerTemp$	$upperTemp$
unit	[-]	K	Pa*s	K	K/Pa	[-]	Pa	K	K
PEEK	36.041	51.6	2.89808e16	403.15	0	0.4266	124139	643	723
ABS	28.8	51.6	2.214900e12	378.15	0	0.2353	72350	463	513

Table 2.4: Cross-WLF viscosity parameters for PEEK and ABS, data derived from Solidworks 2018.

Figure 5.6 shows that the viscosity reduces for higher shear rates. The so called power law model region, is the linear region in Figure 5.6. Mackay et al. (2017) reports that for ABS, the power law region starts at a shear rate of $80\,s^{-1}$, while it can be observed form that for PEEK, this region starts at about $600\,s^{-1}$.

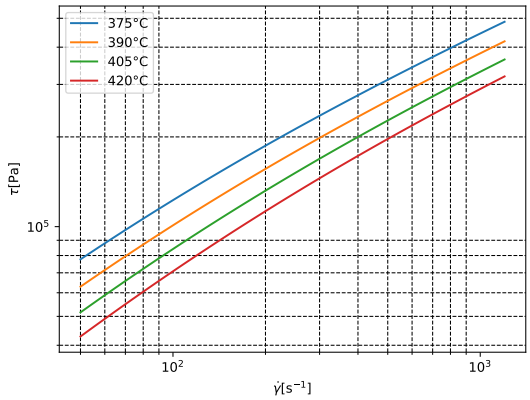

Figure 2.6: Shear stress as a function of shear rate according the Cross-WLF viscosity model of PEEK 450G, data obtained from Solidworks 2018. The model is valid for shear rates under $5 \cdot 10^4 \mathrm{s}^-1$

2.2.3 Liquefier dynamics

In basic extrusion based printing systems, the extruder axis moves linearly proportional to the X,Y and Z axis. When the extrusion head accelerates, the feeder axis accelerates proportionally. This synchronicity is programmed in the G-code.

This assumes an infinitive stiffness between the source of the force and the nozzle tip and absence of thermodynamics.

In a liquefier system both are present. Their combined effect is that the extrusion of the material lags a bit behind the XY motion, depositing the material at a slight offset from the target position.

This magnitude of this lag is not a simple offset constant, but is dependent on time, hence feeder dynamics.

Bellini noticed that the fluid outflow is not directly proportional to the feed rate of the material at the entrance (Bellini, 2002), also see: Bellini (2004). Go and Hart (2017) call feeder dynamics "deviations from ideally straight paths and sharp corners and temporal change in proportion between XY and extruder motion."

Bellini found that the material needs time to ramp up the flow and even has a small lack in time. She proposed to model the system using an electric analogy: a simple RC low pass filter with a small time lag. She obtained the following transfer function:

$$G(s) = \frac{Q_{out}}{Q_{in}} = \frac{\mu}{T \cdot s + 1} \cdot e^{-\tau s} = \frac{0.8865}{0.45s + 1} e^{-0.04s} \tag{2.21}$$

In this equation is μ the gain, T_s the time constant and τ the time lag. Bellini concluded that the steady-state error (12% under extrusion), see Figure 2.7 was caused by slippage of the filament rollers at sudden changes. The steady-state error was not corrected since this would need a simple proportional factor. The time delay in the model is small and does not have a significant influence. The typical time needed to ramp up the extrusion from 1.5 mm^3/s to 4 mm^3/s is about 1.5 s. The idea of this modelling approach is useful and constitutes the basis for chapter 4.

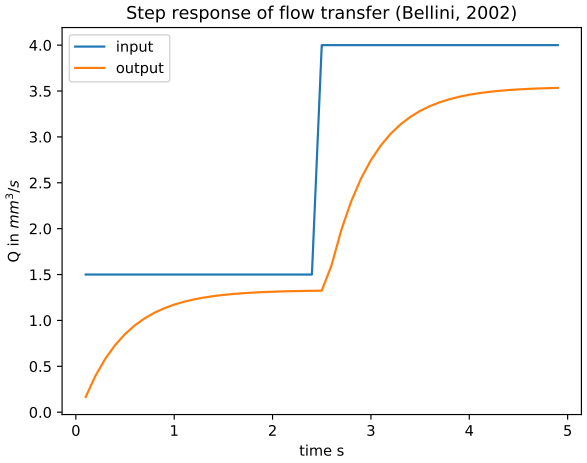

Figure 2.7: Plot of the step response of the transfer function model of Bellini, adapted from Bellini (2002).

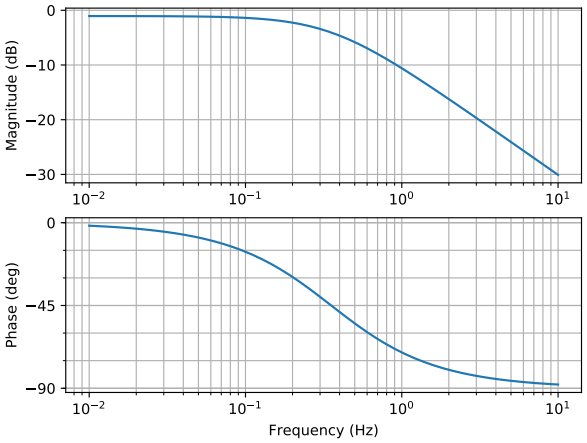

Figure 2.8: Plot of the frequency response of the transfer function model of Bellini (2002) (neglected the time delay). The cutoff frequency is 0.35 Hz

2.2.4 Thermal behaviour

Specific heat capacity

Energy has to be transferred to the material by electric heaters to raise the temperature. The amount of energy needed is dependent on the specific heat, the amount of material and temperature gradient. The specific heat at the average temperature can be described using (Çengel & Ghajar, 2011, p. 8):

$$c_p = \frac{E}{m\Delta T} \tag{2.22}$$

According to *VICTREX® PEEK 450G* (2012) the value of the specific heat capacity at 23 °C is given by Equation 2.23, while Hirschen and Gülhan (2009) write that the specific heat of PEEK changes with temperature according Equation 2.24.

These two models are compared in Figure 2.9.

$$c_{p,Victrex} = 2.2 \frac{\mathrm{kJ}}{\mathrm{kg} \cdot \mathrm{K}} \tag{2.23}$$

$$c_{p,Hirschen} = 6.1 \cdot 10^{-3} \frac{\mathrm{kJ}}{\mathrm{kg} \cdot \mathrm{K}} + 3.5 \cdot 10^{-3} \frac{\mathrm{kJ}}{\mathrm{kg} \cdot \mathrm{K}^2} \cdot T \ \mathrm{K} \tag{2.24}$$

Table 2.5: Units of thermal parameters in equation 2.22-2.24

Parameter	Name	Unit
c_p	Specific heat capacity	$\mathrm{kJ} \cdot \mathrm{kg}^{-1} \cdot \mathrm{K}^{-1}$
m	Mass	kg
ΔT	Temperature gradient	K
E	Internal energy	kJ
T	Temperature	K

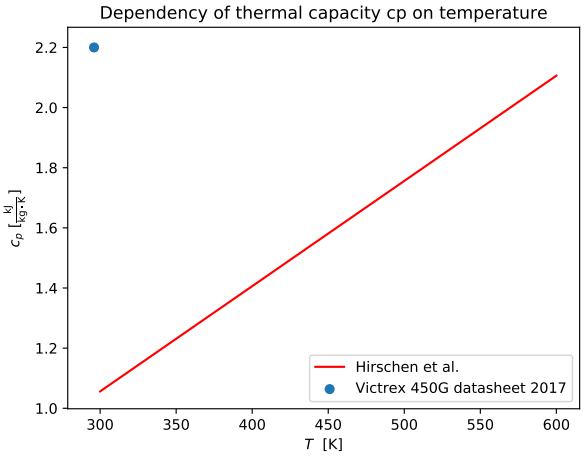

Figure 2.9: Dependency of thermal capacity c_p on temperature

Hirschen and Gülhan (2009) do not specify the PEEK variant that they used. This equation requires validation to use with PEEK 450G. The same accounts for Equation 2.28. This model is applicable for 300 <T <600 K, which is below the processing temperature in the used 3D printing process. In this project, the processing temperature is 678K, as we will see in section 5.4 on page 86.

Heat conduction

Çengel and Ghajar (2011, p. 18) write that Fourier's law describes heat conduction in cylindrical coordinates according Equation 2.25. Heat flux can be described with Equation 2.26 according Çengel and Ghajar (2011, p. 10).

$$\dot{Q}_{cond} = -k \cdot A \frac{dT}{dr} \tag{2.25}$$

$$\dot{q} = \frac{\dot{Q}_{cond}}{A} \tag{2.26}$$

According *VICTREX® PEEK 450G* (2017), the thermal conductivity k of PEEK 450G at 23 °C is given by Equation 2.27. Hirschen and Gülhan (2009) describe the heat conductivity of PEEK as a function of temperature with Equation 2.28. Figure 2.10 shows a plot of the comparison between the two models.

The equation described by Hirschen and Gülhan (2009) is valid in the range 300 <T <600 K. The material variant is unspecified. A recession in the thermal conductivity is observable around the glass transition temperature (419 K) in the model of Hirschen and Gülhan (2009).

$$k_{Victrex} = 0.29 \frac{\mathrm{W}}{\mathrm{m} \cdot \mathrm{K}} \tag{2.27}$$

$$k_{Hirschen} = -2.89 \cdot 10^{-1} \frac{\mathrm{W}}{\mathrm{m} \cdot \mathrm{K}} + 4.14 \cdot 10^{-3} \frac{\mathrm{W}}{\mathrm{m} \cdot \mathrm{K}^2} T - 1.01 \cdot 10^{-5} \frac{\mathrm{W}}{\mathrm{m} \cdot \mathrm{K}^3} T^2 + 8.16 \cdot 10^{-9} \frac{\mathrm{W}}{\mathrm{m} \cdot \mathrm{K}^4} T^3 \tag{2.28}$$

Table 2.6: Units of thermal parameters in equation 2.25-2.28

Parameter	Name	Unit
$\dot{Q}_{cond}$	Heat transfer rate	W
k	Thermal conductivity	$\frac{\mathrm{W}}{\mathrm{m}\cdot\mathrm{K}}$
A	Area	m^2
dT	Thermal difference	K
dr	Radial distance	m
T	Temperature	K
$\dot{q}$	Heat flux	$\frac{\mathrm{W}}{\mathrm{m}^2}$

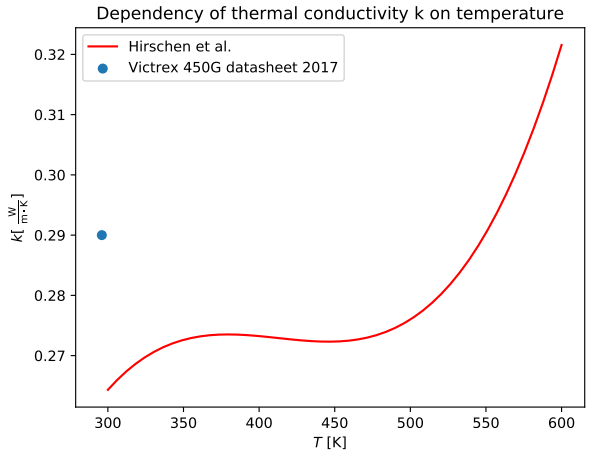

Figure 2.10: Dependency of thermal conductivity k on temperature

In an extrusion based 3D printing process, the heat flux is the factor that limits the flow rate. Go and Hart (2017) write: "The coupling between heat transfer and flow in the liquefier determines the required heater length, which in turn influences the required force". The longer this liquefier has to be, the more dominant the mechanical feeder dynamics will become. The stiffness relation will be described in more detail in subsection 5.2.1 on page 76.

PEEK is a thermal insulator compared to other polymers. Together with the larger diameter of the print tube (5.3 mm), this reduces the heat penetration to the core of the rod more than in thin filament printers. The thermal time constant will be large. Figure 4.8, on page 67 visualises the thermal response.

Numerical models for thermal conductivity in liquefiers The thermal behaviour is hard to describe due to the high importance of local effects, such as the placement of heaters. Some researchers made numerical models of extrusion in different liquefiers and different materials, The quality of the verification for these models is disputable.

Bellini (2002, p. 59) describes a finite element Analysis (FEA) model of the liquefier for ABS. This model assumes uniform wall temperature. The model was validated by comparing the pressure drop with Bellini's analytical model.

Go et al. (2017) made an FEA model of a liquefier for ABS. This model was constructed using rheological data from a Carreau viscosity model, obtained from a material database. Although the model is not validated in the study, it demonstrates the dependency of the thermal situation on the flow rate of the extrusion. The walls were modelled with a constant temperature. From a control perspective it may be necessary to control the wall temperature based on volumetric flow rate, but the risk of burning the material would increase for that case. Figure 2.11 shows that the thermal situation in the liquefier changes with flow rate. The heat transfer is slowed down by a form of thermal resistance.

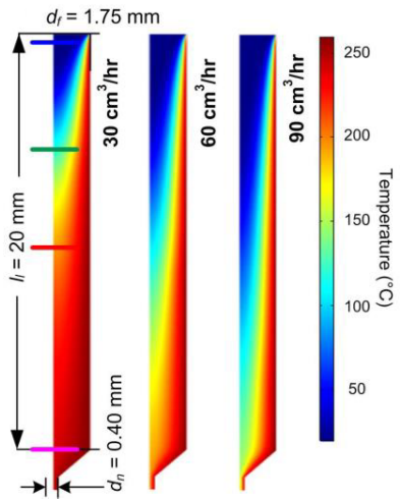

Figure 2.11: Model of the temperature distribution of ABS in a liquefier adopted from Go and Hart (2017, p. 18)

The constant wall temperature assumption (described by both models) requires that the nozzle must have ideal heat conductivity and has no significant heat loss. These assumptions do not apply to the Bond3D printing system for the following reasons:

- Heat loss to the environment, (a nozzle with a temperature of 400°C operates in an environment of 200°C.)
- The thermal conductivity of the nozzle is limited,
- The temperature of the wall is not equal for the whole length of the liquefier tube,
- The volumetric flow rate of extrusion changes with time due to starts, stops and travel moves in the printing process.

A constant heat flux assumption would be a more accurate assumption.

Volumetric expansion

Materials expand with increasing temperature. PEEK has a volumetric expansion of 4 to 5% when heated from room temperature to processing temperature which is considerably high. According to *VICTREX® PEEK 450G* (2017), the volumetric expansion is different below and above the glass temperature. Averaged for the 3 dimensions, the coefficients of thermal expansion (α_V) above and below $T_g = 143$°C are:

- Below T_g: $55 \cdot 10^{-6} \cdot \mathrm{K}^{-1}$
- Above T_g: $140 \cdot 10^{-6} \cdot \mathrm{K}^{-1}$

Volumetric expansion can be modelled using the following formula (Wikipedia, 2018b):

$$F \equiv \frac{\Delta V}{V} = \alpha_V \cdot \Delta T \tag{2.29}$$

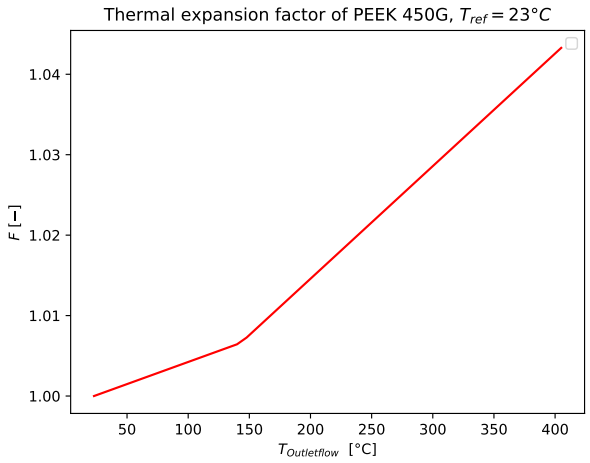

Figure 2.12: Thermal expansion factor

The temperature in the liquefier rises during a stop period, such as a travel move or a pause. The volume increases due to the increase of the average temperature, forcing out extra material. This results in a shortage of material at a start of the next printed segment. This behaviour is observable in Figure 4.1 on page 61.

2.2.5 Die swell

The pressure drop equations Equation 2.1, Equation 2.6 or Equation 2.2, show that minimising the land length of the nozzle: L_2 or L, L_c would result in a reduction of the pressure needed and the dynamical effects. Another phenomenon compromises this effect: die swell.

Die swell occurs due to orientation and stretching of the molecules by the converging section of the nozzle.

Die swell was described by McKinley (2004) and is the reason that the channel needs to be sufficiently long for a given radius: Rabinovitch, Summers, and Booth (1992) remark that there is a decreasing trend of die swell for increasing land length at any shear rate.

It should be mentioned that 3D printing does not correspond to extrusion in open space. Due to the exit effects, such as the normal force applied by the previous layer, the pressure situation may be totally different, hence other nozzle designs with relative short land lengths may provide better results.

The swelling ratio is defined as the ratio of the maximum diameter of the extruded material to the diameter of the die opening. Within the narrow nozzle opening, the melt is under stress, storing deformation material elastically. This stress is relaxed as the polymer leaves the nozzle, allowing release of the elastically stored energy resulting in radial expansion of the melt. (Hopmann, Christian and Michaeli, 2016)

Other extrudate distortions include "sharkskin" (Koopmans & Molenaar, 1998) and instabilities caused by entrance vortices (B. Bird, C. Armstrong, & Hassager, 1987, p. 94).

It should be reminded that the nozzle has a land length to prevent die swell and sharkskin distortions. Using Equation 2.6, it should be noticed that the effect of this land length on the total pressure drop is high. The effect of land length was evaluated in preliminary investigations to this study by Bond3D. The ratio $L/D = 6.67$ was found to be suitable for the Bond3D system. This was evaluated in open-air extrusion. Later studies might reveal that the land length could be shortened.

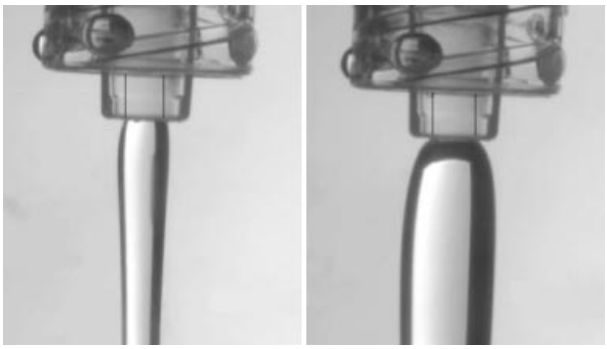

Figure 2.13: Die swell, demonstrated in open air, adopted from McKinley (2004)

2.3 Compensation of accuracy problems

Section 2.2 described the complexity of the fluidic behaviour in the nozzle. People operate extrusion printers without expert knowledge of all the causes of the observable problems. The tricks they use to solve them are described in this section.

'Tricks' are described to compensate for errors in the extrusion process.

In this report they are categorised in the following way:

- Slicer based compensation approaches
- Firmware approaches.

The first category consists in a group of simple empirical, or guesswork determined compensations. These are options that can be set in a slicer software and become part of the G-code that describes the motions. The latter category is more complicated. Modern firmwares have options to adjust the control of the printer's motion with tuning parameters, although obtaining the right values of these parameters can be a challenging process.

2.3.1 Introduction to slicer based approaches

Slicer based approaches are discussed in this subsection: Simplify3D is a commercial slicer software and provides help to solve problems found in 3D printing with their troubleshooting guide. (Simplify3D, 2018)

The following strategies are available for compensation of the 'oozing and stringing' problem and the 'blobs and zits' problem:

- Decrease of travel time
- Retraction
- Decrease of thermal settings
- Wipes
- Priming and coasting

Decrease of travel time

Travel time is the time that the extrusion head moves in the open space, while not extruding. Decreasing travel time results in a respectively more fluent printing. This can be done by decreasing travel speed and decreasing travel distance. Landry (2015) writes: "The stringing between the 20 and 40mm gaps are much worse than the 10mm". The filament has more time to ooze out of the hot end. Travel speed: increasing the travel speed reduces the time of oozing and the amount of oozed material, see: Figure 2.14. Landry (2015) advises an XY travel speed of 150-250mm/s for PLA. Another strategy is to prevent travel over empty space, using combing. Combing can result into longer printing times when the combing distance is set too long, but may reduce the need for retractions. (Ultimaker, 2019)

Retraction

Retraction is based on the principle of releasing pressure from the liquefier at the stop of a printed segment: the potential energy that is stored in the compressed material is released at the top of the liquefier instead the exit of the nozzle tip.

Retraction is a common principle applied in extrusion based printing. Retraction can be applied to stop oozing, . (Landry, 2015) describes how adequate settings can be obtained for a PLA printing system. (Landry, 2015) advises a distance of 0.5 to 5mm. "Using more than necessary can cause jams, blobs, and other extrusion related issues" (Landry, 2015). Bowden extruders require higher retraction distances than direct drive alternatives in general. This is due to the lower cumulative stiffness of the system and material compared to direct drive alternatives. Retraction distance and the opposite; 'engagement' distance are programmed to be equal. Non-equality would result in under- or overextrusion. Engagement is defined as the distance that the extruder has to travel to build up the required pressure at the start of extrusion.

Retraction and engaging take time to perform. During a standstill in XY-motion, while performing a retraction move, oozing will take place.

A 3D printing system benefits from a feeder motor with a high angular velocity. This decreases the duration of this move. The grip that the knurling wheels have on the filament can be a limiting factor during a fast engage of extrusion in filament based systems.

The Bond3D system does not use knurling wheels and continuous filament, but uses rods as can be seen in Figure 2.2 on page 20. Before November 2018 (when the tests in this report were performed, a spindle with a small motor was used in the Bond3D printing system. This feeder has a high torque to provide the high pressure needed for extrusion. The feed rate is limited to 1.5 mm/s. The Bond3D feeder can not pull although release of pressure is possible.

The optimal retraction distance is specific to the design of the printer and settings including volumetric flow rate. Chapter 4 will explain why this is the case.

Decrease of temperatures

A decrease of the temperature increases the viscosity of the material. A high temperature means that the material will be more liquid, through which it can drip from the nozzle (even though retracted). By using a lower temperature the material is less liquid and will string less. When the nozzle is cooled to much, the amount of force needed to push the material through the nozzle increases, hence the dynamical effects. The reduced temperature improves how well the material 'snaps' when followed by a fast travel move.

A small 'puff' of cold breeze at stops decreases the oozing effects according to prior experiments of Bond3D. Despite of the increased accuracy performance, this strategy was dropped at the start: due to the high temperature dependency of the crystallisation rate of PEEK and its effect on strength, the number of (uncontrollable) thermal distortion factors had to be minimised.

Wipes

Wipes are small XY-movements of the nozzle in a certain pattern at the start and/or ending of a segment. The working principle is based on the fact that the material is slightly dragged behind the nozzle. The start and stops can be improved by dragging the material to places where it does not compromise the start and stop quality, such as small offsets from the start and stops.

Different types of wipes are thinkable. For convenience names are assigned to these wipe concepts:

- 'Reloop': a wipe move that engages at an offset distance of the target start position, subsequently moves backwards to the start and then extrudes the segment.
- 'Backwipe': a wipe that moves the extrusion head to an offset distance of the target start position, than moves backward to the start, engages and extrudes the segment.
- 'Endwipe': after extrusion of a segment, the printhead moves backwards for a small distance, subsequently retracts and this is followed by a travel move to a new target position.

Priming and coasting

Priming and coasting are concepts described in the Simplify3D slicer software.

- Priming means that the nozzle moves to a position slightly before the target start position, subsequently engages and then moves to the target position, while extruding. This move is performed with a velocity that is optionally different to the normal printing velocity. The segment is printed as normal.
- Coasting means that the extruder motion is stopped, or reduced at a small distance before the target stop position. The XY-motion continuous with normal velocity, or reduced velocity.

The interesting part of these approaches is that they are common and validated for large numbers of material and printer combinations. Printing communities and manufacturers have contributed to finding working settings. A benefit of these approaches is that they are simple to apply since they are prescribed in G-code. The motion behaviour of the printhead is explicitly described and can be controlled by manipulating settings in the slicer instead of the firmware.

These strategies can or have to be applied in combinations, simultaneously or sequentially or with pauses. The major downside of retraction, wiping, priming and coasting is that these strategies and their combinations introduce a large number of process parameters that require empirical testing and guesswork and can cause new errors.

These approaches conquer the effects in specific situations, but do not solve the root cause. New situations require several new tests. In chapter 3 tests of these principles are described for the Bond3D system. Chapter 4 describes more in depth the phenomenon that causes the problems and describes how a compensation strategy can be drawn up that can be applied for a wider range of situations by compensating dynamically. The approach of dynamical compensation is not new, but already exists in 3D printer firmwares, see: subsection 2.3.2.

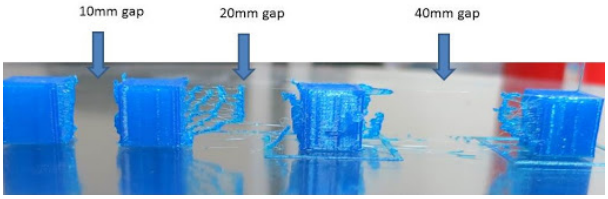

Figure 2.14: Stringing and oozing. The problem increases with travel distance, due to the longer duration, adopted from (Landry, 2015)

2.3.2 'Linear advance' algorithms (firmware approaches)

Engineers and programmers have implemented software algorithms to compensate for the flow rate dependency of the pressure inside the liquefier and hysteresis, that become more dominant at higher flow rates. These are attempts of tuning the liquefier dynamics. An overview is provided in Table 2.7:

Table 2.7: Overview of linear advance algorithms in literarature

Authors:	(Roberts, 2011), (Repetier, 2011).	(Kubicek, 2011a), (Kubicek, 2011b), (Henschke, 2013), (de Bruijn, 2014), (D. Newman, 2016), (L. Newman, 2017).	(Sineos & Sebastianv650, n.d.) (Sebastianv650, 2011), (Sebastianv650, 2018).
Models:	Bernoulli, Hooks law, Linear axial stiffness.	Hagen-Poiseuille, Hooks law, Linear axial stiffness.	Hagen-Poiseuille, Hooks law, Linear axial stiffness.
Compensation:	$\vec{x}_{extra} = k\vec{v}^2$	$\vec{v}_{extra} = k\vec{a}$	$\vec{v}_{extra} = 1/(k\vec{a})$
Base unit* of k:	$\frac{\mathrm{s}^2}{\mathrm{mm}}$	s	$\frac{1}{\mathrm{s}}$

*The base unit is the bare unit that remains after stripping the implementation specific details away, such as steps/distance.

Background:

de Bruijn (2014) claims: "Inside the nozzle there is a pressure depending on the extruding velocity". Kubicek (2011a) adds: "Pressure in the hot end is generated by adding more material than being removed". This pressure is stored in the elasticity of the filament, that could be modelled as a spring, according L. Newman (2017). Sineos and Sebastianv650 (n.d.) remark: "If the material is pushed faster (=printing fast), the filament needs to be compressed more before the pressure inside the nozzle is high enough to start extruding the material".

"The extruder motor moves in linear proportion to all the other motors, maintaining the same acceleration profile and start/stop points. But an extruder is not a linear system, so this approach leads to extra material being extruded at the end of each linear movement" claims Sineos and Sebastianv650 (n.d.). Repetier (2011) remarks: "There seems to be a time shift, too".

"These problems are minor or even imperceptible at low printing speeds, but they become more noticeable and problematic as print speeds increase" (Sineos & Sebastianv650, n.d.).

"There are two reasons for oozing. If we do not print, but the hot end is on, the filament will melt and flow outside. The other reason is pressure, caused by the filament driver. During the print move, a certain pressure was needed. If we stop the extruder, the pressure is still there and will force the plastic outside" state (Repetier, 2011).

Modeling:

There are two approaches for flow modelling. Some authors use the Bernoulli equation to calculate the pressure, while others use the Darcy-Weisbach/Hagen-Poisseulle model. All model the piece of filament between the feeder and the hot end as a linear compressible spring using Hooks's law.

Pressure drop calculation with Bernoulli Roberts (2011) and Repetier (2011) use the Bernoulli equation. This equation describes that a change in speed in a liquid is accompanied by a change in the pressure:

$$\frac{v^2}{2} + g \cdot h + \frac{P}{\rho} = constant \tag{2.30}$$

The pressure could then calculated using:

$$\Delta P = \frac{(v_o^2 - v_i^2)\rho}{2}$$

Pressure drop calculation with Hagen-Poiseuille (Henschke, 2013), (Kubicek, 2011a) and (Kubicek, 2011b) reject the validity of the pressure drop using the Bernoulli equation for the reason that most of the pressure is lost because of friction instead of the velocity change. The Darcy-Weisbach equation, also known as the Hagen-Poiseulle law should be applied:

$$\Delta p = \frac{32\mu \cdot L_c \cdot v}{d^2} = \frac{8\mu \cdot L_c \cdot v}{r^2} \Rightarrow \frac{8\mu \cdot L_c \cdot Q}{\pi r^4} \tag{2.31}$$

Linear axial stiffness The stiffness k for a linear axis, such as a rod or a filament is given by:

$$k = \frac{E \cdot A}{L} \tag{2.32}$$

Hook's Law The pressure can be substituted in Hooks law, Equation 2.33 using the calculated pressure and the diameter of the feeding material: $F = \Delta P \cdot 1/4 \cdot D^2$.

$$x = \frac{F}{k} \tag{2.33}$$

Control algorithms:

Table 2.7 shows that the control strategy in the two right columns relies on the same base theory. The implementation of control differs. Figure 2.15 and Figure 2.16 show theoretical results of the implementation. It can be observed that the strategy requires velocity jumps. Since this is limited by the finite jerk, the required displacement has to be averaged out. How the firmwares handle this factor is a bit different.

The JKN Advance algorithm allows the setting of an extra parameter that accounts for an asymmetry between the compensation during acceleration and deceleration (L. Newman, 2017).

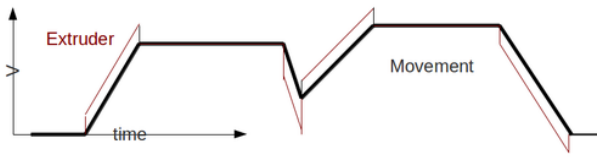

Figure 2.15: Theoretical model of the control algorithm of Kubicek, adopted from (Kubicek, 2011a). In this figure, the time is plotted against the velocity of the plunger. The red line shows that the compensation adds an extra velocity during accelerations and subtracts an the same speed during the deceleration phase. This speed boost compensates for the compliance of the rod.

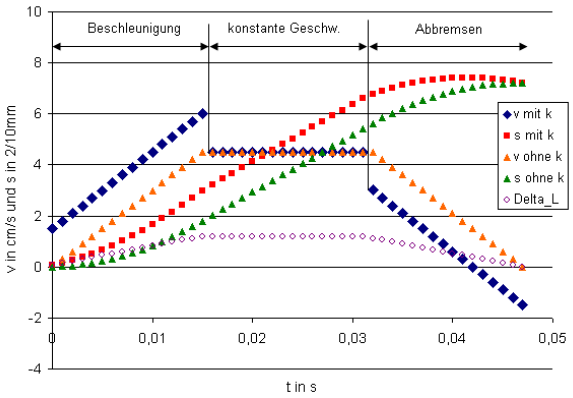

Figure 2.16: Comparison of the feeder motion planning with (blue and red) and without (orange and green) the linear advance controller activated in a trapezoidal motion profile. A. Purple shows the offset distance. Adopted from (Henschke, 2013)

Figure 2.16 demonstrates that this compensation is effectively a retraction move. The major difference are that the correction move (retraction distance) is dependent on the speed and the move is executed simultaneously to XY-motion, instead of a separate move.

The models rely on the following simplifications:

- There is no thermal expansion,
- All material variables are constants. Volumetric flow rate Q and pressure are proportional.

Section 2.2.4 explained that PEEK has a volumetric difference of 4 to 5% between the hot and cold conditions. The large diameter of the liquefier slows down heat penetration and would result in a large thermal time constant. Polymers typically have a shear rate and temperature dependent viscosity and that this results in a pressure drop that is not linear with the volumetric flow rate.

These three aspects may argument why the simplified models that were discussed in this chapter may not hold for the Bond3D printing system.

2.4 Concluding remarks on literature

An overview of the general principle, work flow and relevant components of extrusion based printing was provided in section 2.1.

Extrusion based printing appears as a scientific topic most dominantly in empirical studies. In 2015, (Turner, Strong, & Gold, 2014) concluded that the degree of experimental validation of process models is limited. Today, models validation of these models is still insufficient, making it difficult to draw unambiguous conclusions. The studies that discuss extrusion based 3D printing with PEEK, described in subsection 2.1.3 do not explain how printing accuracy could be enhanced. Strength and stiffness seem to be main topics of interest, although these studies provide a lot of information about the concerns.

An overview of these concerns is presented in Figure 2.3. This chart can serve as a reference for 3D printer troubleshooting in general.

Model based approaches are explained in section 2.2. Two important topics that need to be better understood to improve deposition accuracy are below summarised:

- The flow rate dependent pressure drop and the distance of compression of the material.
- The transient behaviour: the time dependency of the extrusion. (dynamics)

Bellini (2004) proposed both models: A power law fluid based pressure drop model of a liquefier and an electric analogy of the dynamics of the system. These two models were not applied for actual improvement of accuracy and lack proper verification.

Mackay et al. (2017) showed another approach to calculate the pressure dependency by the use of the Boles equation. Mackay et al. (2017) did not use the model to improve accuracy.

The extent of applicability of any of these models to PEEK and the Bond3D printing system is unknown. How PEEK could be modelled using a power law model is uncertain as well. This is further studied in chapter 5.

Accuracy improvement strategies are discussed in section 2.3. section 2.3 discussed compensation tricks that are present in modern slicer software. The 3d printing community devises ways to avoid this problem. The addition of these tricks without actually solving the causes for the problems add up to the complexity of the 3D printing systems and (manual) calibration procedures, although they are easy to apply. In chapter 3 this topic is explained in more depth.

In subsection 2.3.2 more sophisticated solutions found by firmware programmers were discussed. These dynamic compensation technique seems to be promising for improvement of accuracy for the Bond3D printing system. The Bond3D printing system and the material are different than the systems that run these firmwares and their materials. In chapter 4 the dynamics of the Bond3D printing system are identified and a control approach is provided, chapter 5 explains the origin of the dynamics in the Bond3D printing system.

Chapter 3

Enhancing accuracy with empirical determined error compensation

In the beginning of this project, a combination of retraction with wipes, priming or coasting as described in section 2.3 was expected to be the key to produce accurate products. Without any form of retraction, printing small thin walled features reported unsatisfactory results. Retraction and a "wipe during retraction" were investigated preliminary to this study in a small set of experiments by a colleague at Bond3D but theoretical fundamentals were missing and reference like the methods described in the previous chapter were missing. This occurred because the engineers claimed that the Bond3D liquefier system is very different by design to other printers and therefore the significance of the concepts described in the literature section may be very different.

The Bond3D printer has some very specific characteristics such as: a relative large liquefier cross-section working at a very high temperature and a pusher-based feeder system that can only push the material and cannot pull. A one-way clutch mechanism was integrated to prevent the material from moving upwards. Another designed function of the prototype is that the liquefier section moves downwards when the feeder supplies a pressure and moves upwards when the pressure is released (during a retract move). This would help to prevent collisions in a multi-printhead setup. The lower section with the heaters, nozzle and print tube is spring attached to the part that fixes the feeder mechanism. Additionally to these machine characteristics, the behaviour of PEEK is different. Therefore it responds differently to the compensations.

With a very new, untested feeder system and control software and code to generate G-code for experiment geometries, there was a big desire to proof the actual performance of the new designs and to show the big potential of the new feeder system to investors.

Regarding this goal, this chapter is part of the preliminary investigation of this project. It should be considered as a pilot study. It is not the goal of this chapter to find the ultimate settings for the given system, neither to provide scientific proof for the retract, wipes and priming and coasting concepts and neither to cover all available combinations of settings.

The goal is to learn about the behaviour of the liquefier system and to try out some ideas to form a hypothesis on how the behaviour could be enhanced in a more strategic way, while being able to demonstrate achievable small feature performance within a small set of test geometries and benchmark the performance. It is a proof-of-principle approach.

Obtaining hands-on experience with the system provides practical skills in conducting experiments on advanced hardware that is under development. A system that is still in development has to deal with lots of bugs, imperfections and errors and requires the development of troubleshooting skills and workarounds.

Some factors that have not been considered previously in this report that influence accuracy in the Bond3D system will be covered.

3.1 Goal geometry definition

There are several challenges in this chapter that can be assessed with variant of the test crown geometry on the cover of this report.

- Segment start of 10 mm segments
- Segment stop of 10 mm segments

- Pillars, (=only a series of drops at the start of a merlon)
- Shorter segments: 8, 6 and 4 mm long.

Requirements

Bond3D had investigated which features would be needed for their applications and came up with the following target specifications for these single wall test castle produced with a ⌀0.6 mm nozzle:

- A line-width of 0.66 mm
- A layer-height in the range from 0.2 mm to 0.5 mm

The acceptable error tolerances in the horizontal plane are:

1. An error of 0.2 mm for the start of the segment.
2. An error of 0.2 mm for the end of the segment.
3. An error of 0.2 mm for the line width.

3.2 Model synthesis

There are a number of problems observable in videos that were made of the 3D printing process, see Figure 3.1 and Figure 3.2. For these videos retraction was already activated to obtain successful products.

Oozing was observable especially at the stop of a print since material continued flowing from the nozzle and wrong material distributions at the start and endings were observable. Additionally, the formation of blobs, collisions and eventually release from the printing bed were observed.

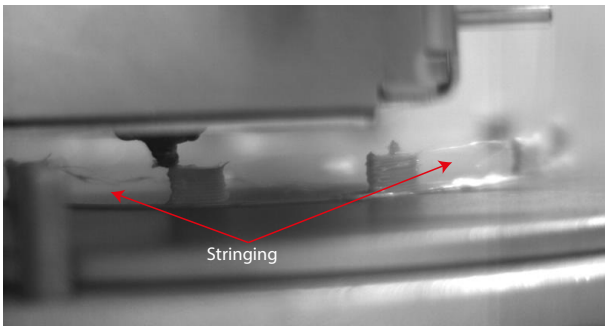

Figure 3.1: Stringing and oozing

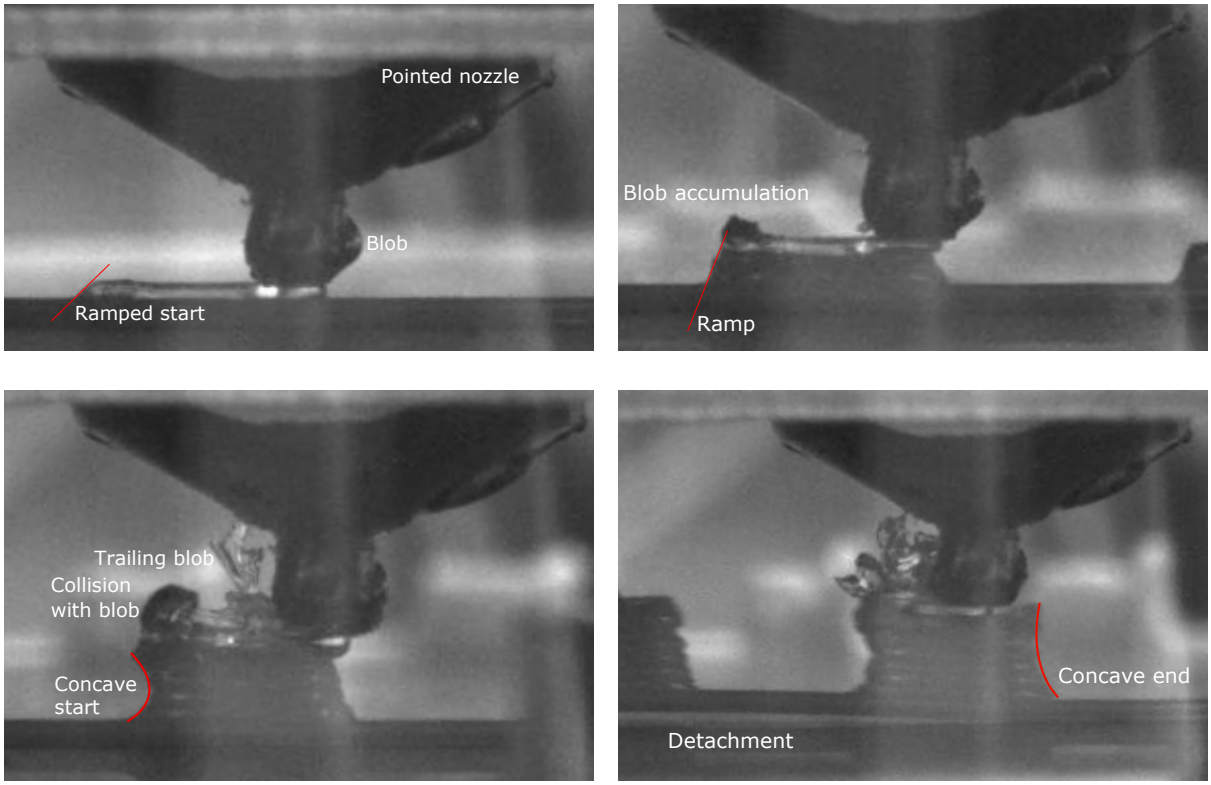

Figure 3.2: Nozzle smearing in a single line sample. Note: retraction was applied

3.2.1 Analysis

Figure 2.14 on page 39 and Figure 3.2 show the major problems:

- Wrong material distribution at the start (ramp or concave)
- Wrong material distribution at the ending (concave ending)
- Accumulation of blobs causing collisions (blobs)
- Build plate detachment
- Oozing

The problems of subsection 3.2.1 may be caused by more of the following causes:

- Wrong amount of material dispensed at start.
  - Pressure forces-out extra material during travel moves
  - Gravity forces-out extra material during travel moves
  - The lack of normal force during travel moves eases flow
- Wrong positioning of layer n, results in extra wrong positioning of layer n+1 (accumulating problem)
  - Poor adhesion and shear cause a ramp formed at the start of each new layer. Material of the next layer forms a new ramp at an offset location.
  - The droplet has to bridge the layer height at the start before it can fuse with the layer below. During XY motion, this leads to a relocation of the layer. This could be considered as bad timing between the xy motion and the extruder motion.
  - Increasing contamination and adhesion on the nozzle's exterior cause sudden large disturbances.
- Over extrusion at the end
  - Momentum of the flow prevents a sudden stop of the flow.
  - Material sticks to the nozzle and is pulled along with the nozzle.
  - The pressure in the nozzle cannot escape in top direction enough since retraction is too slow.

3.2.2 The compensation strategies solution concepts

There is a very large number of parameters that can be adjusted to improve the extrusion to meet the requirements listed in section 3.1. There are many combinations of parameter settings that lead to unsatisfactory results, but from an already defined work point parameters could be adjusted to tune the behaviour, see: Table 3.4.

In subsection 2.3.1 some basic compensation approaches for deposition defects common in the field were described:

- Priming and coasting
- Retraction
- Wipes

At the start of this project, some wipes were investigated by colleagues on the test geometry shown on the cover of this report. Their results were not satisfying: the merlons of the printed test castles were distorted: they had large notches at the start and stops. Not all the merlons were present and large blobs of material showed up everywhere, but without applying these concepts it was not possible to print the geometry at all.

These compensation strategies are relative easy to implement. Bond3D uses a custom G-code generator script. Prior to this research, retraction was implemented and several types of wipes for the start and end of segments, see Table 3.1. A set-up was available and configured with an early version of the software ready to evaluate more iterations of on these concepts.

Table 3.1: Implemented strategies prior to this study

Position	Wipe name	Description
Start	Wipe During	Moving from an offset on the segment to the start is done during retraction.
Start	Wipe Back	Moving from an offset to the start is done after retraction, while extruding at print speed.
End	Wipe During	Moving from the stop to an offset location on the extruded segment is done during retraction.
End	Wipe Back	After extrusion to the end, move back with the endwipe length while printing and subsequently retract

Table 3.2: Parameters of the compensation strategies.

Setting	Description
Prewipe length	The distance of the offset location to the start
Endwipe length	The distance from the stop to the offset location
Retraction distance	The distance that the feeder has pull the material
Retract difference	A difference between the retraction and engaging distance to conquer over extrusion at the start

Additional to these prior strategies, strategies in Table 3.3 were programmed in the G-code generation script. They share the same parameters.

Table 3.3: Additional implemented strategies during this study

Position	Wipe name	Description
Start	Reloop	Move to a position offset, then engage, move back to the start without extruding at print speed and extrude segment.
Start	Priming	Begin at the prewipe distance before the actual start, then engage and than move to the actual start position with the print speed without extruding
Start	Dwell time	Move to the begin of the segment are at a distance just before the segment, engage, wait a small moment and than extrude the segment
End	Coasting (Dry run)	Stop extrusion at the endwipe distance before the stop, continue XY moving at print speed while retracting.
End	Z-lift	Move the extruder upwards prior to retraction

3.3 Material and method

3.3.1 Parameters

It should be mentioned that at the time of this study, the setup is still in development. At the start, the software was not fully implemented and some workarounds were needed to be able to make some prints. The proof-of-principle prototype does not ensure robust test conditions but can to be used to evaluate new solution concepts and parameter-estimation-approaches. This paragraph is written with hindsight. There is a large number of adjustable parameters and environment conditions that may influence the tests conducted in this chapter.

Printer parameters There is a large number of printer related parameters that can influence the accuracy: these are the print speed settings and settings for travel speed, acceleration, deceleration and jerk and smoothing of paths performed by the G-code interpreter, see: (Beckhoff, n.d.). The order of motions (First XY, than to new Z), The zero-height of the Z stage and thermal settings, such as the print bed temperature and the temperature settings for the 4 stages of heating and their PID-tuning values. Two nozzle designs are used, see: Figure 3.5 and Figure 3.2 which is also a printer related factor that can influence the accuracy.

Geometry parameters There are geometry settings that are configured for the test specimens: the layer height, line width, segment length and travel distance and number of layers are the most important factors that may influence the accuracy.

Compensation strategy parameters subsection 2.3.1 described that the principles introduce additional parameters. Retract speed, z-lift distance, z-lift speed and the ones described in Table 3.2 on page 46.

Variation in test conditions There are environment conditions that can influence the testing procedure including changing lab conditions such as humidity, room temperature, cold air breezes. Other factors are nozzle degradation (accumulation of burnt material in the nozzle) and the material batch (and drying process). Not every test could be performed with a clean nozzle hence blobs form on the exterior of the nozzle and there may be accidental detachment from the building plate due to drifting height of print bed over time and wrong adaption to this phenomenon.

Intentional variation in test conditions The hardware is still in the very early stages of development at the time of these tests. Position lag failures occured on the rotary axis caused by obstruction or temperature lags or wrong encoders that required improvement. New nozzles and new heaters were required to speed up the experiments. Changes of the PLC software were applied that change the motion settings and position calibrations etc, and settings to segment smoothing and velocity jumping were adjusted to decrease failure. Despite it would be theoretically feasible and provide scientific robustness it is practically impossible to keep track of the changes and impact on the experiments. The improvement of the system is part of the process.

Influence of the operator The operator has a significant influence on the test conditions: The amount of material purged before the process starts and how well the operator cleans the nozzle between print jobs are some examples. Others are how well manual interventions such as removal of the purged material are performed and the time that the printer has been left at a high temperature. The temperature at the core of the liquefier is lower than the sensors at the wall report, hence the time interval between the start of preheating and running the experiment matters.

Approach of finding good parameter values The number of parameters and uncertainty in the test conditions is very high. Finding optimal result would require testing a very large number of combinations. Executing a single test geometry takes an average time of 30 minutes due to all the complexities with the unfinished software and high chance on total or minor failure of both system and operator.

To deal with the problem of finding adequate values for these parameters, the setup was designed to at least be able to observe the 3D printing process from close by and to be able to record the 3D printing process with a camera.

The setup and test design are explained in subsection 3.3.3. This approach requires that a certain set of parameters is selected as a basic work point

3.3.2 Start work point

A prior study by a colleague defined the start work point. The working conditions were chosen to comply with the requirements, see Table 3.4.

Table 3.4: Default parameter values

Setting	Value and unit	Additional info
Print speed	10 deg/s | 6.55 mm/s*	*For a product with a radius of 37.5 mm
Retraction speed	1.5 mm/s	Retract and engage speed are equal
Retraction distance	1 mm	
Travel speed	200 deg/s | 131 mm/s*	*For a product with a radius of 37.5 mm
Jerk, acceleration and deceleration	INFINITY*	*Velocity jumps are allowed
First move to XY-position, then Z.	TRUE	
Lowest stage print head temperature	Constant 450 °C	
Second stage print head temperature	Constant 160 °C	
Print bed temperature	250 °C	
Top two stages heaters	DISABLED	
Heater and bed PID-tuning values	UNKNOWN	
Nozzle type	⌀0.6 mm	Brass, pointed tip, see Figure 3.2
Product radius	37.5 mm	
Line width	0.66 mm	
Line height	0.3 mm	
Merlon length	10 mm	
Number of merlons	10	
Gap length	12 mm	
Castle height	5 mm	
Number of brims	2	
Prewipe	None	Disabled in the base geometry
Endwipe	Wipe during	
Endwipe length	1.5 mm	

Although it would be sensible to use a smaller nozzle to make smaller details, it was chosen to first investigate the behaviour and limitation for the default nozzle.

3.3.3 Setup and measurement method

Two PoPs were used to conduct the tests in this chapter.

The PoP have the following properties, see 3.3b:

- 1 Rotary axis: a geared stepper motor with encoder drives the heated Printbed
- 1 Linear axis
- A printhead mounted to a z-stage
- A heated print bed of 250 °C
- A cylindrical glass that surrounds the print bed
- Limit switches facilitating homing.
- An IDS camera aimed at the printed product to record the printing process.

There are two important properties that are different for the two setups: PoP1 has a printhead that is mounted a bit off-centre and uses a nozzle with a pointy shape, see: Figure 3.2 on page 45, while PoP2 has a nozzle that is mounted in the centre and has a conic shape, as observable in Figure 3.5 on page 52. It has to be noticed that the G-code is generated by assuming a polar coordinate system and that eccentricity breaks the the validity of this assumption. Adjustment factors could be included by the G-code generator script to compensate for the small radius offset. The system uses a rod pulling system as described in Figure 2.2 on

page 20. The print bed is fixed in height and the printhead assembly moves in Z-direction in the PoPs while being mounted via a load cell.

A colleague assisted by providing some test results of the 'reloop' concept produced with the FeMo prototype.

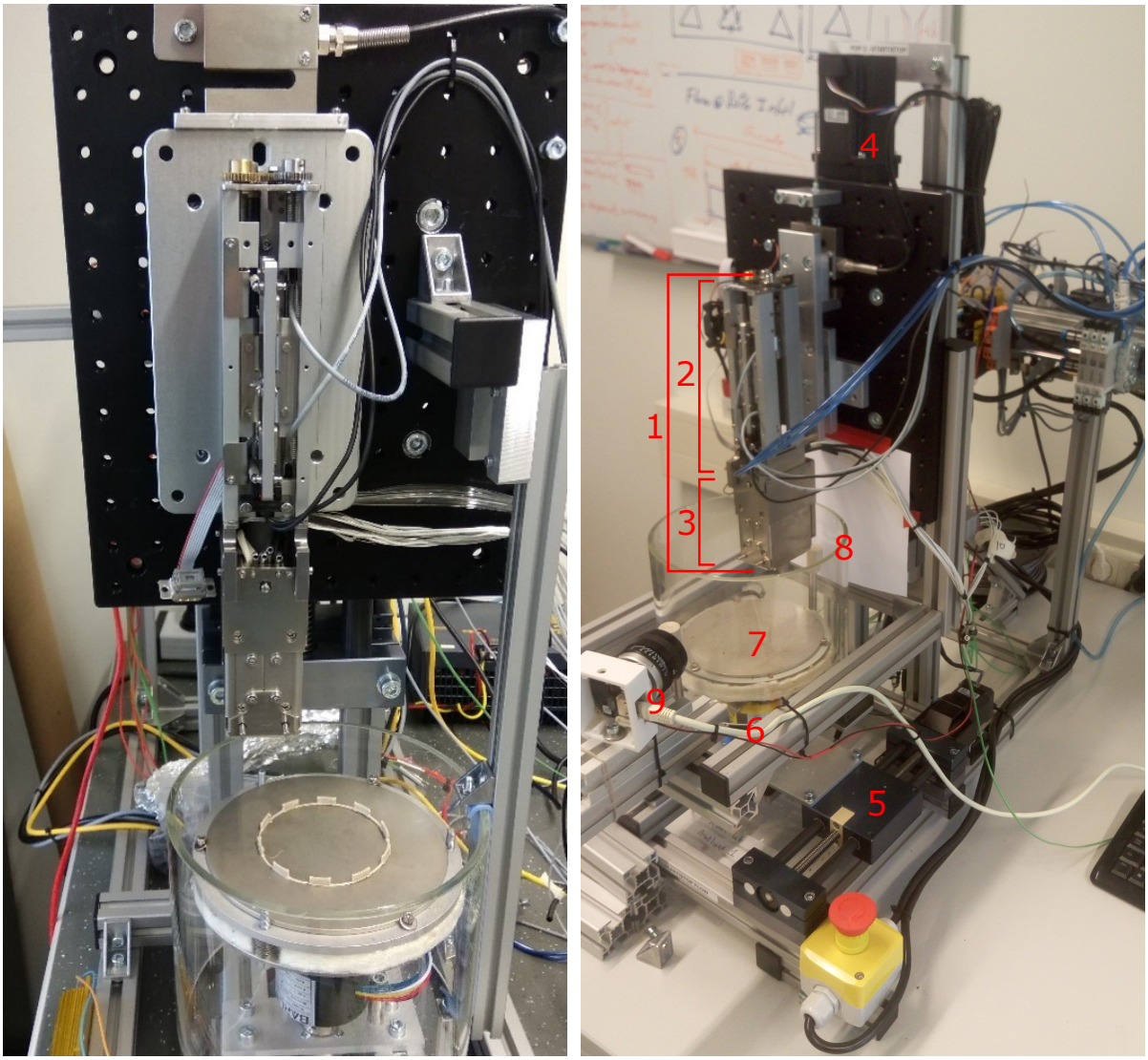

(a) PoP1 setup

(b) PoP2 setup

Figure 3.3: PoP setups. A printhead (1) consisting of a feeder (2) and extruder (3) is mounted to the Z-axis (4). The horizontal motion is provided by a linear axis (5) and a rotary axis (6). The heated print bed (7) is placed in a jar (8) that moves along with the horizontal motion. A camera (9) records the printing process.

Method for preparing tests The procedure for preparing and printing is different from the procedure described in Figure 2.1 on page 19. Appendix L shows an example of a geometry definition script.

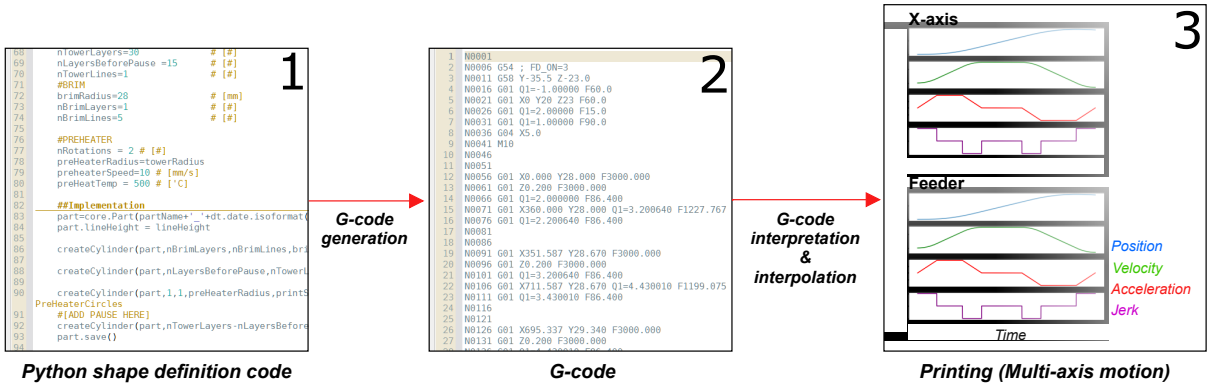

Figure 3.4: G-code preparation using the G-code generator applied to a shape definition code written in Python. An example can be found in Appendix L

The G-code is generated using a Python script[1]. This ensures better control of the actual printed geometry and allows for a quick implementation of the solution concepts. The G-code is generated for the specific test setup[2]. The gcode is loaded into the job executor software[3]. The job execution software is at an early state of development and therefore requires some workarounds:

G-code of the test geometries

1. Product scripts start generally with two brim layers.
2. 10 or more merlons are placed on this brim according test specific parameters.
3. Camotics (Coffland, 2017) was used to analyse the programmed G-code for debugging when a new test shape was programmed
4. G-code is manually checked if it matches the expected code, however this is prone to overlooking of details.
5. The produced G-code is transferred to the printer.

Print procedure Despite the advanced features that could be incorporated in the final product, in the stage described in this chapter, the process involved quite a lot of manual effort. Therefore the process was more susceptible to possible mistakes.

1. Load PEEK into the feeder
2. Start the job executor
3. Start preheating of the build plate
4. Start preheating of the nozzle
5. Home axes
6. Start the recording of the Ueye Cockpit camera software and set the camera settings to make a good recording with a bitrate $< 12\,\mathrm{mb/s}$.
7. Start plotting of measurements
8. Start purging until no bubbles and burnt material leave the nozzle anymore, usually about 10-20cm is needed
9. Start the GUI of the job executor and load the print job
10. Run the print job
11. Shut down the camera software
12. Stop the plotting of measurements
13. Force quit the job executor since the post printing routine is unimplemented
14. Set cooling of the nozzle to preheat temperature (300 °C) or cold.

One of the major problems concerns the fact that in case of any error, the state of the system freezes. The nozzle is left at an elevated temperature while not extruding any material.

This results in a high residence time of the material in the hot build room, accumulating burnt polymer. This increases the chance of failure in the next print. A wrong homing position of the Z-stage is often the cause of the initial problem. When the nozzle is too close to the printbed the motor current overshoots and stops the print job. The homing position of the Z-stage is a variable that needs to be adjusted manually every print

job. To speed up the process, the Z-axis homing position could be set from the G-code generator. The height of the printbed varies over time and therefore several runs are often required to find a running procedure.

Due to the instability of the system and difficulty to analyse the G-code manually, it is hard to assess whether a failed process is caused by wrong calibration or or whether the actual settings are not actual settings are not able to produce a good product.

The majority of the tests are video captured using an IDS camera. Due to time constraints, it was not possible to record every test.

Photographs of the best results were taken by a camera with a telecentric lens with a grid background. This allowed to make images that have equal aspects on the foreground and background well suitable for measurements. The analysis requires manual calibration of the grid with the grid of a vector graphics editor (Inkscape) for every image to process.

Measurement protocol

1. From the best printed test geometry select the best and worst printed merlon. Cut the crown to enable a flat photograph.
2. Load camera profile settings in XIMEA cam tool
3. Make a photograph from the top with the telecentric lens with XIMEA cam tool
4. Make a photograph from the side with the telecentric lens with XIMEA cam tool
5. Save the files
6. Load the files into Inkscape
7. Manually match Inkscape grid to image grid
8. Measure start and stop concave
9. Measure line width at the start, mid and stop.

Only the best test objects were photographed due to the long duration of taking the measurements.

Assessment criteria

The test geometries are assessed by the following criteria:

- Maximum start error (mm) of the best feature on a test object
- Maximum stop error (mm) of the best feature on a test object
- Maximum line width error (mm) of the best feature on a test object
- Maximum length error (mm) of the best feature on a test object

3.3.4 Design of test

In subsection 3.2.2 a large number of solution concepts was described and subsection 3.3.1 elaborated the large number of parameters. Section 3.3.2 described the basic work point, but what matters is how the actual improvement regarding the requirements of section 3.1 can be met.

The objective is to evaluate a relative large number of parameters. A multivariate analysis method like a DOE could contribute to effectively evaluate the influence of the parameters. The proof of principle setup is far from robust and therefore it was chosen to do not rely on such an approach.

This study there had the opportunity to observe the printing process in execution and this allows to run and adapt the experiment series, based unmeasured criteria such as under-extrusion, over-extrusion, blob formation, blob movement etc. It should be mentioned that in some cases it was decided to rerun an experiment in case of a failure.

The parameters and tricks are evaluated for several geometries they were chosen to be as following:

1. Basic test castle with medium long merlons (10 mm), see Figure 3.5 (right) and Figure 3.6 (Row 1)
2. Test geometry with the shortest possible details, pillars, see Figure 3.6 (Row 2)
3. Test geometries with segment lengths inbetween the length of the previous two geometries see Figure 3.6 (left) and Figure 3.7 (Row 3)

The division of the problem into in these sub-problems was done because in the first experiment, the start and end problems are distinguishable from each other, the pillar demonstrates the absolute minimum feature and the intermediate long segments bring start problems closer to the end problems, narrowing down the space for compensation and settling of dynamics.

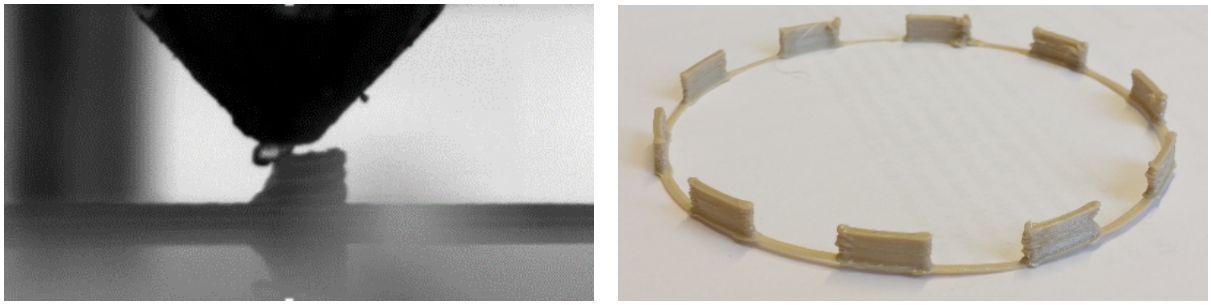

Figure 3.5: Capturing the printing of a short segment with a camera (left) and the completed 'castle with merlons' geometry (right). The height is 5mm.

Some properties were not altered. The base working point was defined in Table 3.4 and for specific experiments additional tables have been made to demonstrate the settings.

The details are shown in the following series of tables.

Segment end

The base geometry for this test series is the crown described in Table 3.4 and shown in Figure 3.5. This test has only one independent variable: `Endwipelength`. This variable describes the offset distance from the target end at which coasting should start. Coasting is retraction during a travel move at print speed.

Table 3.5: Exp1: coasting experiment design end

exp	sample	Endwipelength
1.1	169	1
1.2	172	0.5
1.3	173	2
1.4	174	2
1.5	175	0.5
1.6	176	4
1.7	177	0

Pillars

In order to demonstrate the smallest possible features and to observe the retraction behaviour more in-depth, pillars were produced. The default geometry has the same settings as the previous experiment, but instead of merlons, dots were created by extruding a small amount of material, while standing still. The location for these pillars was initially on equally spaced distances at all the start positions of the merlons however since the pillars at the brim weld had a higher chance of causing failure, the positions were translated with a small offset later-on. In the early experiments, moving in Z-direction happened before after XY-motion and this caused collisions. The setting were switched to reduce this problem. The `Forward` variable describes the travel distance of the plunger during an 'engage' move. The `Retractdifference` is the result of substration of the `Retractdistance` from this value. The `Lineheight` was increased since it seemed that the material had the natural preference to form round blobs.

Table 3.6: Exp2: small pillars experiment design

exp	Forward	Retractdifference	Lineheight	sample	Other
2.1	1	0.1	0.3	179	
2.2	1	0.03	0.3	180	Towers are placed at weld of brim
2.3	1	0.03	0.3	181	With aluminiumfoil to cover
2.4	1	0.03	0.3	182	
2.5	0.8	0.03	0.3	183	
2.6	1.3	0.03	0.3	184	
2.7	1.3	0.05	0.3	185	
2.8	1.3	0.04	0.3	186	Extra brim layer
2.9	0.8	0.04	0.3	187	
2.10	0.8	0.04	0.3	188	
2.11	0.8	0.035	0.3	189	
2.12	0.8	0.04	0.5	222	
2.13	0.8	0.04	0.2	223	
2.14	0.8	0.04	0.15	224	
2.15	0.8	0.04	0.6	225	
2.16	0.8	0.04	0.5	226	First move to Z than XY at layer change from here
2.17	0.8	0.04	0.5	227	gcode same as 2.16
2.18	0.8	0.04	0.5	None	SC
2.19	0.8	0.04	0.5	None	SC
2.20	0.8	0.04	0.5	None	SC and strange pipe mark in Gcode
2.21	0.8	0.04	0.5	None	SC and fixed strange pipe mark
2.22	0.8	0.04	0.5	None	SC and the same as 2.22
2.23	0.8	0.04	0.5	None	SC and an extra brim layer

Note: SC='Sanity check'.

Segment start

For the start of the segment several concepts were tested, shown in Table 3.7. In order to do the tests with the 'reloop' concept, the generator had to be extended to make this feature feasible. The intent was to have an equal line width for all the tests, but due to a programming error the line widths for the 'reloop' concept were less than this value.

The 'reloop' concept was tested in another test series by a colleague on the more advanced Cartesian FeMo prototype. A big difference is that the rotary axis of the PoP rotates in one way during the whole print, accumulating material on the trailing side of the nozzle. The FeMo returns to the start position by moving back in opposite direction, directly over the deposited segments, 'ironing' the accumulated material during this motion.

Table 3.7: Exp3: startwipes experiment design starts

exp	Prewipe	Prewipelength	Segmentlength	Linewidth	Forward	Retractdifference
3.01	Wipe During	0.5	9.5	0.67	1	0
3.02	None	1	10	0.67	1	0
3.2	Priming	0.5	9.5	0.67	0.99	-0.01
3.3	Reloop	0.5	9	0.56	0.98	-0.02
3.4	Dwell time (zero)	1	8.5	0.67	0.99	-0.01
3.5	Reloop	1	10.5	0.55	0.99	-0.01
3.6	Reloop	1	10.5	0.55	0.95	-0.05
3.7	Reloop	1	10.5	0.52	0.95	-0.05

Shorter segments

Table 3.8: Exp4: 5 mm short segments experiment design

exp	Prewipe	Endwipe	Endwipelength	Prewipelength
4.1	No prewipe	During	0.5	0
4.2	Reloop	During	0.5	0.5
4.3	Reloop	During	0.5	0.5

Table 3.9: Exp5: shorter segments experiment design

exp	Segmentlength	Endwipe	Endwipelength	Lineheight	sample
5.1	10	Coasting	0.5	0.3	233
5.2	8	Coasting	0.5	0.3	234
5.3	6	Coasting	0.5	0.3	235
5.4	4	Coasting	0.5	0.3	236
5.5	4	Coasting	0.5	0.5	237
5.6	4	Coasting	0.5	0.5	238
5.7	4	No wipe	0	0.5	239
5.8	4	No wipe	0	0.5	240
5.9	3	No wipe	0	0.3	241

3.4 Results

At this stage of the process, the accuracy gain was high enough to examine visually from the printed samples. The video captures are stored within the sample database of Bond3D.

Since this is a proof-of-principle study, and the intent of this study is to form an hypothesis rather than proofing one, and measurements are difficult and time-consuming, it was chosen to only report on the best results.

Taking all the measurements is a time-consuming task and is of little value since robust test conditions cannot be provided by the PoP in this stage of the process. This impairs the applicability of DOE and multivariate statistics that would otherwise motivate taking them.

The most accurate printed features evaluated on the assessment criteria of section 3.3.3 are shown in Figure 3.6 and Figure 3.7. Their measurements are shown in Table 3.10.

Table 3.10: Errors of the best features on the test geometries, corresponding to the left-most sub-figures in Figure 3.7.

Geometry	Start error (mm)	Stop error (mm)	Line width error (mm)	Length error (mm)
10 mm segment	0.4	0.16	0.65	1
Pillars	0.2	0.2		-
4 mm segment	1	0.3	0.6	0.8

They were achieved using the following settings:

Table 3.11: Settings for compensation strategies for small features with optimal results

	retraction distance (mm)	extruder forward distance (mm)	coasting distance (mm)	line height (mm)	exp	sample
10 mm segment	1	1	0.5	0.3	1.5	175
Pillars	0.76	0.8		0.5	2.17	227
4 mm segment	1	1	0.5	0.5	5.7	239

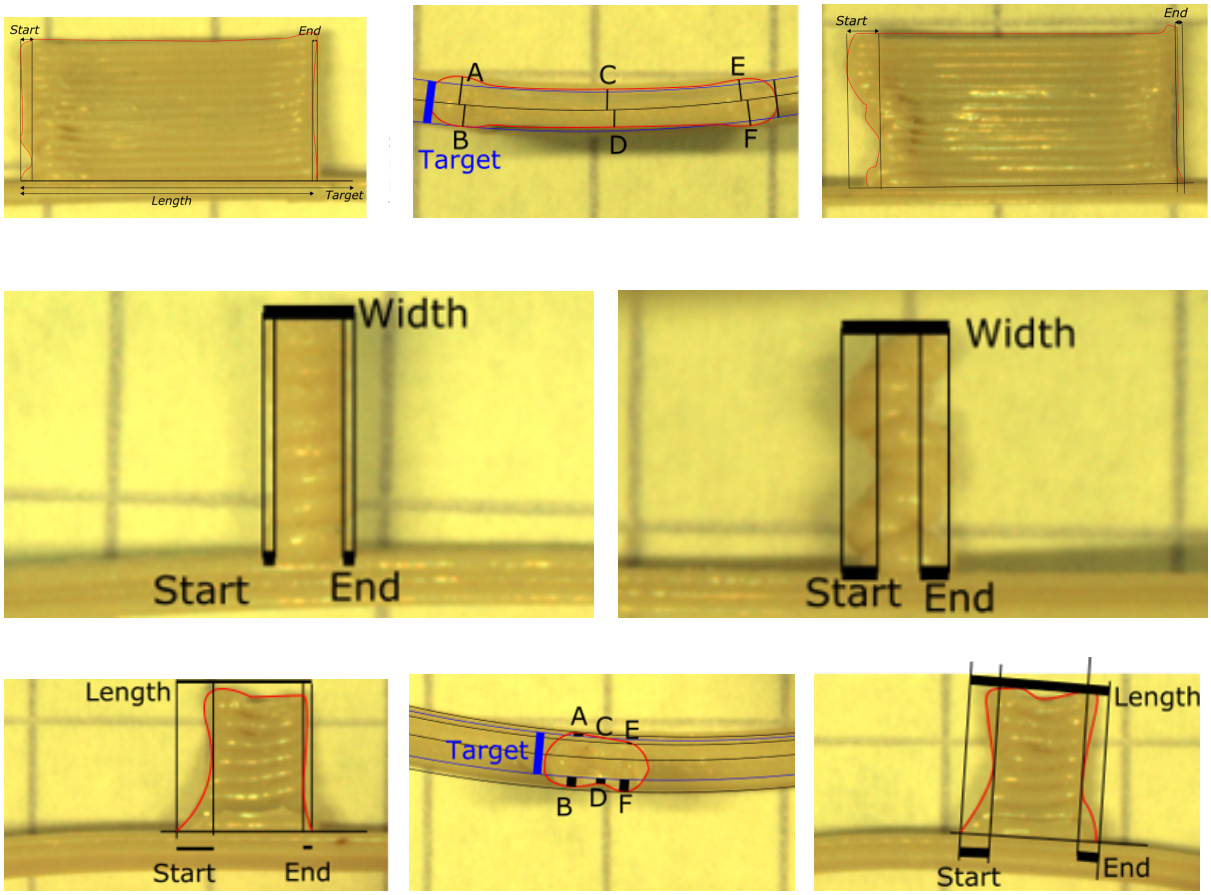

Figure 3.6: Close-up of the best obtained small features. TOP: 10 mm merlons with a line height of 0.3mm, MID: pillars with a layer height of 0.5mm, BOTTOM: 3mm segments with a line height og 0.5mm. The right images show the worst features on the same test object.

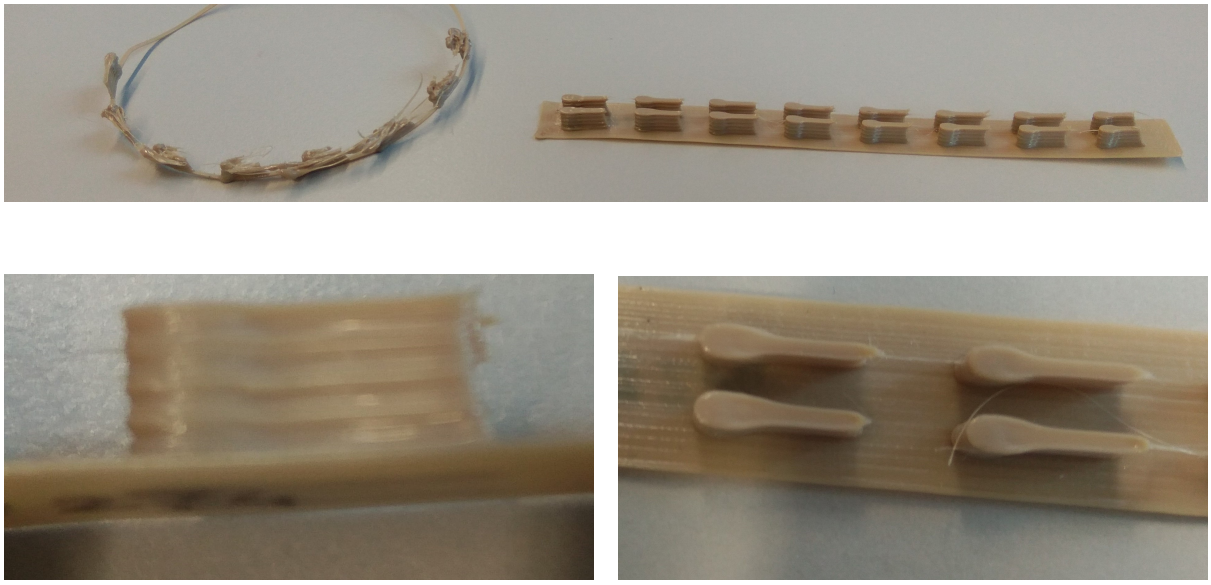

Figure 3.7: Results obtained with the reloop solution concept. No successful printed products have been made on the PoP using the reloop concept. The results on the FeMo satisfy if the criterion is to obtain straight start edges, however the top view shows a large amount of over extrusion at the start.

1. Segments of 10mm The 10 mm segments could be best printed at a line height of 0.3 mm. Coasting prevents material hanging on the nozzle, and it results in cleaner travel and therefore does not form a droplet at the start of the next segment. Coasting for an excessively long distance causes stringing. A coasting distance of 0.5 mm provides the best results.

2. Pillars Pillars could be built by movement to a place and extrude some material (advance of the extruder) and subsequently retract less than previously advanced. Fast travel moves result in a snapping cut. The observed defects were most frequently caused by collisions of the nozzle with the pillar. The bending of the pillars causes an offset in the placement of the new blob from the target location resulting in either an alternation of blobs or in an accumulation of blobs and increasing collisions leading to the same failure mode as shown in Figure 3.2.

A close up detail of the procedure shows that while printing pillars, there is not actually a clean space between the nozzle and the pillar on arrival and during the print, see: Figure 3.8. The substrate layer is pressed firmly by the new layer. A blob forms at the trailing side of the nozzle and as long as contact of this blob with the pillar is prevented there are no problems.

Figure 3.8 shows traces of the layer creation of a pillar. There is not a 'gap' between the pillar and the nozzle tip on arrival. At the end of extrusion (after stage 5) retraction causes the nozzle to move slightly upwards (by design of the printhead) and then snaps away quickly. The surface tension (and elasticity of the material) seem to be responsible for reforming the deposited material to a more drop-like shape. Another observation is that a newly deposited layer squeezes the previous layer slightly. A last observation is that a blob forms on the trailing side of the nozzle. In the case that the blob comes into contact with the pillar, it makes serious distortions to the pillars shape, and may cause a collision with the pillar on the next layer.

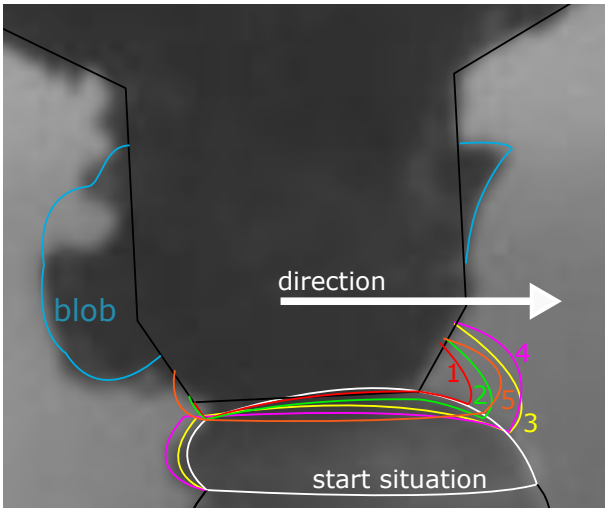

Figure 3.8: Close up of the nozzle while printing pillars. The numbers indicate the progress of the material distribution.

3. Short segments The shortest single wall segments that were achieved had a length of about 4 mm. It was needed to increase the line height to manage this result.

The longer the travel takes, the more material oozes out. The retraction procedure quite slow with a maximum velocity only of only 1.5 mm/s.

3.5 Validation

The intended values were described in section 3.1. The specifications are:

- A line-width of 0.66 mm
- A layer-height from 0.2 mm to 0.5 mm

The acceptable error tolerances:

1. An error of 0.2 mm for the start of the segment
2. An error of 0.2 mm for the end of the segment

3. An error of 0.2 mm for the line width

The obtained results did not meet all of the requirements. Table 3.10 shows the errors. The shortest object possible, a pillar had a diameter of 1.6 mm. The shortest possible segment had a length of 3.8 mm. The segment length for the 10 mm segment was 9 mm.

3.5.1 Discussion

Wiping and coasting settings that are working for a segment of a length of 10 mm for example, do not work for a segment of 4 mm long. The wipes have the disadvantage that they cause process instability: the chance that material sticks to the nozzle and forms blobs, increases heavily.

The coasting approach works very well to decrease the formation of blobs at the end of segments, but calibration is needed to let the segments have the target length.

The reloop strategy is a very good method to improve the straightness of the start at the cost of a drop-shaped top profile.

Retraction is found to be essential to create successful experiments. Retracts succeed in releasing the pressure from the liquefier and is not bothered by the one way clutch mechanism, although a retraction speed of 1.5 mm/s is slow. Higher retraction distance results in a longer duration of oozing. A retraction in the order of 1 mm takes 0.67 seconds and engaging for the same distance takes another 0.67 seconds. This is considerably long when compared to the actual printing of a short segment. (at 6.55 mm/s this takes 0.6 s for a 4 mm segment).

Depressurisation causes the nozzle tip to be lifted slightly and this drags some material at the stop side of a segment. This is an unwanted side effect. The retraction speed could be set to the upper velocity limit of the motor to achieve the best results, the faster the pressure can be released from the feeding material, the better. The snapping of the fast travel move causes a relative clean break between the material on the nozzle and printed geometry. If the distance is too long, it takes too much time to complete this motion, preventing a good snap, since the travel move starts after completion of the retraction move.

The amount of oozing decreases for higher travel speeds. Higher travel speeds and acceleration settings make the machine prone to position lags.

This chapter was a good exploration on the topic of improving accuracy problems. The experimental design of this approach was valuable for the understanding of the system, the relevant variables and its capabilities.

Although it was a satisfactory exploration, the experiments could not be carried out in a robust way:

The test-setup was modified during the tests and in between test series since they were debugged in the same period. Another important factor is that the nozzles had to be interchanged because they became clogged during operation. The heaters were replaced during the test series to allow faster heat up of the nozzle. Black spots of material could disturb the way the product was formed, the purging procedure in advance to each print was able to flush the majority of burnt material out of the nozzle in advance of a print, but sometimes the nozzle had to be replaced because of clogging. Material batches were not documented in this stage of the process yet.

- Burnt material accumulates to internal walls in the liquefier due to the high wall temperature and the sometimes long residence time between experiments.
- Hot material sticks very strong to the brass nozzles causing accumulation of material on the exterior of the nozzle that is randomly deposited.
- In later experiments, such as those described in chapter 5 it was discovered that the actual temperature of the material is not at a stable temperature when the temperature sensor is stabilized on the set point temperature.
- Multiple times during the day, the Z-levelling had to be recalibrated manually.
- The nozzles and nozzle types (conic or straight) were changed within test series (due to clogging).
- The print bed is slightly warped and this additionally causes adhesion problems.
- The printhead prototype used on the PoP has a mechanism that lowers the printhead for about two tenths of a millimetre on pressurisation to prevent collisions in a multi-printhead setup. This mechanism may cause an unwanted lift on depressurisation, pulling material upwards.

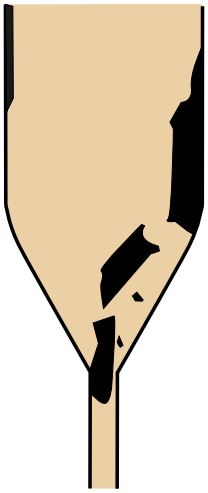

Figure 3.9: Schematic drawing of degradation of the polymer and accumulation of bunt polymer to the wall that causes nozzle obstruction

It is very hard to predict if new experiments conducted with the same settings would lead to comparable results.

The combustion products for burning PEEK (charring) at 450°C are crosslinked PEEK, 1,4-Diphenoxybenzene and 4-Phenoxyphenol (Patel et al., 2010). Since the latter two substances are volatile gasses at the elevated temperature they will cause extra pressure, bubbles and oozing.

These tests were done to actually provide some hypotheses about the printer behaviour and to evaluate in what extent empirical compensations lead to an improvement in accuracy. Especially the last experiment set (short segments) is interesting.

The short segment test showed that the parameters have to be changed specific for each geometry. This is a major defect of this type of compensation, since the intent of 3D printing is to make unique geometries.

3.6 Conclusions and recommendations

In this chapter the following topics were explored:

- Wiping
- Coasting
- Retracting
- Z-lift
- Layer height dependency

The outputs of the experiments in this chapter answer how accuracy could be improved for predetermined geometries, but are not independent of geometry. The approaches used in this chapter are static compensations for dynamic behaviour.

This chapter should be considered as a pilot study: the design of these prototypes enables quick modifications, easy observations and easy user interventions, but repeatability is impossible to ensure. Adapting settings and the application of intuition and observation were used to determine which tests had to be carried out. Therefore only local optima were found.

The results of this chapter show that in some cases good results could be obtained. Proofing principles and proofing the capability of the printer was of much larger importance than ensuring repeatability of the experiments. For Bond3D this was enough for making new plans on feeder design.

This study was a good practical exploration and it provides some information about the factors and disturbances that have a major impact on accuracy. This includes the burning of material, insufficient purging, smearing and collisions.

Other factors that complicate repeatability of the experiments in this chapter are:

- Unawareness of the difference between the motion profiles described in G-code and actual motion: jerk, acceleration and deceleration.
- The absence of an enclosed environment,

- Unawareness of changing conditions over time such as contamination of the nozzle and an expanding print bed,
- The necessary workarounds and manual interventions, such as the removal of purged material at the start of a print using tweezers,
- Ongoing changes to hardware, firmware and G-code generator and absence of a version control system in this early stage,
- Lack of knowledge about factors that influence accuracy,
- Unawareness of the difference between the actual material temperature and the temperature reported by the sensors,
- Limited logging of lab conditions (such as humidity and temperature).

Except for the enclosed environment all of these conditions have improved during the experiments.

The results of this chapter show that by performing tests and examination of the the behaviour it is very hard to make prediction about the results.

The printing conditions are hard to maintain constant and the variables are likely to be interdependent. A model based approach would help. This is done in the next chapters of this thesis.

Chapter 4

Enhancing accuracy by black box modelling of liquefier dynamics

4.1 Introduction to modelling feeder dynamics

This chapter discussed the phenomenon: "Liquefier dynamics" which has been discussed in subsection 2.2.3 on page 31. The goal of this chapter is to find a system characterisation that could be used to design a feed forward controller. The occurrence of feeder dynamics in the Bond3D printing system was discovered during the series of the experiments in chapter 3. The measured line width differs much from the set point line width, see Table 3.10. The G-code was analysed and showed no deviations from the expected result. A test print with two print speeds was made and showed a print speed dependency of line width, see Figure 4.1. The goal of this chapter is to describe how to measure the system's dynamical behaviour and to investigate the extent to which the system can be modelled as a linear dynamical system as the initial goal of this chapter. System identification methods such as step responses and frequency responses can be used to define the system parameters.

The ratio between the velocity of the feeder and the velocity of the gantry (= print speed), here defined as C_1 is fixed with a value of 148.75. This ratio describes the proportionality of horizontal velocity to the velocity of the feeder plunger that pulls the rod when extruding at the `lineheight` and `linewidth` settings of 0.2 and 0.66 mm respectively.

This ratio can be calculated using the following equation:

$$\frac{v_{print}}{v_{feeder}} = \frac{rodArea}{beadArea} = \frac{\pi \cdot radius_{rod}^2}{linewidth \cdot lineheight} \equiv C_1 \tag{4.1}$$

Observations, see: Figure 4.1:

- Thick start of the object.
- Over extrusion at slow printed parts
- Under extrusion at fast printed parts
- Decreasing line width on slow printed parts
- Increasing line width on fast printed parts
- Gap with a strict transition after a change from slow to fast

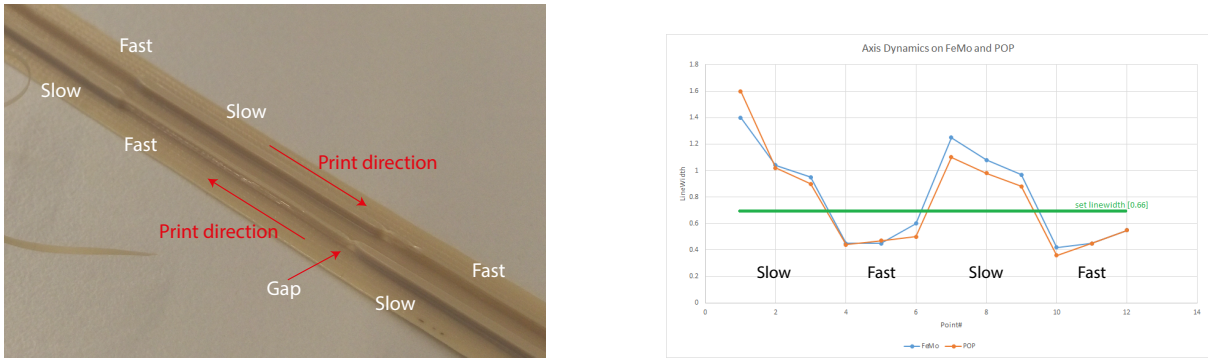

Figure 4.1: The change of line width due to changing print velocity. The intent was to obtain a constant line width. The thick section is printed at low speed, the thin section at high speed. This demonstrates the effect of feeder dynamics. The right image demonstrates that the behaviour occurs both on PoP and FeMo prototypes.

The liquefier is treated as a dynamical system in this chapter. The assumption that the extruded flow and the gantry motion are proportional was proven to be invalid. The response of the flow is much slower than the response of gantry axes, leading to the deposition of the wrong amount of material at the wrong places.

This chapter focuses only on the extrusion in an open space.

4.2 Model

In the case that the dynamic response of the liquefier can be modelled, inherently a compensation strategy could be designed that is applied to either the gantry, the liquefier, or both simultaneously. In the first instance the correction will be applied to the feeder. In later studies, the remaining problem and time lags could be solved by adding additional control to the gantry.

There are two types of behaviour that could be expected to contribute to the system dynamics:

1. The thermodynamics of the liquefier: the heat transport to the material and the volumetric expansion of the material in the liquefier, governed by the equations in subsection 2.2.4. This system can potentially be approached by the model in parallel, shown in: Figure 4.2 (left).
2. The limited mechanical stiffness (compliance) of the rod and the extruder mechanics, and the fluidic resistance of the nozzle. The mechanical system that presses the material through the nozzle restriction acts as a spring and damper in series, see: Figure 4.2 (right).

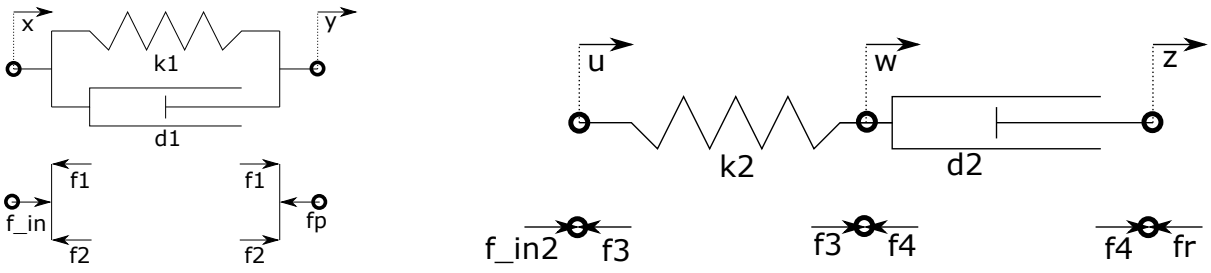

Figure 4.2: Free body diagrams of mechanical analogy of the thermal and mechanical system responsible for the dynamics. Left:thermal, right: mechanical

The models do not include time delays and the thermal and mechanical contribution are isolated from each other. In reality the behaviour is much more complex: the resistance results in a temperature increase and at an increased temperature the viscosity drops, which in turn results in a decrease in resistance.

Although this coupling exists, a first attempt is made to solve the problem without this coupling. If the effects of this coupling are minimal this could result in an adequate but simple solution.

4.3 Method

Using system identification, the coefficients that characterise the system can be obtained and a transfer-function can be found. Using this transfer-function, a compensation strategy can be implemented that could enhance the accuracy of depositing.

Roover (1997) describes two main streams which can be distinguished in the modelling of a system: analytic modelling (white box) and experimental modelling (black box). Contrary to analytic modelling, experimental modelling does not impose any physical structure on the model. Experimental modelling concerns the modelling on the basis of experiments conducted on real systems. The measurements from experimental models relate the resulting model to real life but lack physical interpretation. System identification is generally applicable and the resulting models are well suited for controller design.

Since controller design is one of the purposes, black box modelling was chosen as the approach to enhance accuracy in this chapter.

The steps needed to develop a control approach were the following:

1. Verify parameters in steady-state (What are the errors without considering dynamics)
2. Analyse the dynamical response using a step response analysis. In this case, the step response is the response to a sudden stop of the extrusion velocity.
3. Construct response models in the time domain based on the step response.
4. Analyse the transfer using a frequency response analysis.
5. Construct a transfer function.
6. Construct a control algorithm taking care of the real world physical limitations.
7. Design the control strategy
8. Verify the control strategy

An important characteristic of using this approach is that the system the system is forced to behave in a linear and time-invariant manner. This means that the parameters that characterise the system are independent of the extent of the input. This implies that when an input signal with amplitude A leads to an output signal of A2, and an input signal with amplitude B leads to an output signal with amplitude B2, a signal with amplitude A + B has to lead to a signal A2 + B2. This is also called the superposition principle. Time invariance means that the behaviour of the system does not change with time. (Astrom, 1995).

4.3.1 Verify whether the line width the line width converges to the set point line width

Figure 4.1 shows that there is at least some form of convergence towards the target line width observable. The first step was to find out whether a steady-state error was observable, like Bellini observed, see: Figure 2.7 on page 32. If there is an observable steady-state error, there must be a mismatch between the extrusion rate and gantry motion for which must be compensated.

The required test object to study this behaviour has a cylindrical shape and the motion path follows a spiral path, so there are no discontinuities. The line width of the test object were measured using a caliper.

4.3.2 System identification: step response

In the case that there is no steady-state error, the step response could provide information about the behaviour at a sudden start or sudden stop of feeding. The oozing that occurs as an effect of the relaxing of the mechanics is expected to be dominant during the first five seconds, the slow thermal behaviour is dominant during the rest of the measurement. This slow, thermal behaviour is the scope of this step response experiment. This behaviour is expected to be describable with a first order transfer function.

The following step responses can be proposed:

1. The dynamic response at a sudden start of extrusion from a standstill
2. The dynamic response at a sudden increase of the extrusion rate from a base velocity (as Bellini (2002) conducted)
3. The dynamic response at a sudden decrease of the extrusion rate. (to observe any asymmetry)
4. The dynamic response at a sudden stop of a continuous extrusion to a standstill (This demonstrates the effect of oozing, without retraction)

In the case that the system elements are considered as linear and time-invariant, (which we do in this chapter, see discussion), it implies that there is no asymmetry and the response reaches a final position when

the time is infinity long. In the case that the amplitude at the input is doubled, the amplitude of the output also doubles (superposition principle). Under this assumption, there would not be a difference in the outcomes of the listed step response experiments for finding the characterisation parameters.

The step response experiment that was chosen to conduct was number 4: measuring the time-based development of the length of the oozed material strand.

The oozing length was measured as a function of time. The was conducted as follows, see Figure 4.3:

- A camera was fixed at the height of the nozzle, with a view perpendicular to the oozing strand.
- A measurement grid was calibrated by filming a ruler as reference.
- Filament was extruded at a continuous rate for a sufficiently long time to reach the steady-state
- The material strand was suddenly cut-off with a pair of tweezers and the extrusion was stopped at the same time.
- The video was played back frame by frame, the position of the fluid front coming from the nozzle and time were logged.

The experiment was repeated for four continuous print speeds. [50, 20, 12.2 and 2] mm/s,

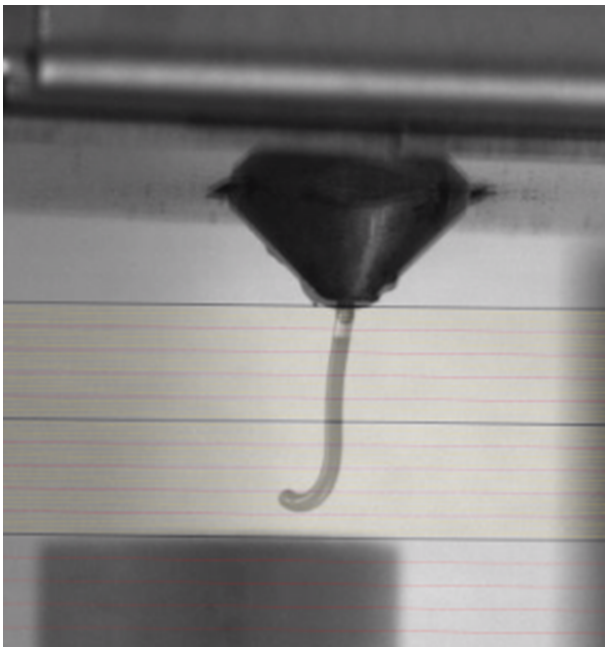

Figure 4.3: Measuring oozing by observing the development of oozing length after a sudden stop. (Step response measurement)

The step response was suitable to analyse the slow, thermal behaviour with a time constant in the order of magnitude of seconds. The approach is not capable of measuring the response during the first second of oozing accurately, because of the limited frame rate of the camera (30 FPS) and the manual stopping and cutting procedure. The cutting of the strand was used as the visual trigger to zero the time. This approach does consider the system in open-air extrusion, which is practical for observation purpose.

4.3.3 System identification: frequency response analysis by measuring line width.

- A frequency response was used to characterise the response for a broader bandwidth and, more important, during actual printing conditions.
- The pressure situation in the liquefier that drives the oozing in free space is caused during the printing process. An important difference with the open air pressure situation is that during actual printing, the substrate acts as an extra force that impairs extrusion.
- The pressure that settles in the liquefier was higher during actual printing than during printing in open air.

Frequency response method A frequency response experiment was carried out in the following way: in the PLC real-time controller a sine wave was added to the position of the extruder axis based on the rotary position of the print bed, see: Equation 4.2.

$$feederoffsetposition = A \cdot \sin(N_{sines} \cdot rotaryaxis.position) \tag{4.2}$$

With $rotaryaxis.position$ in radians.

The PLC system uses set point positions for the location of the plunger. The PLC system is designed with a set of axes that are coupled to eachother, such as a G-code axis, a jogging axis and an offset axis. $feederoffsetposition$ is the position of the plunger on the offset axis. A is the amplitude of the applied sine function. $Nsines$ is the number of sines that occur in one full rotation. Since we want to measure the width of the line, this must be a natural number.

The line width is measured after completion of the test shape, using a calliper. The measurements are obtained at a 90 degree offset from the nozzle. A systematic error would occur if this nozzle was not calibrated. The nozzle was positioned by aligning it with a marking on the object, jogging the axis with 90 degrees and centring the caliper at this marking. The first quarter of collected measured data points are moved to the end, to make the first data point appear to be directly under the nozzle.

- There will be a drop in magnitude: while the target line width would have an amplitude of 1.3 mm for example, the measured line width would have an amplitude of 1 mm for an input frequency of 0.5 Hz for example.
- A phase shift: if the input line width is compared with a function of the output line width, a shift in phase would be noticeable.
- Optionally: a delay, that may be constant in time or not.

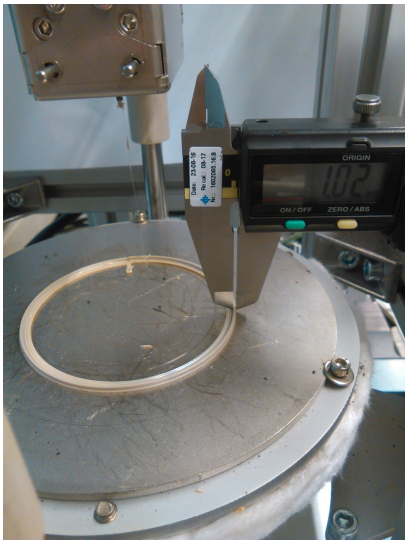

Figure 4.4: Frequency response measurement setup: measuring line width using a clamped caliper.

Although an excitation on the velocity of the feeder would have been directly proportional to the set point line width, the PLC software works by specifying position set points. The set point line width as a function of time is given in: Equation 4.3.

$$linewidth_{object} = linewidth_{gcode} - \frac{\pi \cdot A \cdot N_{sines} \cdot radius_{rod}^2 \cos\left(\frac{N_{sines} \cdot t \cdot v_{print}}{radius_{object}}\right)}{lineheight_{gcode} \cdot radius_{object}} \tag{4.3}$$

Table 4.1: Units of the oscillation parameters in Equation 4.3

Parameter	Name	Value	Unit
$linewidth_{object}$	Target line width	-	mm
$linewidth_{gcode}$	Average target line width	0.66	mm
$radius_{object}$	Radius of the total object	35	mm
$radius_{rod}$	Radius of the feeding rod	2.5	mm
$lineheight_{gcode}$	Layer thickness of the object	0.2	mm
v_{print}	Linear velocity of the bed directly under the nozzle	See: Table 4.2	$\mathrm{mm/s}$
A	Amplitude of the oscillation	See: Table 4.2	mm
N_{sines}	Number of oscillations in a full rotation	See: Table 4.2	$-$

The parameters are selected by taking the following into account:

- The input sines are chosen that a complete number of sines, fits within one full rotation of the build plate.
- And the velocity of the feeder does not overshoot the limit value of $1.5\,\mathrm{mm/s}$.
- The long residence time at slow print speeds requires that the temperature for 1mm/s experiments needs to be set to 410 °C and for 2mm/s to 430°C, while the other experiments are executed at a set point of 450°C.
- The upper limit is given by the fact that the amplitude of the response should be measurable using a caliper and be bigger than 0.05 mm.
- The number of measurements is chosen to at least prevent aliasing and to provide more than enough data points for a data fit.

- This experiment allows studying the bandwidth between 0.10 and 10 Hz.
- It is not possible to find a frequency response for a single print speed, but for low frequencies small print speeds have to be used and for high frequencies fast print speeds have to be used.

The experiment specific inputs shown in Table 4.2:

Table 4.2: Frequency response experiment design

Experiment#	N_{sines}	A	v_{print}	$n_{measurements}$
0	1	0.1	2	40
1	3	0.08	10	40
2	1	0.25	5	40
3	2	0.13	40	40
4	5	0.05	50	40
5	1	0.24	1	40
6	1	0.24	100	40
7	1	0.24	10	20
8	2	0.12	2.5	40
9	2	0.12	5	40
10	6	0.04	5	72
11	3	0.08	40	20

1. The line width was measured, see Figure 4.4 for equal distributed discrete steps in a full rotation. The order was randomised. The rotation axis could be jogged to the required positions using the GUI. A clamped calliper was used to measure the line width. The number of measurements per test object was chosen to be high enough to prevent aliasing. (more sines per rotation require more measurements)
2. Using a least-square fit to a sine function, see Appendix E, the amplitude and phase of the output were calculated, see Figure 4.5.
3. By comparison with the set point line width sine function, the magnitude drop and phase shift were calculated and visualised in a bode plot.

Using a least squares fit algorithm for sines, see Appendix E, a function for the output can be obtained. An example is shown in Figure 4.5. The results can be displayed and analysed in a bode and phase diagram.

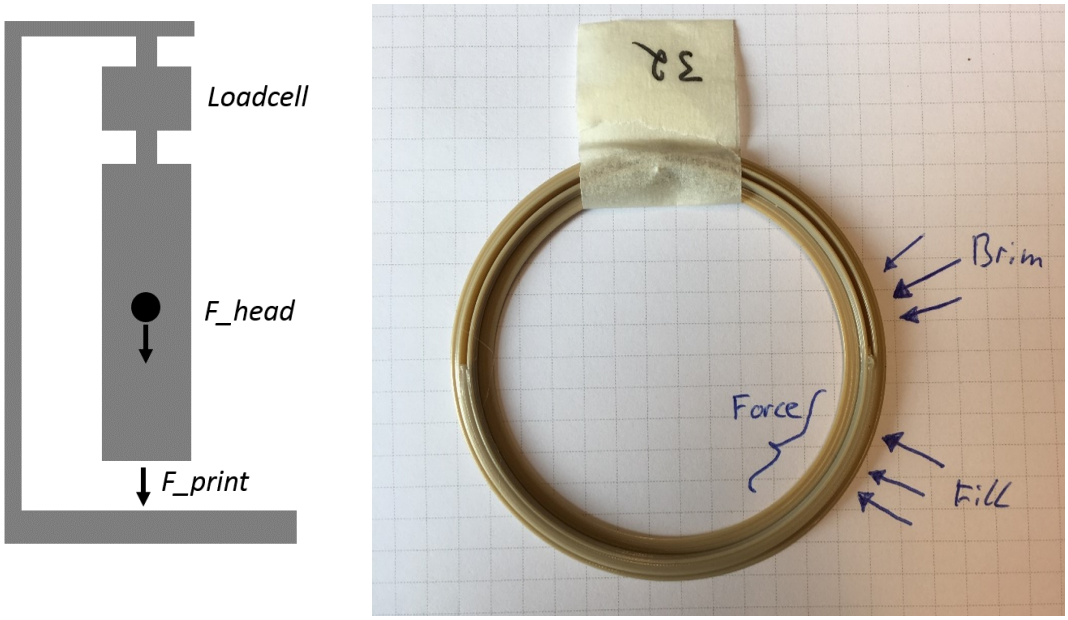

Figure 4.6: Force frequency response setup (left) and test geometry (right)

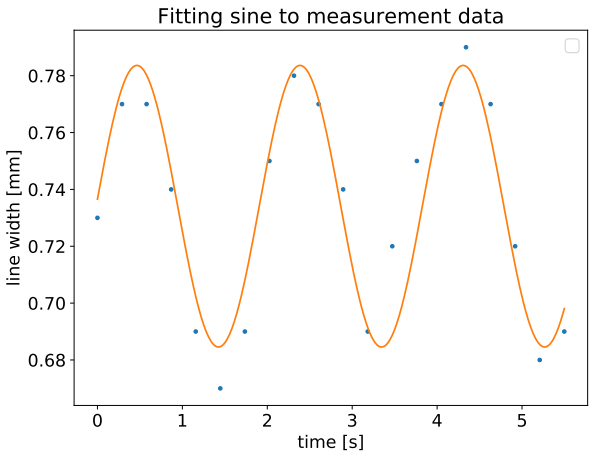

Figure 4.5: Procedure of fitting a sine to the measurements. This procedure was repeated for each test object.

Frequency response by measurement of printing force A likewise approach in which a force measurement was conducted by a colleague. The results of this test could be used to verify the results from the other test. Instead of measurement of the line width using a caliper, the system a force measurement using a load cell, see Figure 4.6. The transfer of the force could be measured during printing in a narrow channel, see Figure 4.6,

4.4 Results

4.4.1 Steady-state error

The steady-state error is insignificant: ultimately the system converges to the target line width, the error was smaller than 0.02 mm for all measured printing speeds.

Figure 4.7: Obtained geometries after long continuous printing at different printing. This tests confirms convergence to set point of 0.66 since all geometries have ultimately the same line width.

4.4.2 Step response

The model described the amount of oozing material at a sudden stop. In other words, it directly describes the error. This model has to be derived from a part of a step response, since the data points at low values of the time are dominantly influenced by the mechanical compliance of the rod and are hard to measure using the used setup. The values at a high values of t are influenced by gravity and probably gaseous combustion products.

Burchett (2014) describes an approach to estimate a transfer-function, but requires steady-state values to be available for estimation of the gain and the dead time of the system. The described log-incomplete response, is useful to find estimates of the values of tau that could be loaded into an algorithm that optimises a fit function to the measured approach. Niemann and Miklos (2014) describe an approach to find a transfer-function if a part of the step response is known. This approach is used in the analysis of the step response in this chapter and was used to find the models that are shown in Figure 4.8.

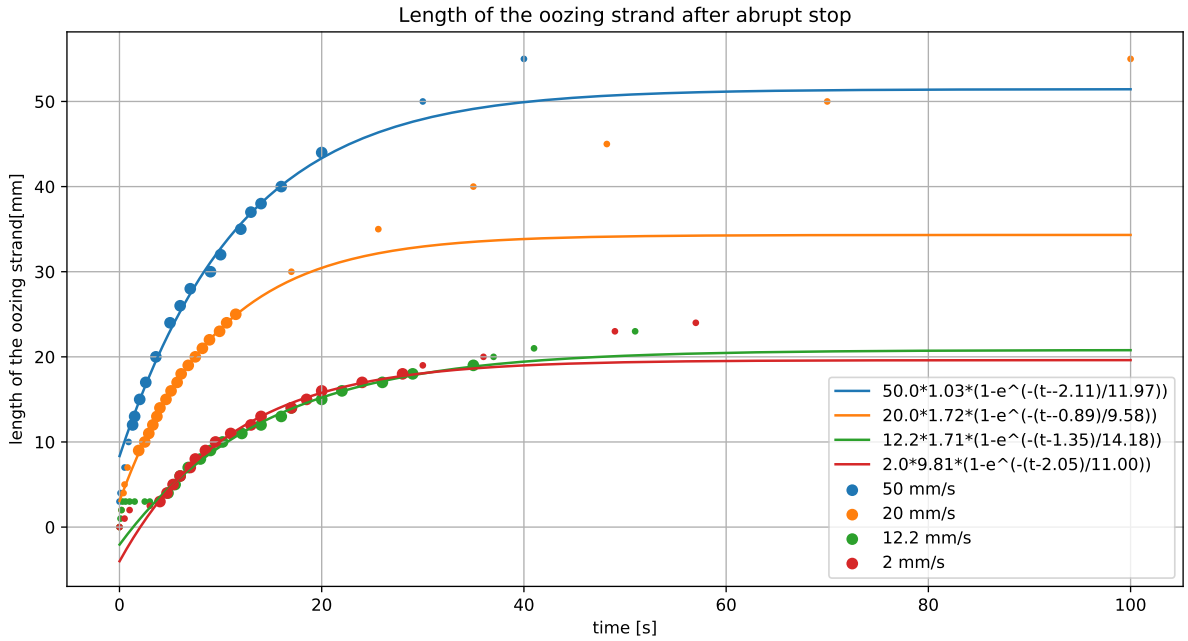

Figure 4.8: Step response of oozing in open air using a 0.6mm nozzle for different values of steady-state v_{print} with a line width of 0.66 mm and line height of 0.2 mm. Logarithmic models were fit to the data in the form: $y = v_{print} \cdot k \cdot (1 - e^{-(t-t0)/\tau})$. Points at the start and end are not taken into account for model constitution, here displayed as small dots.

Transfer-function models have to be found for t between 1 and 20 seconds of the experiment. The gain and the dead time should be independent of the input velocity in the case that the system is linear. This will not be the case in this analysis, hence the step response is not normalised to a unit step response.

Figure 4.8 shows the measured step response. At the start the position was not accurately measurable and due to small curling, the true length of the strands may have got a systematic error of 3mm. Also the stopping of the extrusion and the cutting of the filament may introduce an timing error of about 0.5 s.

The script that was made to find the transfer models by extrapolation used the log-incomplete response described by Burchett (2014), see: Equation 4.4 to calculate estimates of τ. The high linearity of the graph, see: Figure 4.9, shows that the behaviour in the selected region behaves well according the linear transfer-function model.

$$Z = \log\left(\frac{y - y_{ss}}{y_0 - y_{ss}}\right) \tag{4.4}$$

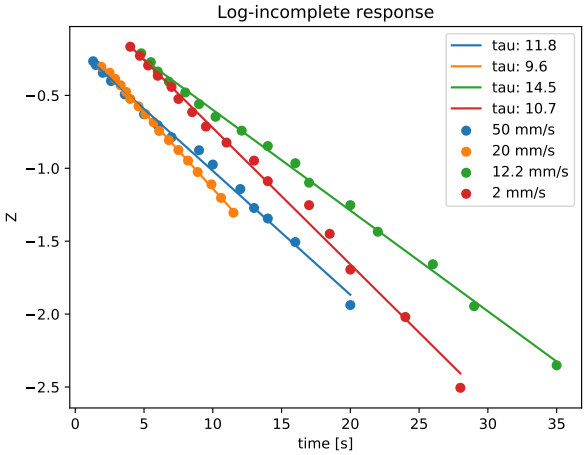

Figure 4.9: Log incomplete response plot used to find estimates of tau. τ =-1/slope. The final models in the transfer-function are slightly different to force slightly better model fits.

Model: The following response describes the behaviour in the time domain, with The oozed length $y(t)$ as the response:

$$y(t) = v_{print} \cdot k \cdot (1 - e^{-(t-t0)/\tau}) \tag{4.5}$$

The model parameters are shown in Table 4.3.

Table 4.3: Model parameters

v_{print} [mm/s]	$k[\frac{\text{mm}}{\text{mm/s}}]$	τ [s]	t_0 [s]
50	1.03	11.97	-2.11
20	1.72	9.58	-0.89
12.2	1.71	14.18	1.35
2	9.81	11.00	2.05

It can be seen that each transfer-function has different model parameters for each value of v_{print}. The strange thing is that some models required to set the time delay to a negative value. This makes no sense in real world. Probably it would have been better to set the initial condition to a value higher than zero. This would be a vertical shift of the graph, instead of horizontal. This suggests that the system is not linear or not time-invariant, or none of both. It is possible to construct a transfer-function for a given average input speed, but its validity needs to be evaluated. Since no accurate data for the time delay is available, the time delay is not further used in the analysis.

The general form of the first-order differential equation is:

$$\tau \cdot \frac{dx}{dt} + x = k \cdot y \tag{4.6}$$

Assuming that all initial conditions are zero and after the Laplace transformation the transfer-function becomes:

$$G(s) = \frac{x_{feederexpand}(s)}{v_{feeder}(s)} = \frac{x_{ooze}(s)}{v_{print}(s)} = \frac{k}{\tau s + 1} \tag{4.7}$$

Where values from Table 4.3 for k and τ can be inserted. x_{ooze} is the distance that the material oozes in open-air at a sudden stop. v_{print} is the velocity of the gantry. $x_{feederexpand}$ is the virtual distance that the feeder plunger would have to travel to ooze the amount of material that actually oozes. v_{feeder} is the (continuous) velocity of the feeder plunger, proportionally to the print speed. τ and k are the system's dead time and gain respectively.

4.4.3 Frequency response

Figure 4.10 shows the set point line widths that should be expected when applying the signals from Table 4.2 on the position of the feeder. The response is plotted in Figure 4.12. The label indices correspond with the indices in Table 4.2.

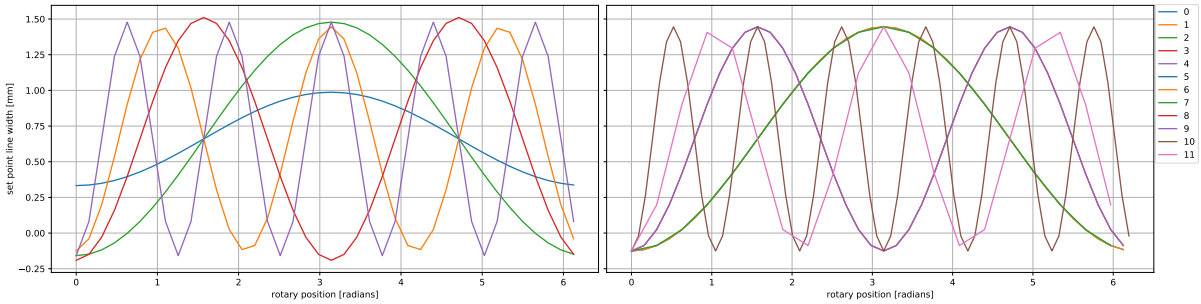

Figure 4.10: Set point line widths (split into 2 graphs for convenience, 0-5 left, 6-11 right). (6 and 7 are directly on top of each other). Note that the line width is negative for some of the oscillations that suggest that the target line width would have a negative value. This does not have a physical other than a very slight retraction of the feeder. For this analysis this is not a big issue, since a high amount of damping is expected.

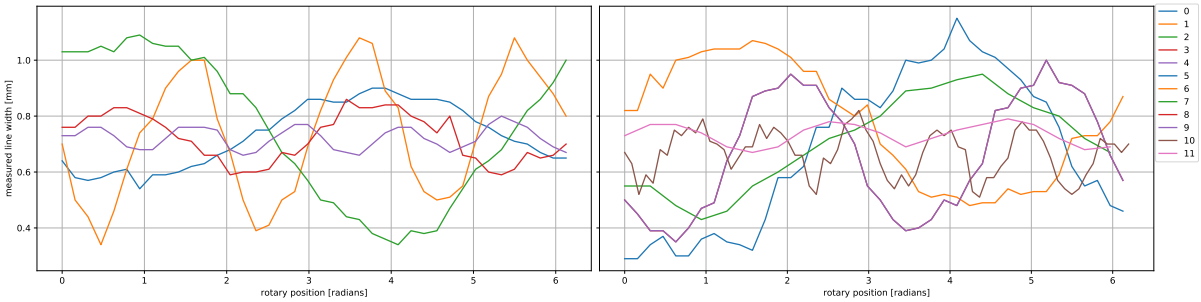

Figure 4.11: Measured line widths (split into 2 graphs for convenience, 0-5 left, 6-11 right)

Bode plot The measurement outputs can be converted back to the time domain by using the print speed. A table was created that contains columns: time, target position, and actual position for each experiment, see Appendix D. Sine fits were made to both the target and actual position and the phase shift and the ratio between the amplitudes was calculated for each experiment.

The colleague that measured the force response, constructed his script but the results are comparable, as can be seen in Figure 4.12. The results of the experiments executed at 1 and 2 mm/s were dropped since they were executed at other set point temperatures and cannot be compared with the other data points.

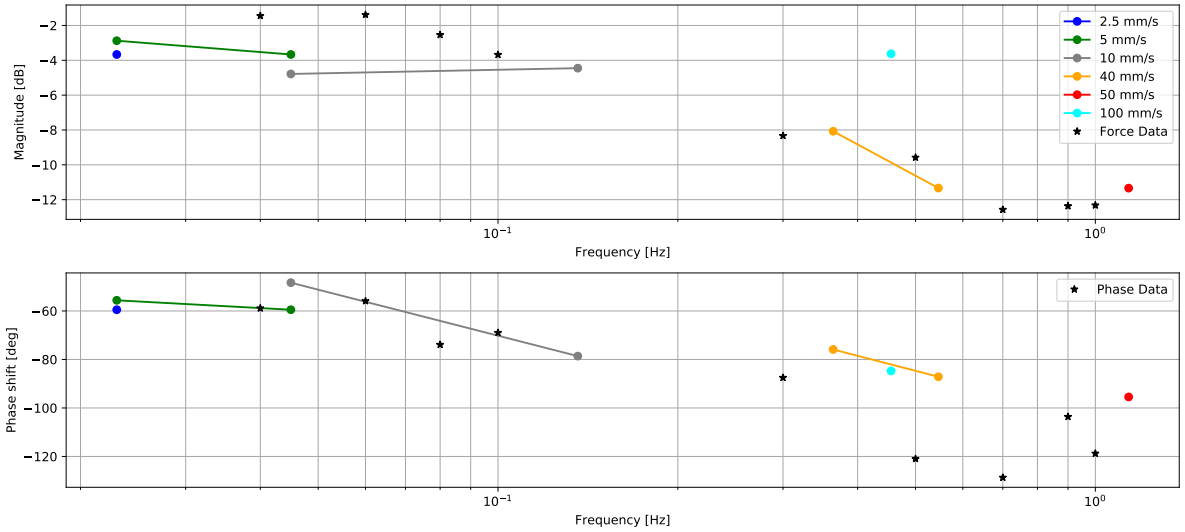

Figure 4.12: Bode plot showing the measured frequency response. This plot relates excitation on the set point line width to the measured line width. Even at low frequencies the phase shift is high and this complicates model construction.

Transfer function model estimation from the frequency response The high value of the phase shift at low frequencies makes it not feasible to fit the model to both the magnitude and phase data. The phase shift data seems to be at a vertical offset, but it could not be found how this could happen. It is suspected that this has to do with the non-linearity of the system, that was already shown in results shown in Table 4.3.

The actual implementation of the control system is a business secret of Bond3D. Therefore it has been chosen to describe this implementation on a separate lay-in sheet, that will not be part of the digital report.

4.5 Validation

Assumptions about the system's behaviour have been made in this chapter. The system seems to have much higher complexity than the behaviour that can be modelled with linear time-invariant transfer-functions. The behaviour of the system has actually been measured and the step responses seem to be able to at least be able to describe the behaviour after an abrupt stop for a given input velocity.

It is possible to find good fits with a first-order transfer-function model, however some horizontal shifting was needed which also required some time shifts. Negative time shifts are strange. In the case that the model would be extended to also contain a vertical shift this would mean that the system would have a start position offset. This is something that might have returned more realistic results. The system is not a linear system since this would have resulted gain and tau values that would have been equal for all measurements.

This suggests that for different (average) print speeds different values of tau and gain should have to be found if the method is valid.

The approach was validated by implementing the control algorithm in the PLC software and running experiments on the test shape shown in Figure 4.14.

Implementation of the control strategy showed good results, but the gain had to be increased for a print speed of 12.2 mm/s. (to a value of 5) The value of τ was also altered, but the results showed that a value of 12 resulted in the best prints.

The results of the frequency response were compared with the results from a study of a fellow researcher who measured the reaction force, as described in section 4.3.3, to verify the measured results. These measurements were performed on another prototype with a similar design, by another researcher and another data interpretation method. The data could be regarded as being highly correlated to the coloured points, although a more scientific analysis would be needed to judge on this more accurately. The frequency response analysis is validated for that reason.

Validation of the implemented control algorithm leading to improved accuracy A control strategy has been implemented, based on the theory and measurements from this chapter. For confidentiality reasons,

this cannot be fully elaborated in this report. The examination board was provided with a confidential inlay. The final result is shown in Figure 4.13.

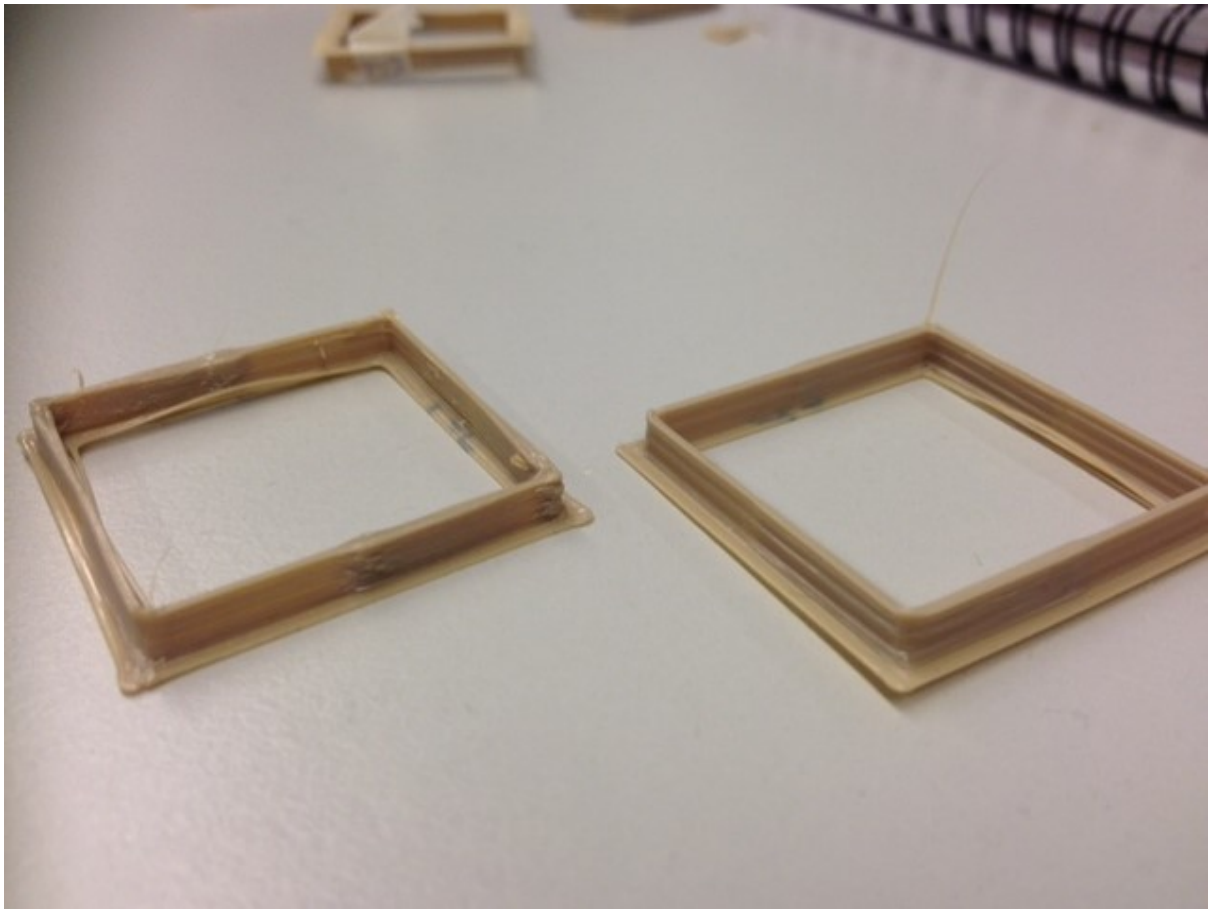

Figure 4.13: Comparison of improved accuracy with a deactivated controller (left) and activated controller (right) printed on the FuMo. The geometry was a 30 by 30mm square where the print speed was alternated between 20 and 4 mm/s. It is observable that the line width is much more constant with an activated controller. A close up of the object with an activated controller is shown in Figure 4.14

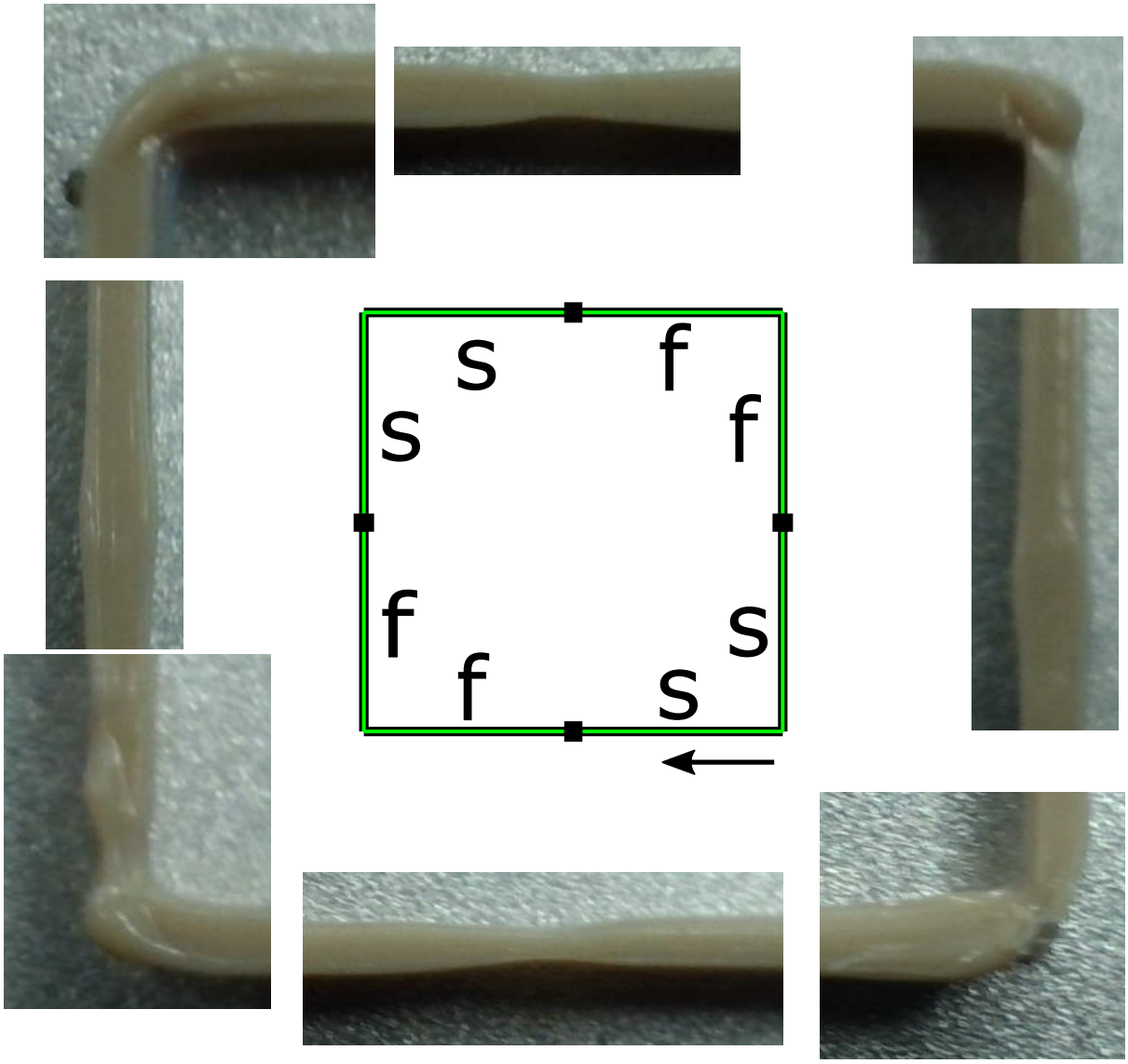

Figure 4.14: Close up of the improved geometry that shows that object with an activated controller still deviates from a square with a constant line width. S=4mm/s, F=20mm/s. The small deviations from the target line width while changing the velocity, proves that the method is correct for print speeds up to at least 20 mm/s.

4.5.1 Discussion

The step response measurement approach is interesting but limited to describe the slow thermal effects. The measurement scale does not allow to capture the fastest material at the beginning, although this could have been captured by using a high-speed camera. The measurement scale of the used camera is not suitable to register the fast extrusion right after stopping the extrusion and by using a manual cutting procedure.

Curling and sticking of the material to the nozzle further complicate the analysis. The lack of observable final steady-state values further complicates the analysis. Gravity and emission of water vapour and other combustion products could have caused that oozing does not seem to end within the time scale of the experiment.

A very important factor is to determine if the step response measurement matches with the actual printing conditions and this is a major factor: in real printing conditions, the pressure situation settles for the situation where the substrate layer works a normal force that increases the restriction value during printing and this normal force disappears when the nozzle moves to a place without support. The frequency response was a measurement of the transfer during an actual printing process, but this process did not include the sudden disappearance of supporting layers.

Table 4.3 demonstrates that different models need to be obtained for different input velocities and that

the system is not linear or time-invariant. It requires to be further analysed using a white box approach to draw better conclusions.

Not all inaccuracy is caused by the dynamics that were described in this chapter. The previous chapter showed that there are much more defects, including pulling of the nozzle, shrinking and sagging defects.

A problem is that the system does not have all the sensors, therefore the temperature of the material may have been different for each experiment. The thermal distribution in the liquefiers varies with flow rate.

It would have been better to complete the experiments with new, unused nozzles since later insights revealed that the nozzles that were used wear over time since burnt material accumulates to the wall of the nozzle, see Figure 3.9 on 58. This has had its impact on the fluidic resistance and is a typical example of a factor that compromises the time-invariance assumption.

Another factor that compromises the time-invariance factor is that the rod is consumed over time and this changes the compliance of the system. This is further elaborated in chapter 5.

The data collection using the measurements with the caliper is acceptable, but not suitable for frequencies higher than 1 Hz and lower than 0.01 Hz and is limited to full waves per rotation. This manual approach is pretty labour-intensive. It would be better to cancel out the print speed dependency, although this would probably require spirals with much bigger perimeters to keep a satisfying measurement resolution and this cannot be done on the used PoP setup.

The understanding of the system is not yet conclusive: The step response experiment showed that some unknown time-delays were needed to actually make the data fit and the frequency response analysis seemed to be unsuitable to approach with linear components due to the high phase shift at low frequency. A linear time delay could be the initiator of this problem, but the effect of a delay term would be a slope in the frequency plot, instead of an offset. The offset could also be print speed dependent. Print speed dependency could be motivated for two reasons:

- Change of the average material temperature for different print speeds
- The resistance of the nozzle in steady-state in the relation $P_{plunger}/Q_{out} = R_{fluidic}$ is not a constant. This is probably caused by shear thinning.

The motor used in this prototype is a limiting factor since the motor's velocity and torque limit the rate at which the D-action could function. For higher printing speeds, where bigger D-actions are required, a stronger motor is required.

4.6 Conclusion

Two approaches to determine the dynamics of the system were constructed in this chapter and a first compensation approach was obtained. The frequency response measurement was validated by comparing the response using a force-based approach and returned similar results. The method seems to be an adequate method to find a compensation strategy in a structured way.

The measurement approaches were satisfying methods to find data about the dynamics of the system, but can be improved. The approach demonstrates the major problem and forms a good base for a better design of control strategies. This chapter revealed a lot of insight about the actual behaviour of the system and a first attempt for a control strategy that made use of the step response model was provide. The frequency response model shows that further study is necessary to improve the model and adequacy of the controller.

4.6.1 Recommendations

It would be useful to use an automatic cutting knife to enhance the measurement accuracy for the step response. This could be synchronised better to the stop of extrusion. With more accuracy on the actual stop moment, it would be possible to estimate the time delays and find a transfer-function in the form:

$$H(s) = \frac{k \cdot e^{-sT_D}}{\tau s + 1} \tag{4.8}$$

Using a function like the Matlab feature `tfest` it would be possible to find a model directly from the measurement data and to design a better control algorithm.

Sets of similar experiments without changing the print speed within that experiment set should be conducted to find different transfer-functions for different base print-speeds. This would probably lead to better (print speed dependent) control parameters.

It would be valuable to find control parameters from an automatic calibration procedure. The approach that measures the force, could be used to automatically find a frequency response model. Further study is necessary to bridge the gap between the transfer-function and appropriate control parameters.

The implemented control strategy acts on the feed rate. The feeder can act slower than the gantry could possibly do. It would make sense to actually apply the a share of the open loop control strategy to the gantry, for example, the time delay.

The approach was a black box approach. That implies that despite the behaviour can be measured, modelled and controlled, the causes are still unknown. A white box approach would probably reveal more in-depth information about the system. This is what's done in the next chapter.

Chapter 5

Enhancing accuracy by analytic modelling of a liquefier

5.1 Introduction: White box model of steady-state liquefier behaviour

A black box model of the liquefier was obtained in the previous chapter. It was shown that controller design by using models of the dynamics makes sense and that adequate controllers can be developed that enhance the performance. The control approach did not take care of the physical nature of the device. Models were solely based on observations. The problem is that the black box model helped to find a control approach that compensates for the error, without taking care of the actual problems. The model does not provide information about the physical causes that could be used in improvement of the design. The behaviour of the system is not linear and not time-invariant. This limits the control method to work only within a small bandwidth of print speeds. The goal is to gain understanding about the system characteristics that contribute to the non-linearity of the system, to improve the system's accuracy. This chapter provides system characteristics of the Bond3D printing system that are of interest for the development of more advanced models, including numerical models.

The actual implementation of a more advanced controller is not within the scope of this master thesis, however the model is verified by measurements.

The physics of the liquefier are further studied. They include: mechanical compliance, a pressure drop that is dependent on print speed and temperature and thermal behaviour and expansion. The components have already been described in the literature section and are applied to the Bond3D printing system in this chapter.

5.2 Model

The literature section described that the following topics are relevant for modelling:

- The stiffness of the material and the system
- Thermal development and expansion
- Non-linear pressure-flow dependency

A graphical overview of molecular behaviour is shown in Figure 5.1. It shows shear thinning and molecular orientation that is responsible for die swell.

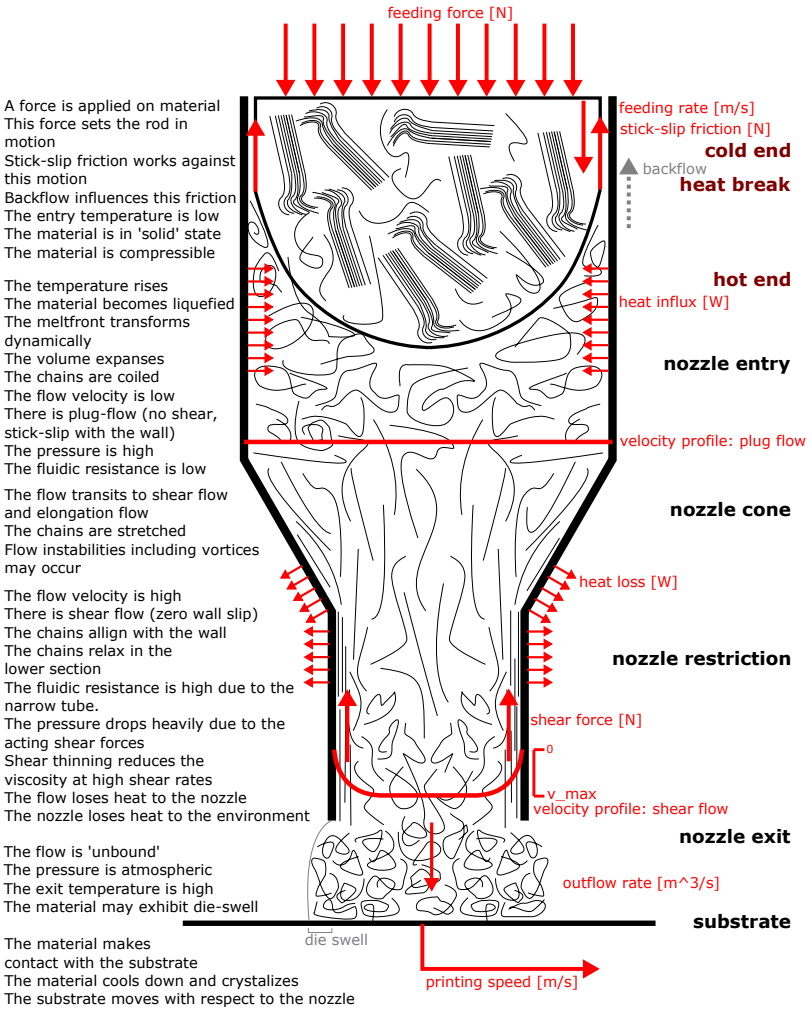

Figure 5.1: Schematic drawing of the liquefier, showing the straightening and tangling of the molecules. When the molecules are not restricted by the wall anymore, they return to their tangled configuration. The feeding rate is provided in $\mathrm{m/s}$ since the displacement of the feeder is controlled. It is proportional to a feeding flow rate by a factor of $19.63\,\mathrm{m}^2$.

5.2.1 Modelling the stiffness of the rod and the system

The stiffness of the rod and the system is graphically represented in Figure 5.1. See Figure 5.3 for a drawing on scale.

Impressibility of the feeding material and the changing stiffness due to varying length are suspected to be the main influence factors for non-linear liquefier dynamics. Shear thinning causes varying restriction for the flow through the nozzle tip.

The stiffness consists of two contributors:

- The base stiffness of the mechanics of the system. This includes bending of the pusher and lead-screw. Any backlash is assumed to be negligible.
- The stiffness of the rod varies with the plunger position due to consumption of the material. For the rod based system this is a good assumption.

Governing equations for the liquefier's column stiffness load case.

The force-displacement relation for a column (truss) with a load is given by the linear expression:

$$F = \frac{AE}{L}u \tag{5.1}$$

Where the term $\frac{AE}{L}$ is defined as the stiffness k, see Equation 5.2. The length L is not a constant in the Bond3D situation. It varies while printing due to consumption of the material.

$$k \equiv \frac{AE}{L} \tag{5.2}$$

The difference in length between relaxed and steady state printing u can be calculated if the force F would be known. This force can be calculated from the pressure drop in the liquefier using Equation 5.3.

$$F = PA \tag{5.3}$$

This pressure drop P is calculated in subsection 5.2.3.

Table 5.1: Stiffness model parameters

Variable	Unit	Description
E	Pa	Young's modulus of the material
L	m	The total length of the column when not subjected to a load
A	m^2	Area of the column
F	N	The load force
u	m	Displacement (The difference in length between unloaded and loaded condition).
P	Pa	Pressure drop in the liquefier

Model of the column stiffness and the effect on oozing in the Bond3D printing system

The length of the column varies during printing in the Bond3D system. Therefore L has to be replaced by $L = f(V)$, a linear function that describes the length of the column as a function of the total amount of consumed volume. Two rods are placed inline with each other in the system that make that the column length varies between 100 and 200 mm, see Figure 5.3.

Since the radius of 1 rod is 2.5 mm and length is 100 mm, the volume of material rod is $100\mathrm{mm} \cdot \pi \cdot (2.5\mathrm{mm})^2 = 1964\mathrm{mm}^3$. This volume is observable as the period in the saw-tooth function.

This saw-tooth function has the following properties:

- For $V = 0$, it has to have a L of 200 mm.
- The period needs to be equal to the total volume of a rod, V_{rod}
- When a rod is fully consumed, $L = 100$.

This function can be described with the following Python code:

```
from scipy import signal
import numpy as np
import matplotlib.pyplot as plt

def f(V):
    """Returns the length of the column as a function of consumed volume"""
    L_max=200 #mm [Maximum column length]
    L_rod=100 #mm [Length of the rod]
    A_rod=19.63 #mm [Area of the rod]
    V_rod=L_rod*A_rod #[Volume of a single rod]

    return (L_max-0.5*L_rod)-(0.5*L_rod)*signal.sawtooth( 1/V_rod * 2 * np.pi * V) #mm
```

The Youngs modulus of the hot melt pool is simplified to be equal to the one of the solid rod at 23°C. The exact size of the melt pool is not known but would be small compared to the total column length. The Youngs modulus of the material at 23 °C is used since no better alternative could be found in the literature. The real temperature for the largest part of the column would not exceed 130°C. This temperature is below the 1.8 MPa heat deflection temperature (152°C) and below the glass transition temperature (143°C). Therefore the elastic modulus value at 23°C is likely to be equal for all temperatures between 23-130°C for PEEK.

The stiffness k has a hyperbolic relation with the length L, see Equation 5.2.

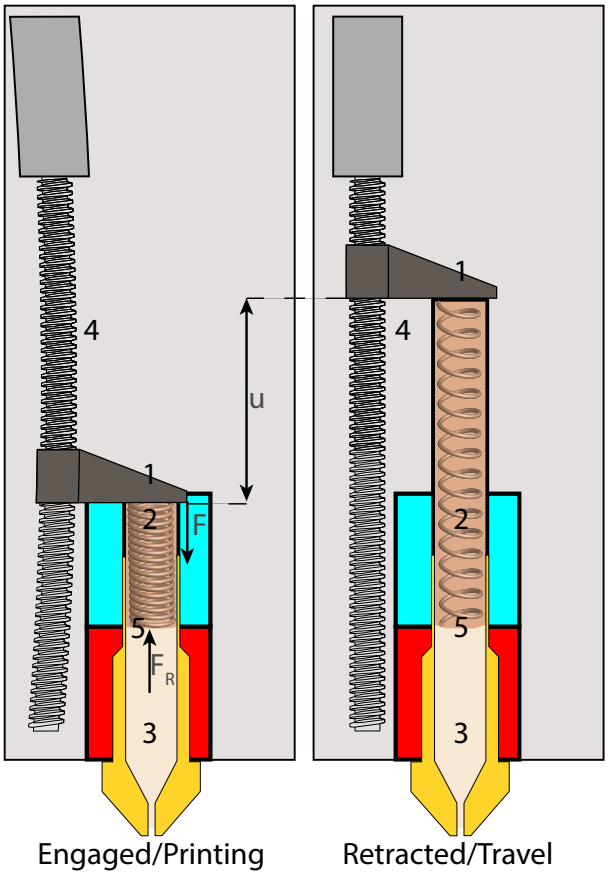

Figure 5.2: Exaggerated close-up of the compliance of the system. The total column(2) has a length difference between loaded (left) and (relaxed) condition (right) of u. The force $F_{plunger}$ that acts on the rod by the plunger(1) that occurs when extruding is responsible for this difference. In steady state situation this force is equal to F_R. The relaxed situation(right) is the situation in which all dynamic effects have settled and the plunger does not put any force on the material anymore and all oozing has stopped. The bending of the feed screw is just for illustration. In the analysis it is assumed to be insignificant compared to the compliance of the column. The drawing is not on scale, for better proportions see: Figure 5.3

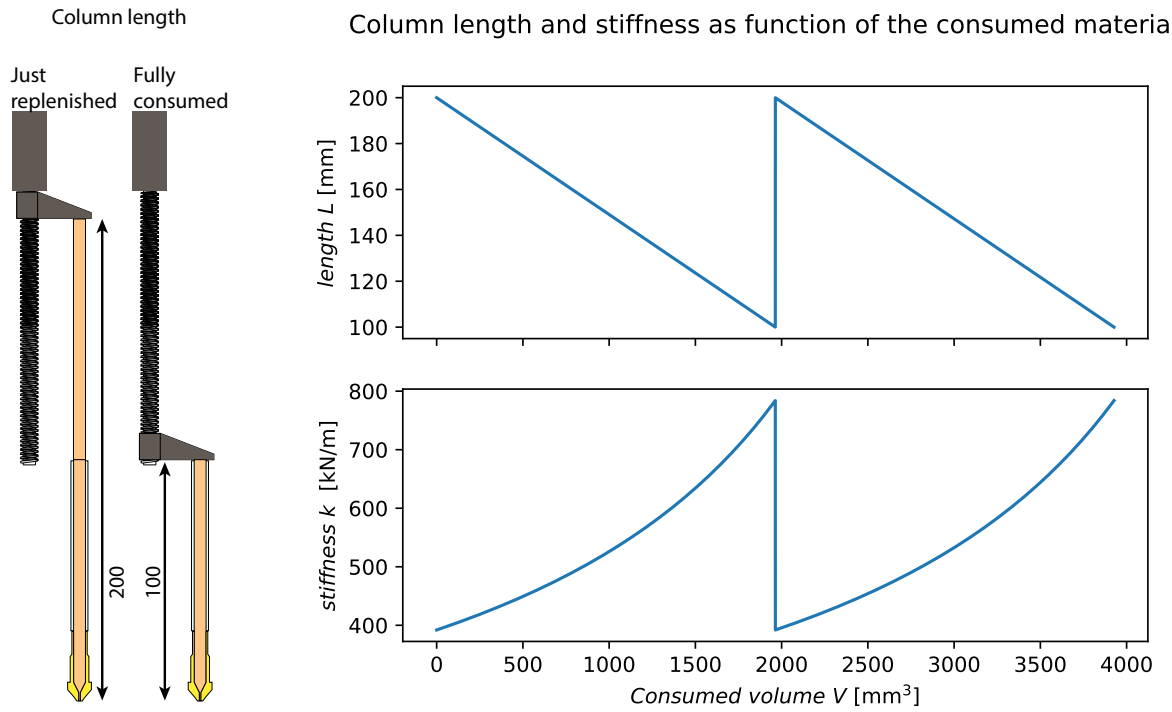

Figure 5.3: Column length and stiffness as functions of the consumed material volume for the Bond3D system, in unloaded conditions. Note the hyperbolic dependency of the stiffness on the volume, caused by Equation 5.2.

Table 5.2: Stiffness model values for the Bond3D system

Variable	Value	Description
L(V)		Total column length as function of the amount of extruded volume, see Figure 5.3.
k(V)		Stiffness as function of the amount of extruded volume, calculated with Equation 5.2.
E	$4 \cdot 10^9$ Pa	Young's modulus of PEEK at 23°C.
L_{rod}	0.1 m	The length of a rod
L_{max}	0.2 m	The distance between the plunger and the nozzle
V_{start}	0 m^3	The amount of material that is extruded before the start of the print job
A_{rod}	$1.96 \cdot 10^{-}5\text{m}^2$	Area of the rod

Table 5.3: Nozzle geometry, see: Figure 2.4 at page 26 for corresponding figure.

nozzle	d [m]	D [m]	α [rad]	L [m]
'default'	$0.6 \cdot 10^{-3}$	$5 \cdot 10^{-3}$	$30/180\pi$	$4 \cdot 10^{-3}$
'small'	$0.47 \cdot 10^{-3}$	$5 \cdot 10^{-3}$	$30/180\pi$	$2.66 \cdot 10^{-3}$

The real pressure drop is discussed in subsection 5.2.3. With hindsight obtained from Figure 5.10, the pressure is about 5 MPa for average conditions when using the regular nozzle. The exit fluid flow rate in this case is 3 mm^3/s the actual temperature is 405°C.

The force F applied by the plunger in this situation is $F = PA = 5 \cdot 10^6$ Pa $\cdot\, 1.96 \cdot 10^{-5}$ m^2 $= 98$ N. The displacement u can be calculated by substitution of the force F and the stiffness k in Equation 5.1. With a known displacement it is possible to calculate the maximum oozable volume and the length of the material strand that would be oozed in open space, see Equation 5.4, and Equation 5.5.

$$V_{ooze} = u \cdot A_{rod} = u \cdot 19.63\text{mm}^2 \tag{5.4}$$

$$L_{ooze} = u \cdot \frac{A_{rod}}{A_{nozzle}} = u \cdot \frac{19.6\text{mm}^2}{0.28\text{mm}^2} = u \cdot 70 \tag{5.5}$$

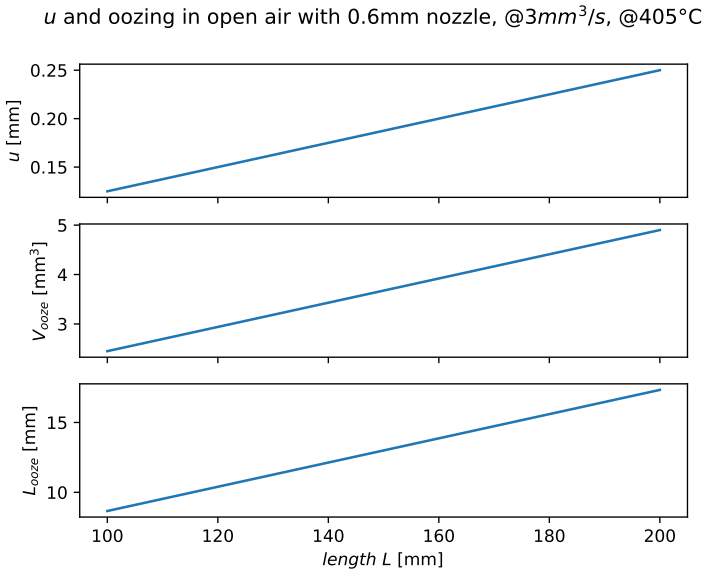

Figure 5.4: Model of the displacement of the column u, the total oozable volume V_{ooze} and the ultimate length of the oozing strand L_{ooze} dependent on the length of the column in the relaxed situation. Full relaxation of the column is assumed. The model applies to oozing from an abrupt stop from $3mm^3$ at an outflow temperature of 405°C. This model only covers the contribution caused by the mechanical compliance of the material column.

The model describes that the total pure mechanically caused oozing can have a maximum length between 8.5 and 17.5 mm and is dependent on the position of the plunger in the relaxed situation. It expects that the fluid restriction remains constant. The restriction is expected to increase for lower flow rates in the real situation.

5.2.2 Thermal development

The volume of the melt pool changes by thermal expansion additional to the change of the rod length over time.

An estimation of the maximum thermal effect on oozing can be made: the maximum size of the meltpool can be guessed based on the placement of the heat break. After a (very) long pause, all material below the heat break will approximate the wall temperature T_{wall}, which is the temperature that the build-in thermocouple tries to measure. Let's call the volume below the heat break $V_{meltpool,max}$.

If the temperature of the outflow T_{out} for a given print speed can be measured it is possible to calculate $T_{diff} = T_{wall} - T_{out}$. When this difference is multiplied with linear thermal expansion factor and the maximum volume of the melt room, the maximum value of the thermal oozable volume can be calculated. This relation was given in Equation 2.29 on page 35.

$$V_{ooze,thermal} = T_{diff,max} \cdot \alpha_V \cdot V_{meltpool,max} \tag{5.6}$$

From section 2.2.4 it is known that for PEEK $\alpha_V = 140 \cdot 10^{-6}\mathrm{K}^{-1}$.
For Bond3D's liquefier $V_{meltpool,max} \approx \pi \cdot (2.5\mathrm{mm})^2 \cdot 20\mathrm{mm} \approx 400\mathrm{mm}^3$.
For a guess value $T_{diff} = 50\mathrm{K}$,

$$V_{ooze,thermal} = 50\mathrm{K} \cdot 140 \cdot 10^{-6}\mathrm{K}^{-1} \cdot 400\mathrm{mm}^3 \approx 3\mathrm{mm}^3 \tag{5.7}$$

This volume would result in an oozing strand with a length of:

$$L_{ooze,thermal} = \frac{3\mathrm{mm}^3}{19.63\mathrm{mm}^2} \approx 60\mathrm{mm} \tag{5.8}$$

A FEA model would provide more accurate estimates.

5.2.3 The pressure drop dependency in the liquefier

Four tasks need to be executed in order to find the pressure drop model for the liquefier:

- Find the range of shear rates in which the liquefier operates.
- Find power law coefficients.
- Constitute the model by insertion of the power law coefficients and geometry in the pressure drop model of Boles and Bellini's pressure drop model.
- Simplify the model.

In subsection 2.2.1 two models were described for the pressure drop in a liquefier. These models both require a power law viscosity models. The paragraph also showed a Cross-WLF viscosity model for PEEK. The main difference with the power law model, is that it has a bend in the log-log plot of the shear rate $\dot{\gamma}$ against the shear stress τ, see Figure 5.8. The power law model is a straight line. The Cross model can cover a wide range of shear rates, including shear rates close to zero. At low shear rates, the fluid is just a Newtonian fluid. The power law cannot model the viscosity for low shear rates, since the shear rate versus viscosity plot has a vertical asymptote, that models the viscosity to be infinity.

The power law model would approximate the behaviour at a satisfying level in the case that the shear rate to determine the power law coefficients match the shear rates that occur in the 3D printing process. The power law coefficients are defined for a region (of shear rates), the so called power-law region, see Figure 5.6.

Determining the wall shear rate

The shear rate depends both on the distance from the wall in the nozzle, as well as the print speed. The material in the inner-core shears less than the material close to the wall. The shear rate is also low for low print speeds and conversely.

The shear is zero on the vertical centre line of the thin section of the nozzle. The wall shear rate is the highest shear rate in the 3D printing process. The value can be calculated with Equation 5.9 according (Steffe, 1996, p. 102).

$$\dot{\gamma}_w = \frac{3n+1}{4n} \cdot \frac{4Q}{\pi \cdot R^3} \tag{5.9}$$

This formula includes the power law exponent n, that is not yet determined. For the calculation of Figure 5.5, a guess value of 0.55 was used and the figure is plotted for several radii.

The shear rate is not likely to exceed $950\,s^{-1}$ for the flow rate conditions in which the Bond3D system operates.

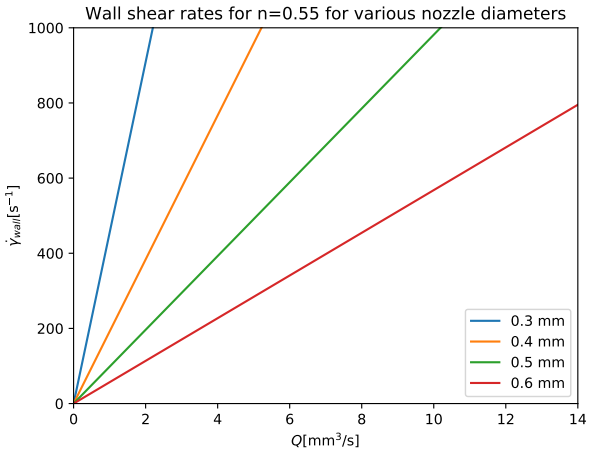

Figure 5.5: Estimates of the wall shear rate for two nozzle diameters.

Power law viscosity model of PEEK suitable for extrusion based printing

3D printing with PEEK takes place in the transition region from Newtonian behaviour towards shear thinning behaviour, see Figure 5.6. This makes the determination of proper power law coefficients a little more challenging.

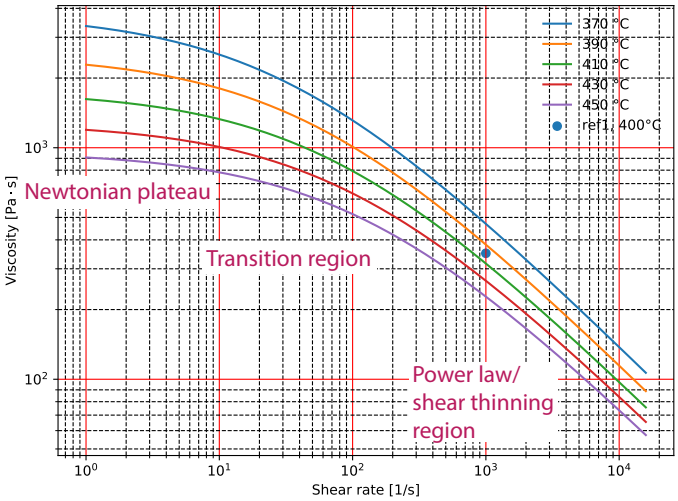

Figure 5.6: Cross-WLF viscosity model of PEEK 450G. The left-most section is called the Newtonian plateau, the rightmost is the shear thinning region, and the bending section is the transition region. The data was derived from Solidworks 2018. The reference point was taken from (*VICTREX® PEEK 450G*, 2017)

The further from 0, the better the viscosity can be described with the power law model. Since the 3D printer operates in the transition region, low shear rates have to be included. This makes that the overall model accuracy is a bit lower, but the applicability a bit larger.

It was found that for PEEK in the 3D printing process, a linear fit in the log-log plot for the region between $600\,s^{-}1$ and $950\,s^{-}1$ can cover most of the behaviour. It should be mentioned that the system can be used also for lower shear rates.

The fitting was done as following: First a function for the Cross-viscosity model was obtained, see Equation 2.15 and Equation 2.17 with the values of Table 2.4 on page 30. A base-10 log-space range of shear rates between the lower and higher limit was generated and the shear stresses were calculated. A linear fit was made. And the coefficients were determined: $k = 10^{intercept}$, and $n = slope$.

This was repeated for a number of temperatures, see section 5.2.3.

A comparison between the obtained power law model and the Cross model is given in: Figure 5.7.

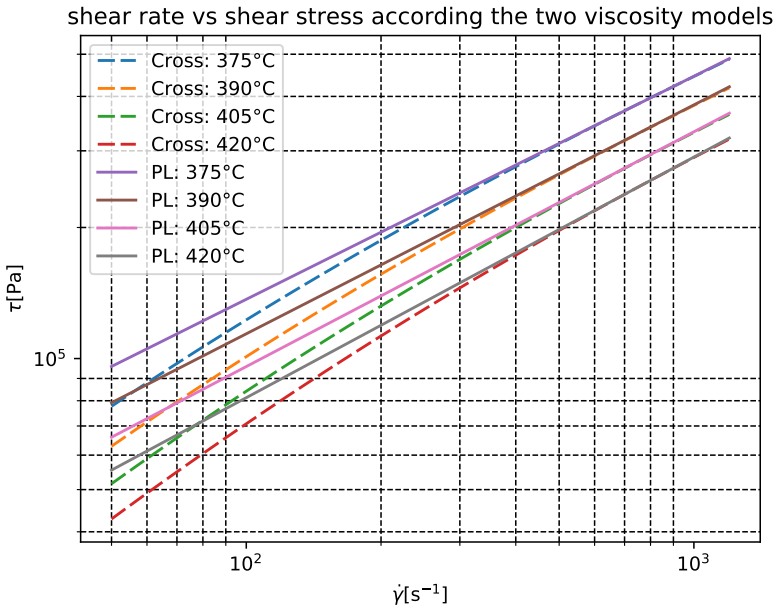

Figure 5.7: Rheogram of the obtained power law model in comparison to the Cross model for PEEK 450G.

It can be observed that the power law model is not an accurate model at low shear rates when compared to the Cross model, but at the higher shear rates (starting at about 250 s^-1) the model does a good job.

Temperature dependency of the power law coefficients for PEEK

Mackay and Bellini used ABS, well defined in the shear thinning region from a shear rate of 80 s^{-1}. For such a power law model with pure shear thinning behaviour, only k changes for changing temperature. This can be an Arrhenius or WLF factor $a(T)$ that is multiplied with a value of k given at a reference temperature.

In the transition region, n has to have a dependency on temperature either to make a good fit. The values for temperature versus k and n are given in Equation 5.10 and Equation 5.10 and shown in Figure 5.8.

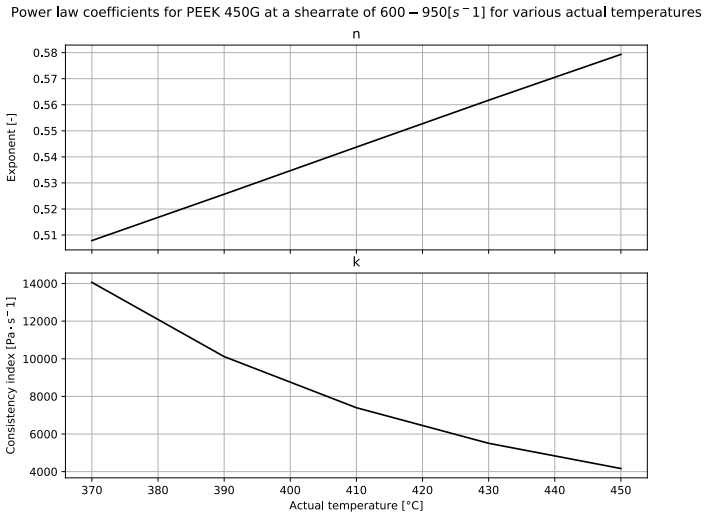

Figure 5.8: Power law coefficients for PEEK 450G for a shear rate of 600 s^{-1} to 950 s^{-1} for a range of temperatures.

The temperature dependent power law coefficients, obtained from the linear fit to the log-log plot of shear rate versus shear stress, can be described as functions. n is a simple linear function: $n = intercept + slope \cdot T$, and k is linear in the base-10 log-log plot of T versus k and becomes $k = 10^{intercept} \cdot T^{slope}$ for the fit in the log-log plot. The temperature has to be provided in °C, since they were plotted in degrees Celsius in Figure 5.8.

$$k(T) = \frac{1.395 \cdot 10^{20}}{T^{6.223}} \tag{5.10}$$

$$n(T) = 8.956 \cdot 10^{-4} T + 0.1765 \tag{5.11}$$

The power law that describes the shear stress as a function of shear rate for PEEK 450G is:

$$\tau(\dot{\gamma}, T) = k(T) \cdot \dot{\gamma}^{n(T)} = \frac{1.395 \cdot 10^{20}}{T^{6.223}} \dot{\gamma}^{8.956 \cdot 10^{-4} T + 0.1765} \tag{5.12}$$

with T in °C, $\dot{\gamma}$ in S^{-1} and τ in Pa, it is plotted in Figure 5.7.

Calculation of the pressure drop by filling in the Boles equation

The values of Table 5.3 and Equation 5.10 and Equation 5.11 were substituted into the Boles equation, see: Equation 2.6 on page 28. The mathematical expression is too large to be comprehensible and the resulting expression would be hard to validate. Therefore it is chosen to provide the result as a simple Python function. A plot of this function is shown in Figure 5.10.

```
import sympy as sp

def getPressureFuncFromSymbolicBoles(geometry,kAndNFunctionsOfTemperatureAsStrings):
    P,T, K, n, Q, a_T, alpha, d, l=sp.symbols('P T K n Q a_T alpha d l')
    bolesEquation = 1.18 * K * a_T * n**(-0.7) * (8 * Q * (3 * n + 1) / (sp.pi * d**3 * n))**n + 2 * K * a_T *
     ↪  (3 * sp.sin(alpha) / (4 * n * (-sp.cos(alpha) + 1)**2 * (2 * sp.cos(alpha) + 1)))**n * (8 * Q * (3 * n
     ↪  + 1) / (sp.pi * d**3 * n))**n / (3 * n * sp.sin(alpha)) + 4 * K * a_T * l * (8 * Q * (3 * n + 1) /
     ↪  (sp.pi * d**3 * n))**n / d
    c=bolesEquation.subs(kAndNFunctionsOfTemperatureAsStrings).subs(geometry).subs({a_T:1})
    return sp.lambdify([Q,T], c) #Returns a function that takes Q and T and provides the pressure drop.

geometry={'name': 'regular', 'alpha': 0.5235987755982988, 'd': 0.0006, 'l': 0.004}
kAndNFunctionsOfTemperatureAsStrings={'K': '10**20.14448225350382*T**-6.2288201451850265',
 'n': '0.17651020236319326+T*0.0008956157030695386'}
 pressureFunction=getPressureFuncFromSymbolicBoles(geometry,kAndNFunctionsOfTemperatureAsStrings)
```

.

Simplifying the pressure drop equations

For better understanding the complicated expression given in the previous paragraph, it was chosen to calculate an approximation. This approximation has the following shape:

$$\Delta P = G(T) \cdot Q^{m(T)} \tag{5.13}$$

where

$$G(T) = A \cdot T^{B}$$

$$m(T) = C + D \cdot T$$

- $G(T)$ is the intercept in the $\log Q \log \Delta P$ plot.
- $m(T)$ is the slope in $\log Q \log \Delta P$ plot.
- A, B, C, D are constants that can be calculated by fitting to data obtained from the Boles model.

For the Bond3D printer situation studied in this report using the regular nozzle:

$$\Delta P_{0.6nozzle} = 3.325 \cdot 10^{13} \cdot T^{-5.012} \cdot Q^{0.176 + 0.000895 \cdot T}$$

For the small nozzle:

$$\Delta P_{0.47nozzle} = 1.349 \cdot 10^{13} \cdot T^{-4.867} \cdot Q^{0.176 + 0.000896 \cdot T}$$

Where the units are in $\mathrm{mm}^3/\mathrm{s}, \mathrm{MPa}$, °C for Q, ΔP, and T respectively. These models relate the temperature and volumetric flow rate to the pressure drop over the liquefier in steady-state.

The model applies to volumetric flow rates in the region of $1 \cdot 10^{-9}$ to $10 \cdot 10^{-9}$ m^3/s and temperatures between 360 and 450 °C. The model is less accurate for low flow rates since the shear rate is low in that case. For low shear rates the power law is inaccurate.

5.3 Method

Two types of measurements have to be performed to study the pressure drop:

- Measurement of the pressure drop.
- Measurement of the temperature of the material.

Ideally, both measurements should be performed for all set point temperatures and volumetric flow rates that occur in the 3D printing process. Ideally both measurements should be performed in open air (The situation during oozing) and during printing (Pressure buildup situation).

To prove the model, ideally different nozzles configurations are necessary.

This study would become overly complex and would take too much time, hence the reduction to the following minimal test:

- For 3 printing speeds, the required force was measured while extruding in steady state, for 3 different wall set point temperatures. The measurements were done with a load cell.
- The actual temperature was measured with a thermal camera.
- This was done using the 0.6 mm nozzle and was repeated for the 0.47mm nozzle.

The difficulty is that the liquefier is a closed system. The temperature is hard to measure. An approximation is assumed to be observable with a thermal camera (Optris PI 640), pointed directly to the nozzle tip. This limits the test to extrusion in open air. The camera is aimed at an angle perpendicular to the material flow that leaves the nozzle, see Figure 5.9.

Using a load cell directly applied between the plunger and rod, the force is measured while the extrusion rate is set to a continuous velocity. The experiment is repeated for different print speeds and for different liquefier set point temperatures and for two different nozzles. This force is multiplied with the area it acts on to find the pressure.

Figure 5.9 shows the used setup.

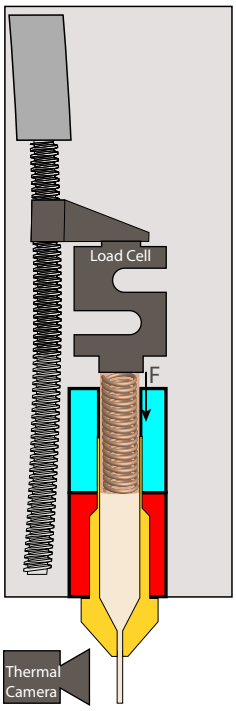

Figure 5.9: Measurement of the pressure drop and outflow temperature

Note: the volumetric flow rates (Q) of the measurement points have to be calculated from the set point feed rate (v) by the use of a scaling factor. This was done using: $Q\ [\mathrm{mm^3/s}] = \mathrm{v\ mm/s \cdot A\ [mm^2]} \cdot \mathrm{F\ [-]} = \mathrm{v\ [mm]} \cdot 20.5\ [\mathrm{mm^2}]$ Where A is the area of the rod and F the thermal expansion factor see: Equation 2.29 on page 35. The precise temperature is unknown. All data points are processed using the same thermal expansion factor: $F = 1.044$. This may introduce a volumetric flow error of about 0.6% in the most extreme cases (370°C and 450°C), which is small but worth to mention.

5.4 Results

Results were obtained using the described method. The steady-state pressure measurement results are shown in Figure 5.10. The steady-state temperature of the extruded material for two different nozzles with equal geometry is shown in Figure 5.11.

The temperature drops down at flow rates higher than 7 mm^3/s. The actual temperature of the material extruded with the Stavax nozzle is close to 405 °C within the tested range of flow rates.

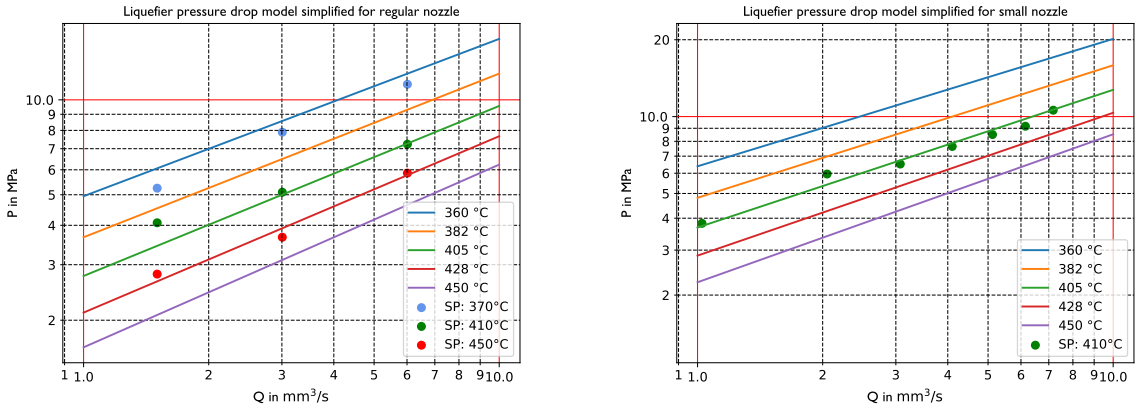

Figure 5.10: Comparison of the pressure drop model and measurements on a log-log scale, using a 0.6 mm nozzle at 1.5, 3 and 6 mm^3/s (left) and right: log-log scale plot of the pressure model and pressure measurements on a set point temperature of 410 °C, using a 0.47 mm nozzle

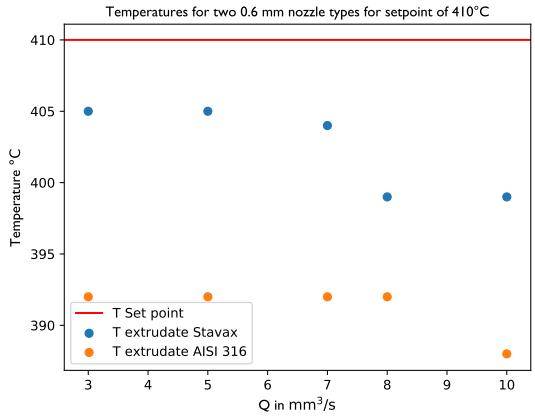

Figure 5.11: Actual temperatures of the outflow material, observed using a thermal camera (Optris PI 640), for a set point temperature of 410 °C. For a Stavax nozzle and for a AISI 316 nozzle with a diameter of 0.6mm. In this chapter, Stavax nozzles were used to determine the pressure drops. In the previous chapters, AISI 316 nozzles were applied.

5.5 Validation

The stiffness model and thermal development were not validated in this analysis. However quick comparison with Figure 4.8 on page 67 shows that they are of the same order of magnitude as those responsible for the step response.

The steady state pressure drop dependency was validated: From Figure 5.10 it can be observed that the actual temperature of the material is about 405 °C for a set point temperature of the wall of 410 °C. Figure 5.10 shows that the measured points are situated on the 405 °C line for both nozzles. This demonstrates that the pressure measurements confirm to the model within the measured range of flow rates.

For higher flow rates, the temperature drops down. At higher volumetric flow rate the heaters have to provide more work to reach the same temperature.

Bellini's model underestimates the pressure drop when the same power law coefficients are used as those applied with the Boles model. Bellini's model has to be shifted upwards in the logarithmic QP plot to make the model agree with the measurement results. This could be done by multiplication of the obtained pressure drop by a factor of 1.5. In Appendix J both models are shown.

The Boles model agrees with the measurement data.

5.5.1 Discussion

The model seems to be more accurate for the higher than for the lower flow rates.

The thermal resistance of the material will become a more dominant factor at higher volumetric flow rates (or shorter liquefiers). The decrease of the actual temperature would lead to a higher pressure drop.

At low flow rates (flow rates that lead to a wall shear rate below $200\,s^{-}1$, see Figure 5.5), the power law model has a larger deviation from the Cross model. The theoretical viscosity will be higher than the actual viscosity, resulting in a larger pressure drop. By looking at the graphs of Figure 5.10 this is not observable. More data points at low flow rates would be necessary to study this effect.

This could also be caused by the fact that the lower shear rates were measured first and that the temperature had not achieved a steady-state. This would result in a higher viscosity and a higher pressure drop value.

The number of measurement points should have been larger for all the experiments for judgement on the scalability to other higher or lower temperatures.

(Kwon et al., 1986) states that the Boles model assumes purely viscous flow and does not consider normal stresses that have a larger contribution at high flow rates and large converging angles.

The flow rates are low, resulting in low shear rates. The model performs excellently at the largest measured points.

Bellini's model does merely consider shear flow and does not consider the effects of elongation flow and this may result in the underestimation of Bellini's model by a factor of 1.5 for the Bond3D system.

In this study, a lot of exponential relations were studied. When these relations are fit within log-log plots, they become linear. This property was used to for making linear fits to log-log data points and transforming the obtained results back to exponents. The input data for this fitting procedure has to be of a `logspace` to result in a `linspace` in the log-log transform. Otherwise, the fitting would be based on a small cluster of points. This thought was used for obtaining the functions for the power law coefficients based on the Cross model for example. The difference between a logarithmic or a linear spacing of shear rates is not observable for obtaining the power law functions.

5.6 Conclusion

The previous chapter considered the system as a black box. In this chapter, an analytic model was proposed of the steady-state behaviour of the liquefier. The goal was to gain more knowledge and insight about the actual design parameters that influence the accuracy of the printing process and to find a model that could be used to support design changes.

The odd behaviour in the bode and phase plot of the previous chapter may be caused by the following problems:

- Changing compliance of the compressible rod with consumption.
- Changes in the fluid restriction with varying flow conditions (shear thinning)
- Changes of the bulk temperature in the nozzle for a range of flow rates

Figure 5.3 shows that the stiffness has a large dependency on the amount of extruded material. This may declare a part of the results observable in Figure 4.8. How stiffness influences the transient conditions remains unclear.

The availability of a Cross viscosity enabled obtaining functions for the power law coefficients k and n that are valid for a certain range of shear rates, for variable temperatures. These functions were compared to the Cross model and show an acceptable approximation within the relevant shear rate range in the 3D printing process.

The power law functions could be substituted in the Boles equation, Equation 2.6, together with the geometrical parameters of the nozzle. The obtained pressure drop function could be simplified to: Equation 5.13. The obtained models agree with the measurements within the range of performed measurements.

Bellini's model underestimates the pressure drop by a systematic error factor of 1.5 for both nozzle types.

The actual temperature of the material is measured using a thermal camera, for the set point of 410 °C, the actual temperature of the material is 405 °C, within the tested domain. At higher temperatures, the actual temperature of the material drops slightly and needs tuning of the thermal controller.

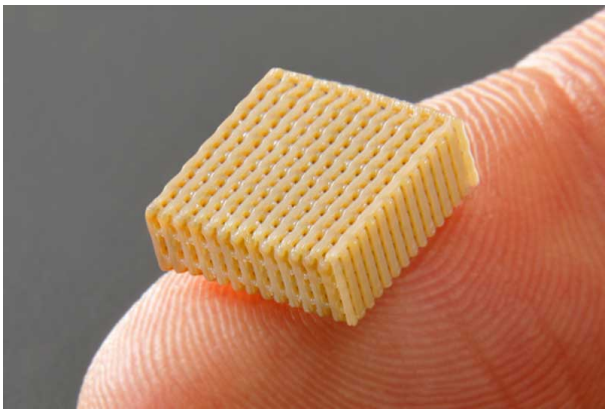

Figure 5.12: The obtained accuracy achieved by colleagues after implementation of feeder dynamics control

5.6.1 Recommendations

The models apply to extrusion in the open air, which is the situation during the oozing process, but is not typical for a 3D printing situation in which the substrate layer provides an extra resistance.

The setup used in this chapter could be used to find information on the difference between the pressure drop in open air extrusion and the actual printing process.

The models perform good within the range of measurements. The number of measurements was little. It would be interesting to be able to conclude on the validity of the model for other temperatures.

This study confirmed that the Boles model can be used to find the pressure drop, without the use of a complex finite element Model (FEM) model, but does require measurements of the actual temperature of the material within the thin section of the nozzle. The limits of the Boles model are not found within this study and need to be found by subjection to a larger frame of flow rates, temperatures, nozzle diameters, nozzle channel lengths and other materials.

Chapter 6

Conclusion

The assignment of this master thesis was to improve the deposition accuracy of an extrusion based printer for PEEK: The right amount of material had to be dispensed at the right place.

Progress was made to the understanding of liquefiers and previously proposed models that presented by other authors were discussed.

The main question of this study was:

Given a high-performance extrusion-based 3D printing system and PEEK 450G as the building material, develop a method to enhance small feature performance.

This question was answered as following:

After an initial study it could be found that tricks such as retracts, wipes, priming and coasting work for specific cases, but often result completely inaccurate product when one of the printing settings (line height, object geometry) has to be changed. The application of 'wipes' is a risky approach since the nozzle is likely to become dirty due to the smearing.

Snapping of the extruded strand is an important factor. In the case of a slow travel move that succeeds a printing move, the material is pulled from its place. Faster travelling has two effects: it enhances how well the material can be snapped and it simply reduces the time that oozing can take place. Additionally to faster travel moves, quicker pressure release by increasing the retract speed decrease the oozing problem.

It was found that the line width of the printed tracks was dependent on time in a second set of experiments. Additional literature was found that could confirm this observation. Liquefier dynamics are the main cause of the problem.

Two different system characterisation methods were applied: a step response experiment and a frequency response experiment. A control strategy was implemented that led to a great improvement. The method was correct, but required different parameters than those estimated by the characterisation. The non-linearity that is observable in the step results of the step response and frequency response was neglected, hence the correction worked only in a small flow regime. The main problem with the previously mentioned approach is that it does not provide any support for designing physical changes to the system, or when parameters are changed. Therefore, the oozing of the system was modelled from a physical point of view. This approach considered 3 important factors: the compliance of the rod, the thermal expansion and the dependency of the pressure drop on both the temperature and the volumetric flow rate. The pressure drop model was validated with steady state pressure drop measurements and good agreement between the model of Boles and measurements was obtained for two different nozzles. No experiment has been carried out to quantify the rod stiffness model and thermal expansion, however estimates of the extent of their effects is in agreement with the step response. A FEM would provide better estimation of the thermodynamics of the liquefier.

Although the implementation of the model was done by other team members, the insights about the dynamics and the temperature and flow rate dependency from this study led to better understanding of the liquefier and formed a good base for further improvement. The approach is likely to be useful to improve nozzle geometry and tuning for other materials and for development of more accurate FEM models.

6.1 Future work

In this master thesis progress has been made to the understanding of liquefiers and models that were presented by other authors were evaluated for PEEK. The measurements provide satisfying results. Better mea-

surement strategies should be designed to find measurements with a higher accuracy. PEEK is a material that will serve in critical applications. Therefore it's behaviour needs to be thoroughly understood.

Temperature will become a more dominant factor for increasing flow rates. And new thermal control strategies may need to be developed. The information cannot be adequately gathered using the PoP prototypes, since they do not have a build room at elevated temperature and measurement of the actual flow temperature of the material when it leaves the nozzle is also difficult.

The measurements provide satisfying results. Improved measurement strategies should be designed to obtain measurements with a higher accuracy.

References

Ashby, M. (2018). *Ces edupack*. Retrieved from https://www.grantadesign.com/education/edupack/ ((Version 2018) [Windows]. Cambridge, United Kingdom: Granta Design.)

ASTM. (2012). *F2792-12a, standard terminology for additive manufacturing technologies, (withdrawn 2015)*. Retrieved from www.astm.org (ASTM International, West Conshohocken, PA, 2012)

Astrom, K. (1995). *Pid controllers*. Research Triangle Park, N.C: International Society for Measurement and Control.

B. Bird, R., C. Armstrong, R., & Hassager, O. (1987). *Dynamics of polymeric liquids: Vol. 1, fluid mechanics* (Vol. 1).

Beckhoff. (n.d.). *Smoothing of segment transitions.* Retrieved from https://infosys.beckhoff.com/english.php?content=../content/1033/tcnci/9007199726065931.html ([Online; accessed 7-April-2019])

Bellehumeur, C., & Li, L. (2004). Modeling of Bond Formation Between Polymer Filaments in the Fused Deposition Modeling Process. *Journal of Manufacturing Processes*, *6*(2), 170–178. doi: 10.1016/S1526-6125(04)70071-7

Bellini, A. (2002). Fused Deposition of Ceramics : A Comprehensive Experimental , Analytical and Computational Study of Material Behavior , Fabrication Process and Equipment Design. *Doctrate thesis*(September), 319. Retrieved from https://idea.library.drexel.edu/islandora/object/idea%3A22

Bellini, A. (2004). Liquefier Dynamics in Fused Deposition. *Journal of Manufacturing Science and Engineering*, *126*(2), 237-246. Retrieved from https://manufacturingscience.asmedigitalcollection.asme.org/article.aspx?articleid=1448627 doi: 10.1115/1.1688377

Berretta, S., Davies, R., Shyng, Y., Wang, Y., & Ghita, O. (2017). Fused deposition modelling of high temperature polymers: Exploring cnt peek composites. *Polymer Testing*, *63*, 251 - 262. Retrieved from http://www.sciencedirect.com/science/article/pii/S014294181730702X doi: https://doi.org/10.1016/j.polymertesting.2017.08.024

Burchett, B. (2014). *First order system identification.* Retrieved from https://www.rose-hulman.edu/ES205/PDFs/s14_lab_5.pdf ([Online; accessed 25-November-2018])

Chua, C. K., Wong, C. H., & Yeong, W. Y. (2017). *Standards, Quality Control, and Measurement Sciences in 3D Printing and Additive Manufacturing*. Retrieved from https://www.elsevier.com/books/standards-quality-control-and-measurement-sciences-in-3d-printing-and-additive-manufacturing/chua/978-0-12-813489-4 doi: 10.1016/B978-0-12-813489-4/00010-6

Coffland, J. (2017). Camotics [Computer software]. Retrieved from https://www.camotics.org

Comb, J. W., Priedeman, W. R., & Turley, P. W. (1994). FDM technology process improvements. *Solid Freeform Fabrication Proceedings*, 42–49. Retrieved from http://www.dtic.mil/cgi-bin/GetTRDoc?AD=ADA290949{#}page=49

Crockett, R. S., Kelly, J. O., Calvert, P. D., Fabes, B. D., Stuffle, K., Creegan, P., & Hoffman, R. (1995). Predicting and Controlling Resolution and Surface Finish of Ceramic Objects Produced By Stereodeposition Processes. *Proceedings Solid Freeform Fabrication Symposium, University of Texas at Austin*, 17–24.

Crump, S., Wales, R., & Walters, B. (1991). Fast, precise, safe prototypes with FDM. *Winter Annual Meeting of the American Society of Mechanical Engineers*, *50*, 53–60. Retrieved from https://sffsymposium.engr.utexas.edu/Manuscripts/1991/1991-15-Wales.pdf{%}0Ahttp://www.scopus.com/inward/record.url?eid=2-s2.0-0026369845{&}partnerID=40{&}md5=84fefc0a925bb2ffa96152287bd9d2fc

Davies, R., Shyng, Y. T., Wang, Y., & Ghita, O. (2015). Extrusion Deposition of Carbon Nanotubes (Cnt)/ Poly Ether Ether Ketone (Peek). Exeter.

de Bruijn, B. (2014). *Machinekit and additive manufacturing.* Retrieved from http://basdebruijn.com/2014/05/machinekit-and-additive-manufacturing/ ([Online; accessed 18-October-2018])

Deng, X., Zeng, Z., Peng, B., Yan, S., & Ke, W. (2018). Mechanical properties optimization of poly-ether-ether-ketone via fused deposition modeling. *Materials*, *11*(2). doi: 10.3390/ma11020216

Eosint p 800 (Datasheet No. 2). (2017, 09). Retrieved from https://www.eos.info/p-solutions/download/datasheet_EOSINT_P800.pdf ([Online; accessed 16-September-2018])

Ganz, M. (2016). *Peek micro moulding for medical parts — a success.* Retrieved from http://www.cmmmagazine.com/micromanufacturing/mouldingtooling/peek-micro-moulding-for-medical-parts-%E2%80%94-a-success/ ([Online; accessed 11-September-2017])

Gibson, I., Rosen, D. D. W., & Stucker, B. (2009). *Additive Manufacturing Technologies: Rapid Prototyping to Direct Digital Manufacturing*. Springer, Boston, MA. doi: 10.1007/978-1-4419-1120-9

Gilmer, E. L., Miller, D., Chatham, C. A., Zawaski, C., Fallon, J. J., Pekkanen, A., ... Bortner, M. J. (2017). Model analysis of feedstock behavior in fused filament fabrication: Enabling rapid materials screening. *Polymer (United Kingdom)*, 1–11. Retrieved from https://doi.org/10.1016/j.polymer.2017.11.068 doi: 10.1016/j.polymer.2017.11.068

Go, J., & Hart, A. J. (2017). Fast Desktop-Scale Extrusion Additive Manufacturing. *Additive Manufacturing*, *18*, 276–284. Retrieved from http://dx.doi.org/10.1016/j.addma.2017.10.016 doi: 10.1016/j.addma.2017.10.016

Go, J., Schiffres, S. N., Stevens, A. G., & Hart, A. J. (2017). Rate limits of additive manufacturing by fused filament fabrication and guidelines for high-throughput system design. *Additive Manufacturing*, *16*(2010), 1–11. Retrieved from http://dx.doi.org/10.1016/j.addma.2017.03.007 doi: 10.1016/j.addma.2017.03.007

Godara, A., Raabe, D., & Green, S. (2007). The influence of sterilization processes on the micromechanical properties of carbon fiber-reinforced peek composites for bone implant applications. *Acta Biomaterialia*, *3*(2), 209 - 220. Retrieved from http://www.sciencedirect.com/science/article/pii/S1742706106001577 doi: https://doi.org/10.1016/j.actbio.2006.11.005

Grasmeder, J. (2017a). *Polymer crystallinity –hpp explained (part 2).* Retrieved from https://www.victrex.com/en/blog/2017/a-closer-peek-at-peek ([Online; accessed 19-September-2018])

Grasmeder, J. (2017b). *Polymer crystallinity –hpp explained (part 3).* Retrieved from https://www.victrex.com/en/blog/2017/polymer-crystallinity-hpp-explained-part-3 ([Online; accessed 11-September-2018])

Henschke, M. (2013). *Advance-algorithmus.* Retrieved from https://www.henschke-geraetebau.de/dr/waerme_filament.html ([Online; accessed 18-October-2018])

Hergenrother, P. M. (2003). The use, design, synthesis, and properties of high performance/high temperature polymers: An overview. *High Performance Polymers*, *15*(1), 3–45. doi: 10.1177/0954008303015001O1

Hirschen, C., & Gülhan, A. (2009). Infrared Thermography and Pitot Pressure Measurements of a Scramjet Nozzle Flowfield. *Journal of Propulsion and Power*, *25*(5), 1108–1120. Retrieved from http://arc.aiaa.org/doi/10.2514/1.41787 doi: 10.2514/1.41787

Hopmann, Christian and Michaeli, W. (2016). *Extrusion Dies for Plastics and Rubber* (4th ed.). München, Germany: Carl Hanser Verlag GmbH & Co. KG. Retrieved from https://www.hanser-elibrary.com/doi/book/10.3139/9781569906248 doi: 10.3139/9781569906248.001

Jerez-Mesa, R., Travieso-Rodriguez, J. A., Corbella, X., Busqué, R., & Gomez-Gras, G. (2016). Finite element analysis of the thermal behavior of a RepRap 3D printer liquefier. *Mechatronics*, *36*(April), 119–126. doi: 10.1016/j.mechatronics.2016.04.007

Kang, J., Wang, L., Yang, C., Wang, L., Yi, C., He, J., & Li, D. (2018). Custom design and biomechanical analysis of 3D-printed PEEK rib prostheses. *Biomechanics and Modeling in Mechanobiology*, *17*(4), 1083–1092. doi: 10.1007/s10237-018-1015-x

Koopmans, R. J., & Molenaar, J. (1998). The "Sharkskin Effect" in polymer extrusion. *Polymer Engineering and Science*, *38*(1), 101–107. doi: 10.1002/pen.10169

Kubicek, B. (2011a). *Another acceleration-extrusion compensation for repraps.* Retrieved from http://bernhardkubicek.soup.io/post/168776124/Another-acceleration-extrusion-compensation-for-repraps ([Online; accessed 18-October-2018])

Kubicek, B. (2011b). *Improved oozing compensation for diy fused deposition 3d printers.* Retrieved from https://web.archive.org/web/20140801235854/http://kariert.org/advanceV2.pdf ([Online; accessed 18-October-2018])

Kurtz, S. M. (2012). *PEEK biomaterials handbook*. doi: 10.1016/B978-1-4377-4463-7.10001-6

Kwon, T. H., Shen, S. F., & Wang, K. K. (1986). Pressure drop of polymeric melts in conical converging flow: Experiments and predictions. *Polymer Engineering & Science*, *26*(3), 214–224. doi: 10.1002/pen.760260306

Landry, T. (2015). *Retraction: just say no to oozing.* Retrieved from https://www.matterhackers.com/articles/retraction-just-say-no-to-oozing ([Online; accessed 01-October-2017])

Mackay, M. E., Swain, Z. R., Banbury, C. R., Phan, D. D., & Edwards, D. A. (2017). The performance of the hot end

in a plasticating 3D printer. *Journal of Rheology*, *61*(2), 229–236. Retrieved from http://aip.scitation.org/doi/10.1122/1.4973852 doi: 10.1122/1.4973852

Martineau, L., Chabert, F., Boniface, B., & Bernhart, G. (2019). Effect of interfacial crystalline growth on autohesion of peek. *International Journal of Adhesion and Adhesives*, *89*, 82 - 87. Retrieved from http://www.sciencedirect.com/science/article/pii/S0143749618302720 doi: https://doi.org/10.1016/j.ijadhadh.2018.11.013

McKinley, C. W. M. . G. H. (2004). *Tubeless siphon and die swell demonstration.* Retrieved from https://web.mit.edu/nnf/research/phenomena/Demos.pdf ([Online; accessed 24-October-2018])

Meyer, T., & Keurentjes, J. T. F. (2008). *Handbook of Polymer Reaction Engineering*. doi: 10.1002/9783527619870

Michaeli, W. (1992). *Extrusion Dies: for plastics and Rubber: design and engineering computations – second edition"*. Carl Hanser Verlag.

Newman, D. (2016). *Stepperaccelplanner.hh, line 491.* Retrieved from https://github.com/jetty840/Sailfish-MightyBoardFirmware/blob/4d8456e54c537dd32775095ed2715d41f5961e6c/firmware/src/MightyBoard/Motherboard/StepperAccelPlanner.cc#L491 ([Online; accessed 23-October-2018])

Newman, L. (2017). *SAILFISH Reference Manual*. Retrieved from http://www.sailfishfirmware.com/doc/sailfish.pdf ([Online; accessed 18-Oktober-2018])

Niemann, H., & Miklos, R. (2014). A simple method for estimation of parameters in first order systems. *Journal of Physics: Conference Series*, *570*. Retrieved from http://iopscience.iop.org/article/10.1088/1742-6596/570/1/012001/pdf doi: 10.1088/1742-6596/570/1/012001

Nikzad, M., Masood, H. S., Sbarski, I., & Groth, A. (2009). A Study of Melt Flow Analysis of an ABS-Iron Composite in Fused Deposition Modelling Process. *Tsinghua Science and Technology*, *14*(SUPPL. 1), 29–37. doi: 10.1016/S1007-0214(09)70063-X

Osswald, T. A., Puentes, J., & Kattinger, J. (2018). Fused filament fabrication melting model. *Additive Manufacturing*, *22*(June), 51–59. Retrieved from https://doi.org/10.1016/j.addma.2018.04.030 doi: 10.1016/j.addma.2018.04.030

Patel, P., Hull, R., Mccabe, R., Flath, D., Grasmeder, J., & Percy, M. (2010, 05). Mechanism of thermal decomposition of poly(ether ether ketone) (peek) from a review of decomposition studies. *Polymer Degradation and Stability - POLYM DEGRAD STABIL*, *95*, 709-718. doi: 10.1016/j.polymdegradstab.2010.01.024

Pierrot, F., Reynaud, C., & Fournier, A. (1990). Delta: A simple and efficient parallel robot. *Robotica*, *8*(2), 105–109. doi: 10.1017/S0263574700007669

Piper-Plastics. (2018). *Near net shapes for high performance polymers.* Retrieved from https://www.piperplastics.com/pages/nearnet.html ([Online; accessed 11-September-2018])

Prime, R. B., General, Z. B. M., Division, P., California, S. J., & Seferis, J. C. (1986). Thermo-Oxidative Decomposition of Poly (Ether Ether Ketone). *Journal of Polymer Science Part C: Polymer Letters*, *24*(12), 641–644. doi: 10.1002/pol.1986.140241204

Rabinovitch, E. B., Summers, J. W., & Booth, P. C. (1992, mar). Die design for rigid PVC—the effect of die land length on extrudate swell. *Journal of Vinyl and Additive Technology*, *14*(1), 20–23. Retrieved from http://doi.wiley.com/10.1002/vnl.730140107 doi: 10.1002/vnl.730140107

Rahman, K. M., Letcher, T., & Reese, R. (2015). Mechanical Properties of Additively Manufactured PEEK Components Using Fused Filament Fabrication. *Volume 2A: Advanced Manufacturing*, V02AT02A009. Retrieved from http://proceedings.asmedigitalcollection.asme.org/proceeding.aspx?doi=10.1115/IMECE2015-52209 doi: 10.1115/IMECE2015-52209

Ramanath, H. S., Chua, C. K., Leong, K. F., & Shah, K. D. (2008). Melt flow behaviour of poly-ϵ-caprolactone in fused deposition modelling. *Journal of Materials Science: Materials in Medicine*, *19*(7), 2541–2550. doi: 10.1007/s10856-007-3203-6

Repetier. (2011). *Extruder pressure control.* Retrieved from https://github.com/repetier/Repetier-Firmware/wiki/Hardware-settings-and-print-quality#extruder-pressure-control ([Online; accessed 01-October-2017])

Richardson, S. M. (2018). *Poiseuille flow.* Retrieved from http://www.thermopedia.com/content/1042/ ([Online; accessed 16-September-2018]) doi: 10.1615/AtoZ.p.poiseuille_flow

Roberts, M. (2011). *Mattroberts' firmware.* Retrieved from https://reprap.org/wiki/Mattroberts%27_Firmware ([Online; accessed 18-October-2018])

Roover, D. d. (1997). *Motion Control of a Wafer Stage* (Doctoral dissertation, Delft). Retrieved from http://www.narcis.nl/publication/RecordID/oai:tudelft.nl:uuid:3db4abf3-50b3-4a5b-8fbc-4d38356ba8b4

Sebastianv650. (2011). *Basic infos about advance feature in marlin.* Retrieved from http://drive.google.com/file/d/0B5UvosQgK3adaHVtdUI5OFR3VUU/view ([Online; accessed 22-October-2018])

Sebastianv650. (2018). *planner.cpp, line 2245.* Retrieved from https://github.com/MarlinFirmware/Marlin/blob/5befb307011607cc5ff391d974f2087e728c6099/Marlin/planner.cpp#L2245 ([Online; accessed 23-October-2018])

Silbernagel, C. (2018). *What is material extrusion.* Retrieved from http://canadamakes.ca/what-is-material-extrusion/ ([Online; accessed 11-September-2018])

Simplify3D. (2018). *Print quality troubleshooting guide.* Retrieved from https://www.simplify3d.com/support/print-quality-troubleshooting/ ([Online; accessed 11-September-2017])

Sineos, & Sebastianv650. (n.d.). *Marlin documentation linear advance.* Retrieved from http://marlinfw.org/docs/features/lin_advance.html ([Online; accessed 18-October-2018])

Solvay. (2018). *Solvay announces winners of additive manufacturing (am) cup, an international 3d printing competition using ketaspire® peek am filament* [Datasheet]. Retrieved from https://www.solvay.com/en/press-release/solvay-announces-winners-additive-manufacturing-am-cup-international-3d-printing ([Online; accessed 20-june-2018])

Steffe, J. (1996). *Rheological methods in food process engineering* (2nd ed.). East Lansing: Freeman Press.

Swanson, W. J., Turley, P. W., Leavitt, P., Karwoski, P. J., LaBossiere, J. E., & Skubic, R. L. (2000). *High temperature modeling apparatus* (No. WO2000078519A1). Retrieved from https://patents.google.com/patent/WO2000078519A1 ([Online; accessed 21-September-2018])

Tseng, J. W., Liu, C. Y., Yen, Y. K., Belkner, J., Bremicker, T., Liu, B. H., ... Wang, A. B. (2018). Screw extrusion-based additive manufacturing of PEEK. *Materials and Design*, *140*, 209–221. Retrieved from https://doi.org/10.1016/j.matdes.2017.11.032 doi: 10.1016/j.matdes.2017.11.032

Turner, B. N., & Gold, S. A. (2015). A review of melt extrusion additive manufacturing processes: II. Materials, dimensional accuracy, and surface roughness. *Rapid Prototyping Journal*, *21*(3), 250–261. doi: 10.1108/RPJ-02-2013-0017

Turner, B. N., Strong, R., & Gold, S. A. (2014). A review of melt extrusion additive manufacturing processes: I. Process design and modeling. *Rapid Prototyping Journal*, *20*(3), 192–204. doi: 10.1108/RPJ-01-2013-0012

Ultimaker. (2019). *fdmprinter.def.json.po line 2793.* Retrieved from https://github.com/Ultimaker/Cura/blob/0e55b25e0bc4ca7777124d625edeefb2dca9e6db/resources/i18n/nl_NL/fdmprinter.def.json.po ([Online; accessed 6-June-2019])

Vaezi, M., & Yang, S. (2015). Extrusion-based additive manufacturing of PEEK for biomedical applications. *Virtual and Physical Prototyping*, *10*(3), 123–135. doi: 10.1080/17452759.2015.1097053

Valentan, B., Kadivnik, Ž., Brajlih, T., Anderson, A., & Drstvenšek, I. (2013). Processing poly(ether etherketone) on a 3d printer for thermoplastic modelling. *Materiali in Tehnologije*, *47*(6), 715–721.

Venkataraman, N., Rangarajan, S., Harper, B., Matthewson, M., Safari, A., & Danforth, S. (2000). Process-property-performance relationship for fused deposition of ceramics (fdc) feedstock materials. *MRS Proceedings*, *625*, 203. doi: 10.1557/PROC-625-203

Victrex®. (2018). *A comprehensive review of the processing guidelines of victrex® peek™ high performance polymer.* Retrieved from https://www.emcoplastics.com/assets/pdf/peek/Processing%20Guide-PEEK.pdf ([Online; accessed 26-September-2018])

Victrex® peek 450g (Datasheet No. 1). (2012, 07). Retrieved from https://www.tafersnc.com/wp-content/uploads/Victrex-450G.pdf ([Online; accessed 4-March-2018])

Victrex® peek 450g (Datasheet No. 1). (2017, 06). Retrieved from https://www.victrex.com/~/media/datasheets/victrex_tds_450g.pdf ([Online; accessed 06-November-2018])

Wikipedia. (2018a). *A comparison of standard plastics, engineering plastics, and high-performance plastics.* Retrieved from https://en.wikipedia.org/wiki/High-performance_plastics ([Online; accessed 25-September-2018])

Wikipedia. (2018b). *Thermal expansion.* Retrieved from https://en.wikipedia.org/wiki/Thermal_expansion ([Online; accessed 12-November-2018])

Wohlers, T. (2016). *Popularity of fdm.* Retrieved from https://wohlersassociates.com/blog/2016/01/popularity-of-fdm/ ([Online; accessed 11-September-2018])

Wu, W., Geng, P., Li, G., Zhao, D., Zhang, H., & Zhao, J. (2015). Influence of layer thickness and raster angle on the mechanical properties of 3D-printed PEEK and a comparative mechanical study between PEEK and ABS. *Materials*, *8*(9), 5834–5846. doi: 10.3390/ma8095271

Wu, W. Z., Geng, P., Zhao, J., Zhang, Y., Rosen, D. W., & Zhang, H. B. (2014). Manufacture and thermal deformation analysis of semicrystalline polymer polyether ether ketone by 3D printing. *Materials Research Innovations*, *18*(sup5), 5–12. Retrieved from http://www.tandfonline.com/doi/full/10.1179/1432891714Z.000000000898 doi: 10.1179/1432891714Z.000000000898

Yang, C., Tian, X., Li, D., Cao, Y., Zhao, F., & Shi, C. (2017). Influence of thermal processing conditions in 3D

printing on the crystallinity and mechanical properties of PEEK material. *Journal of Materials Processing Technology*, *248*(May), 1–7. doi: 10.1016/j.jmatprotec.2017.04.027

Yardimci, M. a., Hattori, T., Guceri, S. I., & Danforth, S. C. (1997). Thermal analysis of Fused Deposition. *Solid Freeform Fabrication Proceedings, September 1997*, 689–698.

Zein, I., Hutmacher, D. W., Tan, K. C., & Teoh, S. H. (2002). Fused deposition modeling of novel scaffold architectures for tissue engineering applications. *Biomaterials*, *23*(4), 1169–1185. doi: 10.1016/S0142-9612(01)00232-0

Zhao, F., Li, D., & Jin, Z. (2018). Preliminary investigation of poly-ether-ether-ketone based on fused deposition modeling for medical applications. *Materials*, *11*(2). doi: 10.3390/ma11020288

Çengel, Y., & Ghajar, A. (2011). *Heat and mass transfer : Fundamentals and applications*. New York: McGraw Hill Higher Education.

Appendices

Appendix A

Cross viscosity model for PEEK

cross.py

```python
#!/usr/bin/env python3
import numpy as np


def calcPeekViscosity(temperature, shear_rate)
    """Returns the viscosity of PEEK in Pa*s.
    inputs: temperature in degC, shear_rate in 1/s.
    Compiled from data of the PEEK450G Cross-WLF model in Solidworks 2018"""
    temp_Kelvin = 273 + temperature
    viscosity_Pa_s = 2.89808e+16 * np.exp((-36.041 * (temp_Kelvin) + 14529.92915) / (temp_Kelvin - 351.55)) /
    ↪   (3300099.99695341 * (shear_rate * np.exp((-36.041 * temp_Kelvin + 14529.92915) / (temp_Kelvin -
    ↪   351.55)))**0.5734 + 1.0)
    return viscosity_Pa_s

if __name__ == "__main__":
    print(calcPeekViscosity(400, 1000))
```

```python
def initLibrary():
    """Returns a library with some Cross model properties of materials, data adopted from Solidworks 2018"""

    material_variables = ['A_1', 'A_2', 'D_1', 'D_2', 'D_3', 'n',
                          'tau', 'Tstar', 'lowerProcessingTemp', 'upperProcessingTemp']
    material_units = ['[-]', 'K', 'Pa*s', 'K',
                      'K/Pa', '[-]', 'Pa', 'K', 'K', 'K']
    PEEK_values = [36.041, 51.6, 2.89808e16, 403.15, 0,
                   0.4266,  124139, 403.15, 370 + 273, 450 + 273]
    ABS_values = [28.8, 51.6, 2.214900e12, 378.15, 0,
                  0.2353, 72350, 403.15, 190 + 273, 240 + 273]
    ULTEM1010_values = [31.81, 51.6, 2.16e13,
                        473.1, 0, 0.1134, 830200, 473.1, 343, 400]
    PEEK = dict(zip(material_variables, PEEK_values))
    ABS = dict(zip(material_variables, ABS_values))
    ULTEM1010 = dict(zip(material_variables, ULTEM1010_values))
    lib = {'peek': PEEK, 'abs': ABS, 'ultem1010': ULTEM1010}
    return lib

if __name__ == "__main__":
    lib = initLibrary()
    print(lib['peek'])
```

Appendix B

Step response measurements data

The data can be extracted from this file Oozed distance in millimetres after a sudden stop from extrusion at a print speed of $[50, 20, 12.2, 2]$ mm/s. With a square cross section area of $0.132\,\mathrm{mm}^2$, and a circular rod area of $19.63\mathrm{mm}^2$.

Table B.1: Step response data in mm, after suddon stop of extrusion at a printspeed of n mm/s part 1

t	L_50	L_20	L_12.2	L_2
0	3	0	0	0
0.1	4		1	
0.2		2	2	
0.3			3	
0.4		4		
0.5	7	5		1
0.6			3	
0.8		7		
0.9	10			
1			3	2
1.3	12			
1.5	13		3	
1.9		9		
2	15			
2.5		10	3	
2.6	17			
2.9		11		
3			3	2.5
3.3		12		
3.6	20			
3.7		13		
4		14		3
4.6		15		
4.7				4
4.8			4	

Table B.3: Step response data in mm, after suddon stop of extrusion at a printspeed of n mm/s part 2

t	L_50	L_20	L_12.2	L_2
5	24			
5.1		16		
5.3				5
5.5			5	
5.7		17		
6	26		6	6
6.1		18		
6.8		19		
6.8			7	
7	28			7
7.5		20		8
8			8	
8.2		21		
8.5				9
8.9		22		
9	30		9	
9.5				10
9.9		23		
10	32			
10.2			10	
10.6		24		
11				11
11.5		25		
12	35			
12.1			11	
13	37			
13				12
14	38		12	13
16	40		13	
17		30	14	14
18.5				15
20	44		15	16
22			16	
24				17
25.6		35		
26			17	
28				18
29			18	
30	50			19
35		40	19	
35				
36				20
37			20	
40	55			
41			21	
48.2		45		
49				23
51			23	
57				24
70		50		
100		55		

Appendix C

Transfer Function

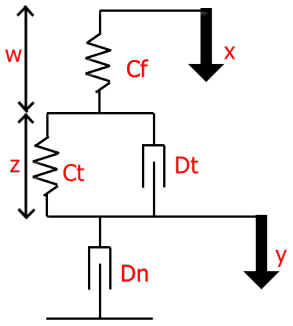

Figure C.1: Model of the system's dynamics

Transfer function from input displacement to output displacement in the nozzle, see Figure C.1.

$$F_3 = C_f \cdot w$$

$$F_2 = C_t \cdot z + D_t \cdot \dot{z} = (C_t + D_t \cdot s) \cdot z$$

$$F_1 = \dot{y} \cdot D_n$$

$$F_1 = F_2 \Rightarrow \dot{y} \cdot D_n = (C_t + D_t \cdot s) \cdot z$$

$$y = \frac{(C_t + D_t \cdot s) \cdot z}{D_n \cdot s}$$

$$z = \frac{D_n \cdot s \cdot y}{C_t + D_t \cdot s}$$

$$F_1 = F_3 \Rightarrow C_f \cdot w = \dot{y} \cdot D_n$$

$$w = \frac{\dot{y} \cdot D_n}{C_f}$$

$$w = \frac{D_n \cdot s}{C_f} \cdot y$$

$$x = y + z + w \Rightarrow y = x - z - w$$

$$y = x - \frac{D_n \cdot s \cdot y}{C_t + D_t \cdot s} - \frac{D_n \cdot s \cdot y}{C_f}$$

$$y + \frac{D_n \cdot s}{C_t + D_t \cdot s} \cdot y + \frac{D_n \cdot s}{C_f} \cdot y = x$$

$$(1 + \frac{D_n \cdot s}{C_t + D_t \cdot s} + \frac{D_n \cdot s}{C_f}) \cdot y = x$$

$$\frac{y}{x} = \frac{C_t + D_t \cdot s}{C_t + D_t \cdot s + D_n \cdot s + \frac{D_n \cdot C_t \cdot s}{C_f} + \frac{D_n \cdot D_t \cdot s^2}{C_f}}$$

$$G(s) = \frac{y}{x} = \frac{D_t \cdot s + C_t}{\frac{D_n \cdot D_t}{C_f} \cdot s^2 + (D_t + D_n + \frac{D_n \cdot C_t}{C_f}) \cdot s + C_t}$$

Appendix D

Frequency response measurement data

This is the measurement data for the experiments described in Figure 4.4. The data can be extracted from this file

```
## arrays in arrays, indices 0-11, SEE TABLE 'Frequency response experiment design' in H4
import pandas as pd
import re
timestamps=[[0.0, 2.36, 4.71, 7.07, 9.42, 11.78, 14.14, 16.49, 18.85, 21.21, 23.56, 25.92, 28.27, 30.63, 32.99,
35.34, 37.7, 40.06, 42.41, 44.77, 47.12, 49.48, 51.84, 54.19, 56.55, 58.9, 61.26, 63.62, 65.97, 68.33, 70.69,
73.04, 75.4, 77.75, 80.11, 82.47, 84.82, 87.18, 89.54, 91.89], [0.0, 0.47, 0.94, 1.41, 1.88, 2.36, 2.83, 3.3,
3.77, 4.24, 4.71, 5.18, 5.65, 6.13, 6.6, 7.07, 7.54, 8.01, 8.48, 8.95, 9.42, 9.9, 10.37, 10.84, 11.31, 11.78,
12.25, 12.72, 13.19, 13.67, 14.14, 14.61, 15.08, 15.55, 16.02, 16.49, 16.96, 17.44, 17.91, 18.38], [0.0, 0.94,
1.88, 2.83, 3.77, 4.71, 5.65, 6.6, 7.54, 8.48, 9.42, 10.37, 11.31, 12.25, 13.19, 14.14, 15.08, 16.02, 16.96,
17.91, 18.85, 19.79, 20.73, 21.68, 22.62, 23.56, 24.5, 25.45, 26.39, 27.33, 28.27, 29.22, 30.16, 31.1, 32.04,
32.99, 33.93, 34.87, 35.81, 36.76], [0.0, 0.12, 0.24, 0.35, 0.47, 0.59, 0.71, 0.82, 0.94, 1.06, 1.18, 1.3, 1.41,
1.53, 1.65, 1.77, 1.88, 2.0, 2.12, 2.24, 2.36, 2.47, 2.59, 2.71, 2.83, 2.95, 3.06, 3.18, 3.3, 3.42, 3.53, 3.65,
3.77, 3.89, 4.01, 4.12, 4.24, 4.36, 4.48, 4.59], [0.0, 0.09, 0.19, 0.28, 0.38, 0.47, 0.57, 0.66, 0.75, 0.85,
0.94, 1.04, 1.13, 1.23, 1.32, 1.41, 1.51, 1.6, 1.7, 1.79, 1.88, 1.98, 2.07, 2.17, 2.26, 2.36, 2.45, 2.54, 2.64,
2.73, 2.83, 2.92, 3.02, 3.11, 3.2, 3.3, 3.39, 3.49, 3.58, 3.68], [0.0, 4.71, 9.42, 14.14, 18.85, 23.56, 28.27,
32.99, 37.7, 42.41, 47.12, 51.84, 56.55, 61.26, 65.97, 70.69, 75.4, 80.11, 84.82, 89.54, 94.25, 98.96, 103.67,
108.38, 113.1, 117.81, 122.52, 127.23, 131.95, 136.66, 141.37, 146.08, 150.8, 155.51, 160.22, 164.93, 169.65,
174.36, 179.07, 183.78], [0.0, 0.05, 0.09, 0.14, 0.19, 0.24, 0.28, 0.33, 0.38, 0.42, 0.47, 0.52, 0.57, 0.61,
0.66, 0.71, 0.75, 0.8, 0.85, 0.9, 0.94, 0.99, 1.04, 1.08, 1.13, 1.18, 1.23, 1.27, 1.32, 1.37, 1.41, 1.46, 1.51,
1.56, 1.6, 1.65, 1.7, 1.74, 1.79, 1.84], [0.0, 0.94, 1.88, 2.83, 3.77, 4.71, 5.65, 6.6, 7.54, 8.48, 9.42, 10.37,
11.31, 12.25, 13.19, 14.14, 15.08, 16.02, 16.96, 17.91], [0.0, 1.88, 3.77, 5.65, 7.54, 9.42, 11.31, 13.19,
15.08, 16.96, 18.85, 20.73, 22.62, 24.5, 26.39, 28.27, 30.16, 32.04, 33.93, 35.81, 37.7, 39.58, 41.47, 43.35,
45.24, 47.12, 49.01, 50.89, 52.78, 54.66, 56.55, 58.43, 60.32, 62.2, 64.09, 65.97, 67.86, 69.74, 71.63, 73.51],
[0.0, 0.94, 1.88, 2.83, 3.77, 4.71, 5.65, 6.6, 7.54, 8.48, 9.42, 10.37, 11.31, 12.25, 13.19, 14.14, 15.08,
16.02, 16.96, 17.91, 18.85, 19.79, 20.73, 21.68, 22.62, 23.56, 24.5, 25.45, 26.39, 27.33, 28.27, 29.22, 30.16,
31.1, 32.04, 32.99, 33.93, 34.87, 35.81, 36.76], [0.0, 0.52, 1.05, 1.57, 2.09, 2.62, 3.14, 3.67, 4.19, 4.71,
5.24, 5.76, 6.28, 6.81, 7.33, 7.85, 8.38, 8.9, 9.42, 9.95, 10.47, 11.0, 11.52, 12.04, 12.57, 13.09, 13.61,
14.14, 14.66, 15.18, 15.71, 16.23, 16.76, 17.28, 17.8, 18.33, 18.85, 19.37, 19.9, 20.42, 20.94, 21.47, 21.99,
22.51, 23.04, 23.56, 24.09, 24.61, 25.13, 25.66, 26.18, 26.7, 27.23, 27.75, 28.27, 28.8, 29.32, 29.85, 30.37,
30.89, 31.42, 31.94, 32.46, 32.99, 33.51, 34.03, 34.56, 35.08, 35.6, 36.13, 36.65, 37.18], [0.0, 0.24, 0.47,
0.71, 0.94, 1.18, 1.41, 1.65, 1.88, 2.12, 2.36, 2.59, 2.83, 3.06, 3.3, 3.53, 3.77, 4.01, 4.24, 4.48]]
```

```
setpointwidth=[[0.33, 0.34, 0.35, 0.37, 0.4, 0.43, 0.47, 0.51, 0.56, 0.61, 0.66, 0.71, 0.76, 0.81, 0.85, 0.89,
0.92, 0.95, 0.97, 0.98, 0.99, 0.98, 0.97, 0.95, 0.92, 0.89, 0.85, 0.81, 0.76, 0.71, 0.66, 0.61, 0.56, 0.51,
0.47, 0.43, 0.4, 0.37, 0.35, 0.34], [-0.12, -0.03, 0.2, 0.54, 0.9, 1.22, 1.41, 1.44, 1.3, 1.02, 0.66, 0.3, 0.02,
-0.11, -0.08, 0.1, 0.42, 0.78, 1.12, 1.36, 1.45, 1.36, 1.12, 0.78, 0.42, 0.1, -0.08, -0.11, 0.02, 0.3, 0.66,
1.02, 1.3, 1.44, 1.41, 1.22, 0.9, 0.54, 0.2, -0.03], [-0.15, -0.14, -0.11, -0.06, 0.0, 0.08, 0.18, 0.29, 0.41,
0.53, 0.66, 0.79, 0.91, 1.03, 1.14, 1.24, 1.32, 1.39, 1.44, 1.47, 1.48, 1.47, 1.44, 1.39, 1.32, 1.24, 1.14,
1.03, 0.91, 0.79, 0.66, 0.53, 0.41, 0.29, 0.18, 0.08, 0.0, -0.06, -0.11, -0.14], [-0.18, -0.14, -0.02, 0.16,
0.4, 0.66, 0.92, 1.16, 1.35, 1.47, 1.51, 1.47, 1.35, 1.16, 0.92, 0.66, 0.4, 0.16, -0.02, -0.14, -0.18, -0.14,
-0.02, 0.16, 0.4, 0.66, 0.92, 1.16, 1.35, 1.47, 1.51, 1.47, 1.35, 1.16, 0.92, 0.66, 0.4, 0.16, -0.02, -0.14],
[-0.15, 0.08, 0.66, 1.24, 1.48, 1.24, 0.66, 0.08, -0.15, 0.08, 0.66, 1.24, 1.48, 1.24, 0.66, 0.08, -0.15, 0.08,
0.66, 1.24, 1.48, 1.24, 0.66, 0.08, -0.15, 0.08, 0.66, 1.24, 1.48, 1.24, 0.66, 0.08, -0.15, 0.08, 0.66, 1.24,
1.48, 1.24, 0.66, 0.08], [-0.12, -0.11, -0.08, -0.03, 0.02, 0.1, 0.2, 0.3, 0.42, 0.54, 0.66, 0.78, 0.9, 1.02,
1.12, 1.22, 1.3, 1.36, 1.41, 1.44, 1.45, 1.44, 1.41, 1.36, 1.3, 1.22, 1.12, 1.02, 0.9, 0.78, 0.66, 0.54, 0.42,
0.3, 0.2, 0.1, 0.02, -0.03, -0.08, -0.11], [-0.12, -0.11, -0.08, -0.03, 0.02, 0.1, 0.2, 0.3, 0.42, 0.54, 0.66,
0.78, 0.9, 1.02, 1.12, 1.22, 1.3, 1.36, 1.41, 1.44, 1.45, 1.44, 1.41, 1.36, 1.3, 1.22, 1.12, 1.02, 0.9, 0.78,
0.66, 0.54, 0.42, 0.3, 0.2, 0.1, 0.02, -0.03, -0.08, -0.11], [-0.12, -0.08, 0.02, 0.2, 0.42, 0.66, 0.9, 1.12,
1.3, 1.41, 1.45, 1.41, 1.3, 1.12, 0.9, 0.66, 0.42, 0.2, 0.02, -0.08], [-0.12, -0.08, 0.02, 0.2, 0.42, 0.66, 0.9,
1.12, 1.3, 1.41, 1.45, 1.41, 1.3, 1.12, 0.9, 0.66, 0.42, 0.2, 0.02, -0.08, -0.12, -0.08, 0.02, 0.2, 0.42, 0.66,
0.9, 1.12, 1.3, 1.41, 1.45, 1.41, 1.3, 1.12, 0.9, 0.66, 0.42, 0.2, 0.02, -0.08], [-0.12, -0.08, 0.02, 0.2, 0.42,
0.66, 0.9, 1.12, 1.3, 1.41, 1.45, 1.41, 1.3, 1.12, 0.9, 0.66, 0.42, 0.2, 0.02, -0.08, -0.12, -0.08, 0.02, 0.2,
0.42, 0.66, 0.9, 1.12, 1.3, 1.41, 1.45, 1.41, 1.3, 1.12, 0.9, 0.66, 0.42, 0.2, 0.02, -0.08], [-0.12, -0.01, 0.27,
0.66, 1.05, 1.34, 1.45, 1.34, 1.05, 0.66, 0.27, -0.01, -0.12, -0.01, 0.27, 0.66, 1.05, 1.34, 1.45, 1.34, 1.05,
0.66, 0.27, -0.01, -0.12, -0.01, 0.27, 0.66, 1.05, 1.34, 1.45, 1.34, 1.05, 0.66, 0.27, -0.01, -0.12, -0.01,
0.27, 0.66, 1.05, 1.34, 1.45, 1.34, 1.05, 0.66, 0.27, -0.01, -0.12, -0.01, 0.27, 0.66, 1.05, 1.34, 1.45, 1.34,
1.05, 0.66, 0.27, -0.01, -0.12, -0.01, 0.27, 0.66, 1.05, 1.34, 1.45, 1.34, 1.05, 0.66, 0.27, -0.01], [-0.12,
0.2, 0.9, 1.41, 1.3, 0.66, 0.02, -0.08, 0.42, 1.12, 1.45, 1.12, 0.42, -0.08, 0.02, 0.66, 1.3, 1.41, 0.9, 0.2]]

measuredwidth=[[0.64, 0.58, 0.57, 0.58, 0.6, 0.61, 0.54, 0.59, 0.59, 0.6, 0.62, 0.63, 0.66, 0.68, 0.71, 0.75,
0.75, 0.79, 0.82, 0.86, 0.86, 0.85, 0.85, 0.88, 0.9, 0.9, 0.88, 0.86, 0.86, 0.86, 0.85, 0.82, 0.78, 0.76, 0.73,
0.71, 0.7, 0.67, 0.65, 0.65], [0.7, 0.5, 0.44, 0.34, 0.46, 0.61, 0.74, 0.79, 0.9, 0.96, 1, 1, 0.79, 0.67, 0.5,
0.39, 0.41, 0.5, 0.53, 0.69, 0.82, 0.93, 1.01, 1.08, 1.06, 0.89, 0.83, 0.62, 0.53, 0.5, 0.51, 0.55, 0.71, 0.87,
0.95, 1.08, 1, 0.94, 0.88, 0.8], [1.03, 1.03, 1.03, 1.05, 1.03, 1.08, 1.09, 1.06, 1.05, 1.05, 1, 1.01, 0.96,
0.88, 0.88, 0.83, 0.75, 0.67, 0.63, 0.57, 0.5, 0.49, 0.44, 0.43, 0.38, 0.36, 0.34, 0.39, 0.38, 0.39, 0.47, 0.54,
0.61, 0.64, 0.68, 0.75, 0.82, 0.86, 0.92, 1], [0.76, 0.76, 0.8, 0.8, 0.83, 0.83, 0.81, 0.79, 0.76, 0.72, 0.71,
0.66, 0.66, 0.59, 0.6, 0.6, 0.61, 0.67, 0.66, 0.7, 0.76, 0.77, 0.86, 0.83, 0.83, 0.84, 0.84, 0.8, 0.78, 0.74,
0.8, 0.66, 0.65, 0.6, 0.59, 0.61, 0.67, 0.65, 0.66, 0.7], [0.73, 0.73, 0.76, 0.76, 0.73, 0.69, 0.68, 0.68, 0.72,
0.76, 0.76, 0.76, 0.75, 0.68, 0.66, 0.67, 0.71, 0.74, 0.77, 0.77, 0.73, 0.68, 0.67, 0.66, 0.7, 0.74, 0.76, 0.76,
0.72, 0.7, 0.67, 0.69, 0.71, 0.77, 0.8, 0.78, 0.76, 0.72, 0.69, 0.67], [0.29, 0.29, 0.34, 0.37, 0.3, 0.3, 0.36,
0.38, 0.35, 0.34, 0.32, 0.43, 0.58, 0.58, 0.62, 0.76, 0.76, 0.9, 0.86, 0.86, 0.83, 0.89, 1, 0.99, 1, 1.04, 1.15,
1.07, 1.03, 1.01, 0.97, 0.93, 0.87, 0.85, 0.76, 0.62, 0.55, 0.57, 0.48, 0.46], [0.82, 0.82, 0.95, 0.9, 1, 1.01,
1.03, 1.04, 1.04, 1.04, 1.07, 1.06, 1.04, 1.01, 0.96, 0.96, 0.86, 0.83, 0.8, 0.84, 0.7, 0.66, 0.61, 0.53, 0.51,
0.52, 0.51, 0.48, 0.49, 0.49, 0.54, 0.52, 0.53, 0.53, 0.59, 0.72, 0.73, 0.73, 0.78, 0.87], [0.55, 0.55, 0.48,
0.43, 0.46, 0.55, 0.6, 0.66, 0.72, 0.75, 0.8, 0.89, 0.9, 0.93, 0.95, 0.88, 0.83, 0.8, 0.72, 0.67], [0.5, 0.45,
0.39, 0.39, 0.35, 0.4, 0.47, 0.49, 0.64, 0.73, 0.87, 0.89, 0.9, 0.95, 0.91, 0.91, 0.83, 0.78, 0.7, 0.55, 0.5,
0.43, 0.39, 0.4, 0.43, 0.5, 0.48, 0.57, 0.63, 0.82, 0.83, 0.9, 0.91, 1, 0.92, 0.91, 0.88, 0.78, 0.66, 0.57],
[0.5, 0.45, 0.39, 0.39, 0.35, 0.4, 0.47, 0.49, 0.64, 0.73, 0.87, 0.89, 0.9, 0.95, 0.91, 0.91, 0.83, 0.78, 0.7,
0.55, 0.5, 0.43, 0.39, 0.4, 0.43, 0.5, 0.48, 0.57, 0.63, 0.82, 0.83, 0.9, 0.91, 1, 0.92, 0.91, 0.88, 0.78, 0.66,
0.57], [0.67, 0.63, 0.52, 0.59, 0.56, 0.68, 0.66, 0.75, 0.73, 0.76, 0.74, 0.79, 0.71, 0.7, 0.68, 0.61, 0.65,
0.69, 0.69, 0.77, 0.72, 0.76, 0.74, 0.71, 0.66, 0.66, 0.55, 0.52, 0.65, 0.63, 0.68, 0.77, 0.79, 0.82, 0.75,
0.71, 0.63, 0.57, 0.54, 0.59, 0.55, 0.59, 0.67, 0.73, 0.75, 0.73, 0.75, 0.69, 0.68, 0.53, 0.51, 0.58, 0.58,
0.62, 0.65, 0.75, 0.78, 0.75, 0.75, 0.71, 0.65, 0.57, 0.54, 0.52, 0.54, 0.59, 0.63, 0.72, 0.7, 0.7, 0.67,
0.7],[0.73, 0.77, 0.77, 0.74, 0.69, 0.67, 0.69, 0.75, 0.78, 0.77, 0.74, 0.69, 0.72, 0.75, 0.77, 0.79, 0.77,
0.72, 0.68, 0.69]]

# Data export:

columns = ['timestamps', 'setpointwidth', 'measuredwidth']
databox = [timestamps, setpointwidth, measuredwidth]

if False:  # export the data to a single file if set to true
    datafile = pd.DataFrame(columns=columns)
    for i, j in enumerate(columns):
        datafile[j] = databox[i]
    datafile.to_csv('all_measurements.csv')

if True:  # if set to true, data is exported to single files per column
    for i, j in enumerate(columns):
        data = pd.DataFrame(columns=[j])
        data[j] = databox[i]
        data.to_csv('data' + j + '.csv')

    if True:  # set to true if data needs to be expanded to cell data, for Matlab for example
        rgx_list = [re.compile(i) for i in [r'\]\"', r'\"\[']]
```

```
        for j in columns:
            def clean_text(rgx_list, text):
                new_text = text
                for rgx_match in rgx_list:
                    new_text = re.sub(rgx_match, '', new_text)
                return new_text

            with open('data' + j + '.csv', mode='r') as file, open('data' + j + '_ml.csv', 'w') as output_file:
                for line in file:
                    line_filtered = (clean_text(rgx_list, line))
                    output_file.write(line_filtered)
```

Appendix E

Least square fitting of a sine function

The data can be extracted from this file

```
#Adapted from:
# Author: DhDd
# 23-5-2013
# https://stackoverflow.com/questions/16716302/how-do-i-fit-a-sine-curve-to-my-data-with-pylab-and-numpy
# Accessed on: 13-11-2018

from scipy.optimize import leastsq
import numpy as np
import pylab as plt
plt.rcParams['figure.figsize'] = (15, 15)

def func(param, t):
    return param[0]*np.sin(2*np.pi*param[1]*t+param[2]*np.pi/180) + param[3]

A = lineWidthAmp # amplitude [mm] "look for a value near the input amplitude
B = SineOmega/rotationTime # frequency [Hz]  number of oscillations per second.
C = 90 # phase [deg]
D = lineWidthAvg # offset [mm]
param = [A,B,C,D]

N = len(data) # number of data points
t = np.linspace(0, rotationTime, N)
t2= np.linspace(0, rotationTime, 20*N)
guess = [np.std(data)*(2**0.5),B,C*2,np.mean(data)]

# we'll use this to plot our first estimate. This might already be good enough for you
data_guess = func(guess,t)

# Define the function to optimize, in this case, we want to minimize the difference
# between the actual data and our "guessed" parameters
optimize_func = lambda x: func(x,t) - data
#optimize_func = lambda x: func((x[0],B,x[2],x[3]),t) - data
fit = leastsq(optimize_func, guess)[0]

# # recreate the fitted curve using the optimized parameters
data_fit = func(fit,t)

plt.plot(t,data, '.', label='data\n%s'%param)
#plt.plot(t2,func(guess,t2), label='first guess\n%s'%guess)
plt.plot(t2,func(fit,t2), label='fit\n%s'%fit)   ###
plt.legend()
plt.show()
print(fit)

fitrad=[0,0, 0, 0]
fitrad[0]=fit[0]             #Amplitude [mm]
fitrad[1]=fit[1]*2*np.pi     #frequency [deg]
fitrad[2]=fit[2]*np.pi/180   #[rad]
fitrad[3]=fit[3]             #[mm]
print('In radians this yields the following function')

print('lw(t) = %.3f + %.3f * sin (%.3f * t + %.3f)'%(fitrad[3],fitrad[0] ,fitrad[1],fitrad[2]))

```

Appendix F

Calculate the pressure drop using the equation of Boles

The data can be extracted from this file

```python
#!/usr/bin/env python3
import numpy as np


def calcPressureDrop(K, n, Q, a_T, alpha, d, l):
    """Boles equation: Pressure drop in the liquefier in SI units
    inputs: K:powerlaw consistency, n:powerlaw exponent, Q:volumetric flow rate, a_T: temperature factor,
    alpha:half cone angle of the nozzle, d:diameter of thin section, l:land length, all in SI units."""
    totalPressure_MPa = 1.18 * K * a_T * n**(-0.7) * (8 * Q * (3 * n + 1) / (np.pi * d**3 * n))**n + 2 * K * a_T * (3 * np.sin(alpha) / (4 * n * (-np.cos(alpha) + 1)**2 * (2 * np.cos(alpha) + 1)))**n * (8 * Q * (3 * n + 1) / (np.pi * d**3 * n))**n / (3 * n * np.sin(alpha)) + 4 * K * a_T * l * (8 * Q * (3 * n + 1) / (np.pi * d**3 * n))**n / d
    return totalPressure_MPa

if __name__ == "__main__":
    K = 10114                   # [Pa*s^n] unique values of K and n should be calculated for each temperature
    n = 0.51                    # [-]
    Q = 20e-9                   # [m^3/s]
    a_T = 1                     # [-] (const) For PEEK, a_T should be set to 1
    alpha = (45 / 180) * np.pi  # [radians] (const)
    d = 0.6e-3                  # [m] (const)
    l = 4e-3                    # [m] (const)
    print(calcPressureDrop(K, n, Q, a_T, alpha, d, l))
```

Appendix G

Thermal properties of polymers

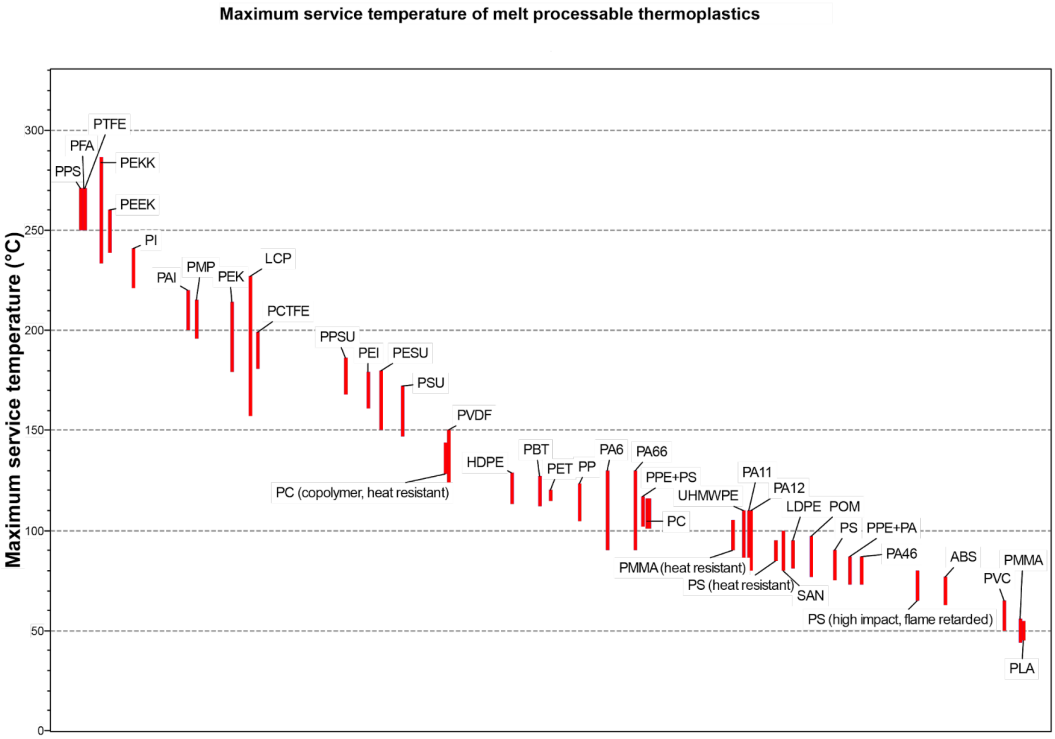

Figure G.1: Comparison of the service temperature limits for unfilled thermoplastics, data obtained from: (Ashby, 2018)

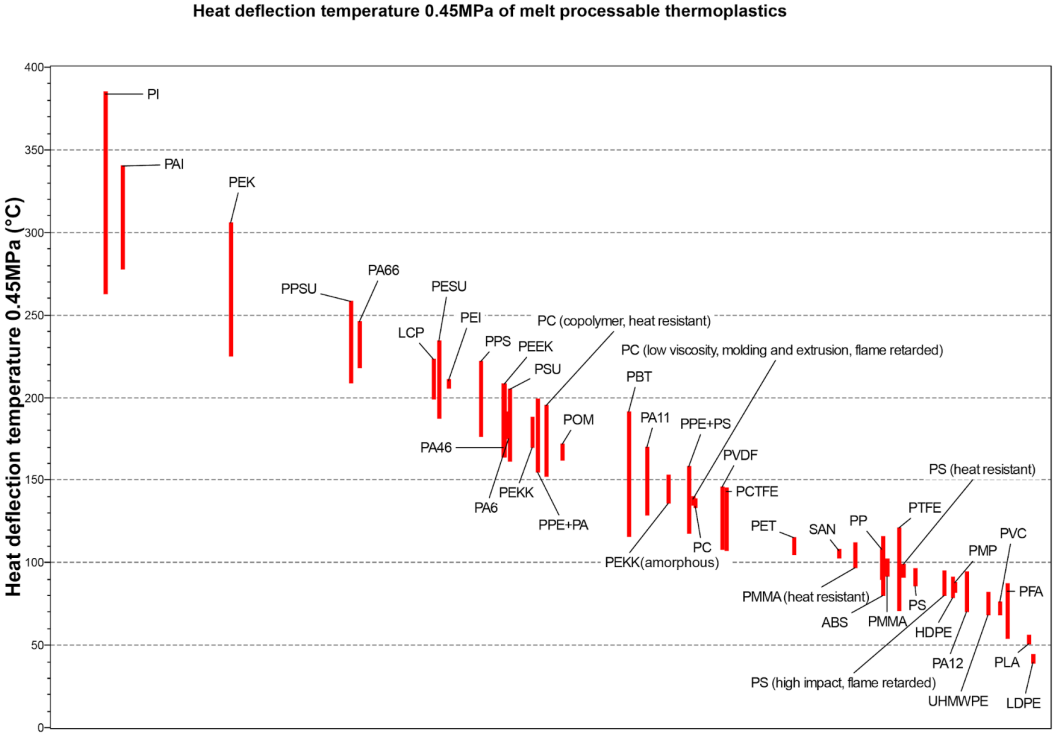

Figure G.2: Comparison of heat deflection temperatures for unfilled thermoplastics under a load of 0.45 MPa, data obtained from: (Ashby, 2018)

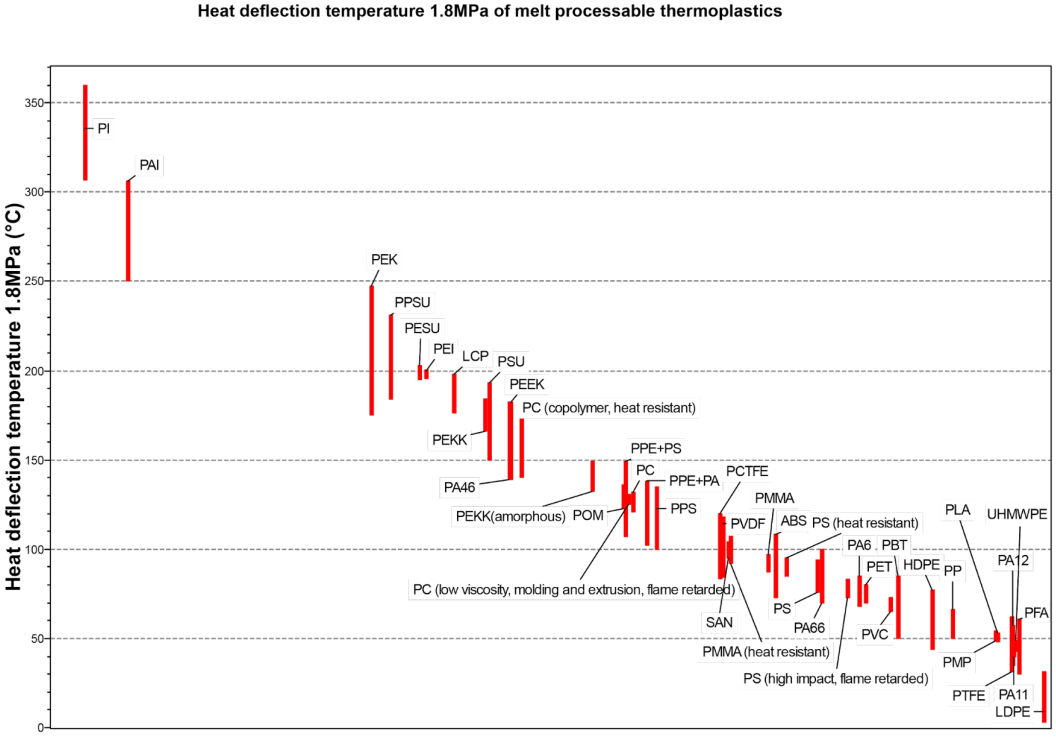

Figure G.3: Comparison of heat deflection temperatures for unfilled thermoplastics under a load of 1.8 MPa, data obtained from: (Ashby, 2018)

Appendix H

List of use cases for PEEK

Polymers have properties that can't be surpassed by metals. These properties include:

- Resistance to oxidation and acids
- Thermal and electrical insulation
- Low magnetic and radio interference
- Low densities and high strength to density ratios.

According (Grasmeder, 2017a) and (Kurtz, 2012), PEEK has the following properties:

- High-temperature resistance, see Figure G.1, G.2 and G.3
- High electrical insulation properties
- FDA (food, medical) approved
- Fire resistance, low smoke and toxicity
- Hydrolysis resistance
- Wear resistance
- High purity
- Easy processing (compared to metals)
- Chemical resistance
- High mechanical strength and high stiffness
- Stiffness tunable to cortical bone (25 GPa)(Kurtz, 2012, p. 35)
- High creep resistance and low fatigue
- Abrasion and corrosion resistance
- Radio translucency
- Sterilizible with steam, radiation and EtO
- Low density (when compared to metals)

Appendix I

Processing techniques for PEEK

Injection moulding Injection moulding with PEEK can be hard since it requires high clamping forces, high temperatures, accurate cooling using heaters elements, cooling channels and thermocouples. These aspects contribute to high tooling costs. Tooling is hard to adapt to changes. PEEK requires thick runner systems and oversized sprues that may dramatically increase material consumption. This can add up to 65%. The semi-crystalline structure of PEEK adds complexity to the cooling phase. An uniform tempering should be taken into account in the design phase. The cooling rates need to be controlled to provide the right crystallinity. (Ganz, 2016) The low surface roughness of the products and the high throughput are the main advantages (Kurtz, 2012, p.99).

Machining PEEK can be machined, but this should be done with care. Heat generation during cuts and grinds can introduce cracks and internal stresses. For medical applications, air is the preferred coolant. (Kurtz, 2012, p.44) The costs per product could be high since a lot of the expensive material is removed. The machine costs could be estimated at €100-150 per hour. Products are often formed in their near net shape before machining to reduce material consumption (Piper-Plastics, 2018). The surface roughness should be assessed for medical applications, since machining can produce features of the same order of size as the adhering bacteria and this could promote adhesion of bacteria. (Kurtz, 2012, p.99)

Selective laser sintering Using an EOS Eosint P800 SLS printing system, solid PEEK can be 3D printed with tensile strengths of 95 MPa and a tensile modulus of 4.4 MPa. This is achieved with a modified variant: PEEK-HP3 (Kurtz, 2012, p. 186). SLS may be unreliable in certain cases, due to differences in arrangement and size of powder particles, SLS has random discrepancies (Chua, Wong, & Yeong, 2017). Other downsides of SLS are the limited re-usability of powder waste material and the high investment costs of a full powder bed. The whole printing bed is transformed in a cookie like structure, containing solidified parts. Each time the powder is recycled the average particle size increases. This changes the spreading and melting characteristics of the powder. PEEK parts made with SLS can have high crystallinity levels (45%) (Grasmeder, 2017b). A disadvantage is that PEEK powder has irregular shapes causing non-uniform layers.

One of the big advantages of SLS is that the building material also serves as a supporting structure. This broadens design freedom dramatically. The throughput is high when compared to extrusion based printing: Using values from (*EOSINT P 800*, 2017), an estimate of the throughput can be calculated by making the following assumptions:

- An average of 25% of the build area would result into product geometry,
- The build area is 700 mm x 380 mm
- The vertical build rate is 7 mm/h
- The set-up an cool-down duration (including material removal) are estimated to be higher than those of extrusion based processes, hence up-time is estimated at 50%, which is a low estimate.

Using these assumptions, the limit of the volumetric build rate can be calculated and this is in the range of: $(700(\mathrm{mm}) \cdot 380(\mathrm{mm}) \cdot 7(\mathrm{mm/h}) \cdot 0.25 \cdot 0.5)/3600 = 65\mathrm{mm}^3/\mathrm{s}$. Despite of the low estimate of the up-time, the build rate is double of the highest rate reported for an extrusion printer: (127 cm^3/h=35 mm^3/s (Go & Hart, 2017).

Appendix J

Bellini and Boles pressure drop models compared with measurements

Pressure drop models compared. The mapping between the actual temperature of the material is unknown, but for a set point temperature of 410 °C the actual temperature is measured to be 405 °C, which agrees to the Boles model. It can be observed that the Boles model models the pressure drop well, while Bellini's model underestimates the pressure drop by a factor of 1.45. It should be notices that Bellini's model performed with ABS at flow rates of about 3 mm^3/s and had a pressure drop of about 1.5 MPa.

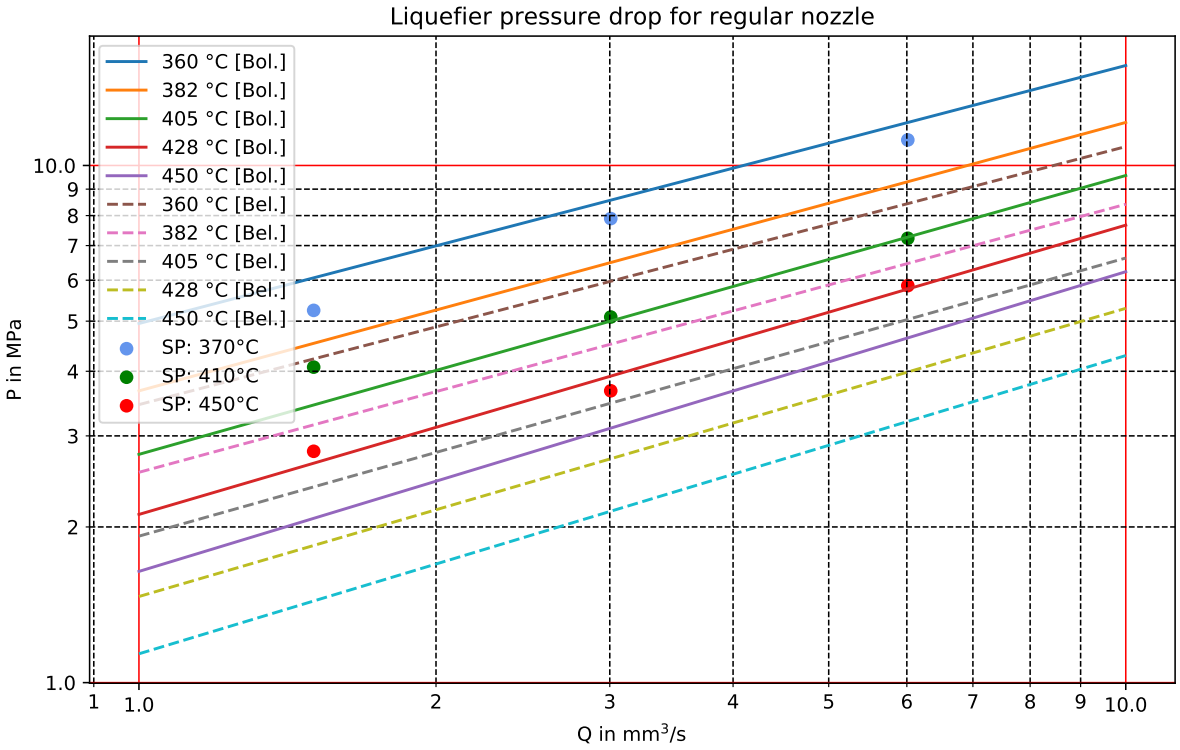

Figure J.1: Comparison of Boles and Bellini pressure drop models for regular nozzle and measurements

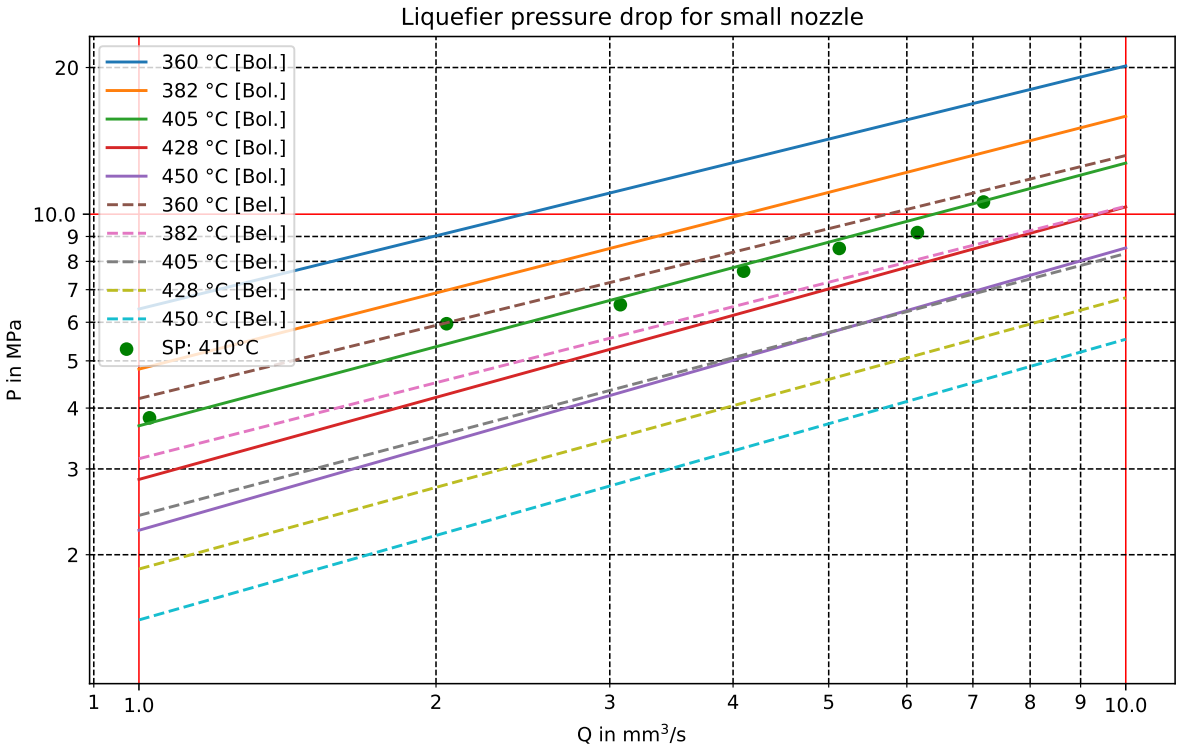

Figure J.2: Comparison of Boles and Bellini pressure drop models for small nozzle and measurements

Appendix K

3D printing technologies

3D Printing Process

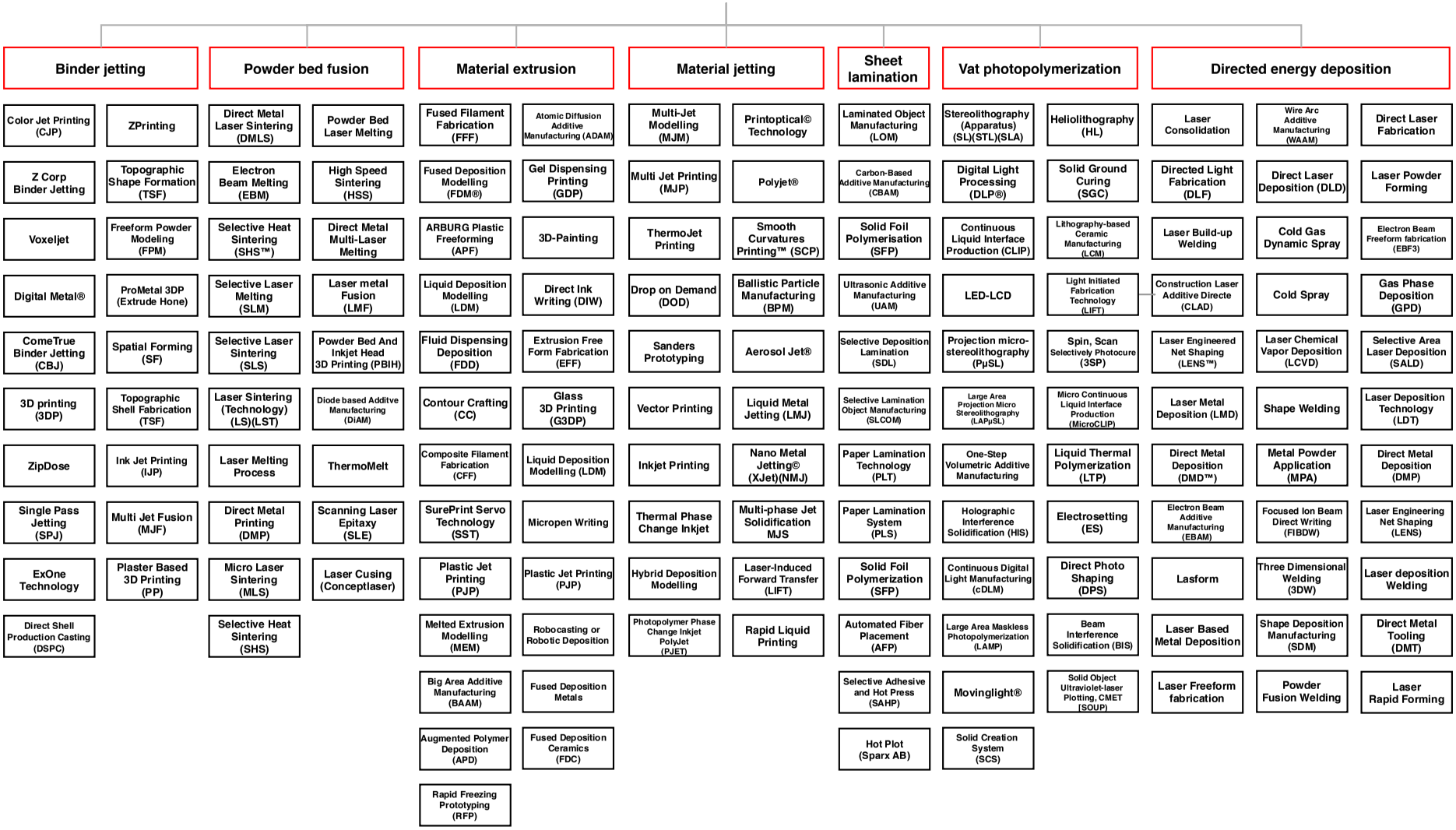

Appendix L

Crown test object definition file

The data can be extracted from this file

```
"""description: This is a file that can be used to define a specific geometry. In this case a Castle that consists of two stacked brim layers and several merlons for studying compensations for start-stop problems. It uses the g-code generator script to make g-code files that can be loaded to various type of printers (PoP, FeMo, FuMo, Ultimaker). Instead of a CAD modelling and slicing workflow, this workflow creates g-code directly and therefore allows better control of path placement.
author: Reinout Holtrup"""
#================================================================================

import numpy as np
import core
import util
from core import POPDriver

##Working file
MyPart = core.Part('castle_exp5') #Initialise part, name of Gcode file becomes castle_exp5.nc
MyPart.driver = POPDriver() #Sets the driver to generate g-code for the PoP.

#Settings:
lineWidth      = 0.44 # equals 0.67 / circumference
lineHeight     = 0.3 #[mm]
brimLineHeight = 0.3 #[mm]
radius     = 75/2 #[mm]
height     = 5-2*brimLineHeight #[mm]

MerlonWidth = 10 #[mm]
MerlonGap   = 10 #[mm]    # is adjusted lateron to fit an integer amount of merlons in a rotation
WipeLength = 0.5 #[mm]
WipeAngle = WipeLength/radius*180/np.pi #[deg] The PoP uses polar coordinates

# Override some default values
MyPart.lineWidth     = lineWidth
MyPart.lineThickness = lineHeight
MyPart.garbageX   = 0
MyPart.safeZlevel = 50  # [mm] sets parking position
MyPart.moveSpeed  = 200 # [mm/s]
MyPart.printSpeed = 10  # [mm/s]
MyPart.fastPfeed  = 1.5
MyPart.slowPfeed  = 0.25
MyPart.wipePullZ =  0
MyPart.wipeLength = WipeAngle   # [mm]
MyPart.P_Clearance     = 1  # [mm] feeder retract
MyPart.P_Clearance_fwd = 1  # [mm] feeder forward
MyPart.brimSpeedFactor  = 1.75

# Raxis
MODULO_RAXIS = True #can be used for better visualisation in CAMotics

# Calculate parameters for Merlons
UnitAngle   = (MerlonWidth+MerlonGap)/radius/np.pi*180
nMerlons    = int(360/UnitAngle)
UnitAngle   = 360/nMerlons
MerlonAngle = MerlonWidth/radius*180/np.pi

```

```
50  GapAngle    = UnitAngle-MerlonAngle
51  # Misc parameters for script
52  nlayers = int(height/lineHeight)
53  LineAngle  = 360
54
55  ##Create geometry: CastleTower
56  #===============================================================================
57
58  #Brim
59  MyPart.newLayer(brimLineHeight)
60  MyPart.addPath((0,360),'brim layer 1', wipe=core.WIPE.NONE )
61  MyPart.newLayer(brimLineHeight*2)
62  MyPart.addPath((360,720),'brim layer 2', wipe=core.WIPE.NONE )
63
64  #Merlons
65  for i in range(nlayers):
66      MyPart.newLayer((lineHeight*(i+3)))
67
68      for j in range(nMerlons):
69          MerlonStart = UnitAngle*j + 360*i +720
70          MerlonEnd   = UnitAngle*j + MerlonAngle - WipeAngle +360*i +720
71
72          pnts = np.array([MerlonStart, MerlonEnd])
73
74          if not MODULO_RAXIS:
75              pnts += LineAngle*(i+2)
76
77          MyPart.addPath(pnts,'castle layer %d merlon %d' % (i,j), wipe=core.WIPE.DURING,
            ↪  prewipe=core.PREWIPE.NONE)
78
79  # Tell my part to write the GCode and the SVG file
80  MyPart.save()
```